

ACOUSTO-ELECTRIC AND RELATED EFFECTS IN SEMICONDUCTORS AT
MICROWAVE FREQUENCIES

A thesis submitted to the
Faculty of Engineering of
the UNIVERSITY OF GLASGOW
for the degree of
DOCTOR OF PHILOSOPHY
(Electrical Engineering)

BY

DAVID HARRY ROBERT PRICE

Department of Electrical Engineering,
The University, Glasgow.

May, 1970.

ProQuest Number: 11011936

All rights reserved

INFORMATION TO ALL USERS

The quality of this reproduction is dependent upon the quality of the copy submitted.

In the unlikely event that the author did not send a complete manuscript and there are missing pages, these will be noted. Also, if material had to be removed, a note will indicate the deletion.



ProQuest 11011936

Published by ProQuest LLC (2018). Copyright of the Dissertation is held by the Author.

All rights reserved.

This work is protected against unauthorized copying under Title 17, United States Code
Microform Edition © ProQuest LLC.

ProQuest LLC.
789 East Eisenhower Parkway
P.O. Box 1346
Ann Arbor, MI 48106 – 1346

CONTENTS

Abstract		iv.
Chapter	1. INTRODUCTION	
	1.1 Field of Interest	1.
	1.2 Review of the Field	1.
Chapter	2. DEFORMATION POTENTIAL COUPLING	
	2.1 Introduction	7
	2.2 Physical Basis of Deformation Potential Interactions	7.
	2.3 Calculation of the Gain of a Deformation Potential Amplifier	12.
Chapter	3. HOT ELECTRON HALL MEASUREMENTS	
	3.1 Introduction	20.
	3.2 The Hall Effect	21.
	3.3 Apparatus	22.
	3.4 Specimen Preparation	29.
	3.5 Measurement Technique	33.
	3.6 Results	39.
	3.7 Calculation of Electron Temperature	41.
Chapter	4. DEFORMATION POTENTIAL AMPLIFIER	
	4.1 Introduction	60.
	4.2 Apparatus and Amplifier rods	60.
	4.3 Transducers	62.
	4.4 Measurement Technique	67.
	4.5 Results	68.
	4.6 Comparison of Theory and experiment	69.
	4.7 Discussion of the Deformation Potential Amplifier as an Electronic Device.	75.

Chapter	5.	ACOUSTIC ATTENUATION MEASUREMENTS AT LOW TEMPERATURES I - THEORETICAL ASPECTS	
	5.1	Introduction	77.
	5.2	Geometric and Surface Effects	78.
	5.3	Bulk Effects	82.
	5.4	Attenuation by Thermal Phonons	84.
	5.5	Summary of the Predicted Behaviour of the Acoustic Attenuation	104.
Chapter	6.	ACOUSTIC ATTENUATION MEASUREMENTS AT LOW TEMPERATURES II - EXPERIMENTAL ASPECTS	
	6.1	Introduction	107.
	6.2	General Description of Microwave Systems	108.
	6.3	X-band Microwave System	109.
	6.4	S and L-band microwave systems	117.
	6.5	Cryostats	121.
	6.6	Specimens	126.
	6.7	Measurement technique	130.
Chapter	7.	ACOUSTIC ATTENUATION MEASUREMENTS AT LOW TEMPERATURES III - RESULTS AND INTERPRETATION	
	7.1	Introduction	135.
	7.2	Experimental Results concerning the temperature Dependence and the Frequency Dependence of the acoustic attenuation.	136.
	7.3	Interpretation of the Attenuation Results	137.
	7.3.1	Temperature Dependence	
	7.3.2	Frequency Dependence	
	7.3.3	Limits of the Landau-Rumer region.	

	7.4 Other Experimental Results	140.
	7.5 Conclusions	143.
Chapter	8. ROOM TEMPERATURE ACOUSTIC ATTENUATION MEASUREMENTS	
	8.1 Introduction	145.
	8.2 Discussion of Bragg Scattering	147.
	8.3 Experimental Details	158.
	8.3.1 Optical Apparatus	
	8.3.2 Microwave Apparatus	
	8.3.3 Experimental Technique	
	8.4 Acoustic Attenuation at Room Temperature	162.
	8.5 Results	166.
	8.5.1 Longitudinal Wave Specimen	
	8.5.2 Shear Wave Specimen	
	8.6 Interpretation of Shear Wave Attenuation Results	169.
	8.7 Maximum Operating Frequencies of Acousto-Electric Devices.	173.
APPENDICES		
	Appendix A	175
	Appendix B	185.
	References	190.
	Acknowledgements	196.

ABSTRACT

This study is concerned with acousto-electric effects and the related phenomenon of acoustic attenuation, in semiconductors.

An account is presented of a theory of acoustic amplification based on the diffusion-mobility approximation, for the case where the coupling between the acoustic wave and the conduction electrons is a function of the deformation potential of the material. Experimental results obtained for the amplification of a 9 GHz acoustic wave in germanium are compared with the predictions of this theory. These results, and others obtained in germanium by another worker, are found to be in agreement with the theoretical predictions provided the theoretical expression is correctly evaluated. In evaluating the expression it is necessary to recognise that certain of the quantities in the expression were electric field dependent under the experimental conditions. In order to obtain the required values of electron temperature and the other electric field dependent quantities, a series of measurements were made of Hall mobility as a function of electric field. This unusual method of obtaining values of the electron temperature, and its justification are considered.

A review is included of the existing theories of the attenuation of microwave frequency acoustic waves in insulators at low temperatures. Special attention is paid to the

temperature dependence and to the frequency dependence of the attenuation. The predictions of these theories are compared with the results of a series of attenuation measurements made in the temperature range 15-120°K, at frequencies of 1.0, 3.6 and 8.8 GHz. The measurements were made on three materials, zinc oxide, cadmium sulphide and cadmium selenide. An extensive comparison of theory and experiment is possible, and in all cases the theoretical predictions are verified.

The study of acoustic attenuation was extended by a series of measurements made at room temperature in zinc oxide. The diffraction of a laser beam by an acoustic column was used as the basis of the method of measuring attenuation, rather than the pulse-echo technique used in the low temperature measurements. The method and its advantages are discussed, as is their experimental demonstration. The theories of the attenuation of acoustic waves at room temperature are discussed. Experimental results are presented which show that the attenuation of the longitudinal mode propagating along the c-axis of one specimen exhibited the anticipated frequency dependence; whereas the attenuation of the shear mode propagating parallel to the a-axis in another specimen did not show this dependence. An explanation of the behaviour of the attenuation in the shear specimen is presented.

A number of experimental systems were used during the course of the work, each is described; as are the methods of preparing the different types of specimen used.

CHAPTER 1 INTRODUCTION

1.1 Field of Interest

This thesis is concerned with acousto-electric effects and the related phenomenon of acoustic attenuation in semiconductors. The former effects involve the interaction of an acoustic wave with the conduction electrons in a solid, whereas the interaction between an acoustic wave and the thermal phonons in the solid is the source of the latter effect. In general when an acoustic wave propagates in a semiconductor both types of interaction occur. The acoustic frequencies of interest were in the microwave range.

During the course of this work attention was not only directed to the study of the above effects, but also to the prediction of the properties of certain acousto-electric devices.

1.2 Review of the field

The influence of an acoustic wave on the conduction electrons in a solid appears to have been first treated by PARMETER (1953), who introduced the term acousto-electric effect. The effect considered was the generation of an electric current as the result of the propagation of an acoustic wave through a solid containing conduction electrons. The acoustic wave was expected to be attenuated as a consequence of the interaction. The details of this treatment were later criticised by BLOUNT (1959).

In a discussion of the acousto-electric effect, WEINREICH (1956) pointed out that if a specimen in which an acoustic wave was propagating was subjected to an electric field of such a magnitude that the drift velocity of the conduction electrons was greater than the velocity of sound; then amplification of the acoustic wave might be expected.

A general relation between the open-circuit acousto-electric field and the attenuation coefficient of the acoustic wave was deduced by WEINREICH (1957). This relation, which is independent of the detailed mechanism of the wave-particle coupling, was obtained from a consideration of the conservation of momentum. The first experimental observation of the acousto-electric effect appears to have been made by WEINREICH and WHITE (1957), who detected the open-circuit acousto-electric voltage caused by a 60 MHz acoustic wave travelling through a germanium specimen.

POMERANTZ (1964) observed the amplification of a 9 GHz acoustic wave caused by the application of an electric field of the appropriate magnitude to a germanium specimen at 4.2°K . The measured gain however was smaller than that predicted by a factor of fifty. A possible explanation of this discrepancy was suggested by CONWELL (1964), who pointed out that a substantial reduction in the gain of an acoustic amplifier operating at low temperatures might be expected as a result of the heating of the electrons by the applied field.

This explanation could not be checked quantitatively because no data was available concerning the electric field dependent values of the electron temperature and electron mobility, at the electric fields at which the experiment was conducted.

Acoustic amplification was first observed by HUTSON, McFEE and WHITE (1961), at a frequency of 45 MHz in a cadmium sulphide specimen. In this case the coupling between the acoustic wave and the conduction electrons arose principally from the piezoelectric properties of the cadmium sulphide, whereas in germanium the coupling is a function of the deformation potential of the material.

A number of theoretical treatments of acousto-electric phenomena have been presented, some of which are discussed in Chapter 4.

The interest in acousto-electric devices has been mainly as solid state amplifiers operating at microwave frequencies. During the course of this work the potential importance of acousto-electric amplifiers has decreased as the result of advances in the technology of competitive devices, especially parametric and transistor amplifiers. Certain acousto-electric devices other than amplifiers have been investigated. A potentially significant example of such devices is the acousto-electric oscillator WHITE and WANG (1966) TWOMEY (1970).

The ability to launch with moderate efficiency acoustic waves with frequencies in the microwave range, is of great importance in experimental investigations of acousto-electric phenomena and acoustic attenuation. Prior to 1958, the most commonly used type of transducer took the form of a polished slice of piezoelectric material which was bonded to the specimen. It was found difficult to make measurements at frequencies greater than about 300 MHz with such transducers. This situation was improved when BARANSKII (1958) showed that it was possible to excite an acoustic wave having a frequency in the microwave range, by placing the end of a piezoelectric rod in the high electric field region of a re-entrant coaxial cavity. This work was followed by further advances in transducer techniques, these were concerned mainly with the preparation of very thin resonant transducers using evaporation methods. Both piezoelectric and magnetostrictive transducers were prepared in this way. QUATE, WILKINSON and WINSLOW (1965) and COHEN and GORDON (1965) have shown that light diffraction by an acoustic column has a number of advantages over the pulse echo technique McSKIMMIN (1964) as a method of investigating the propagation of a microwave frequency acoustic wave through a solid. The ease with which light diffraction experiments can be performed has been considerably enhanced by the availability of laser light sources.

The availability of relatively efficient methods of launching acoustic waves at microwave frequencies stimulated interest in acoustic attenuation measurements at these frequencies. A number of experimental investigations were made at low temperatures, including those of JACOBSON (1960), deKLERK and KLEMENS (1966) and LANGE (1968). A number of materials have been studied, of these quartz has been the most extensively investigated. The extent of the agreement between the experimental results and the predictions of the theories mentioned below, varied considerably.

A theory of acoustic attenuation at low temperatures based on a three phonon interaction model was given by LANDAU and RUMER (1937). This theory predicts that the attenuation of longitudinal acoustic waves should not occur as a result of three phonon processes, because such processes do not satisfy the relevant selection rules. However it was shown experimentally that the attenuation of both longitudinal and shear microwave frequency waves at low temperatures showed the same general behaviour, and moreover this behaviour was in agreement with the predictions of Landau and Rumer. SIMONS (1963) (1964) and MARIS (1964) have shown that three phonon processes involving a longitudinal acoustic phonon can satisfy the appropriate selection rules if account is taken of the uncertainty in the energy of the thermal phonons arising from the finite nature of their lifetimes. The treatment of attenuation at low temperatures

was further extended KWOK, MARTIN and MILLER (1965) GUREVICH and SHKLOVSKII (1967) by using powerful perturbation techniques to include the effect of higher order three phonon processes. A much fuller discussion of the theories of acoustic attenuation at low temperatures is given in Chapter 5.

Two mechanisms have been proposed to account for acoustic attenuation at room temperature. The first involves the relaxation of the acoustically perturbed thermal phonon distribution by means of thermal conduction. This appears to have been first suggested by Kirchoff in 1868, and applies only to the attenuation of longitudinal waves. The second mechanism was proposed by AKHEISER (1939) and applies to both shear and longitudinal waves.

Potentially the most important applications of acousto-electric devices are in the microwave frequency range. Consequently the magnitude of the acoustic attenuation influences the performance of the device. One important parameter of an acousto-electric device which is directly influenced by acoustic attenuation is the high frequency cut-off of the device. In general the cut-off will occur at a frequency at which the attenuation of the acoustic energy by the lattice is so large that no appreciable acousto-electric interaction is possible.

2.1 Introduction

The first section of this chapter introduces the concept of a deformation potential, and outlines the physical basis of wave-particle interactions caused by deformation potential coupling. The second section contains a discussion of various methods of calculating the gain of a deformation potential amplifier. A detailed account is given of one such method, which does not appear to have been given previously.

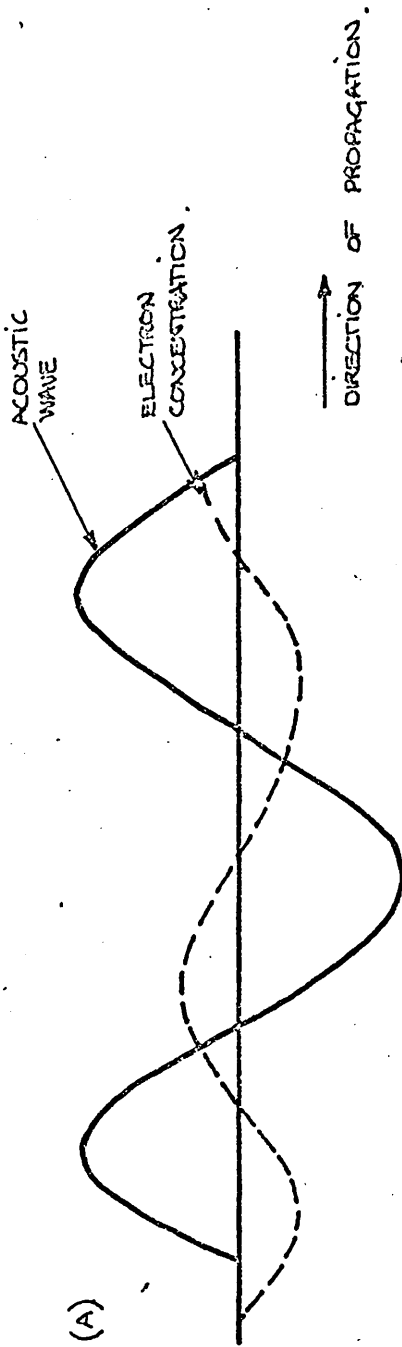
2.2 Physical basis of deformation potential interactions

A current carrier moving in a semiconductor experiences a potential resulting from the combined effects of the ion cores of the material and the other current carriers. This potential may be calculated self consistently by the Hartree-Fock method WILSON (1953). The effect of an acoustic wave propagating through a semiconductor is to periodically displace the atoms from their equilibrium positions. This distortion will cause a periodic perturbation of the potential experienced by a current carrier. This variation in the carrier potential can be described in terms of a perturbation in its Hamiltonian ($\hat{H} = T + V$). This change in the Hamiltonian will result in a change in its eigenvalues, i.e. the carrier energy levels.

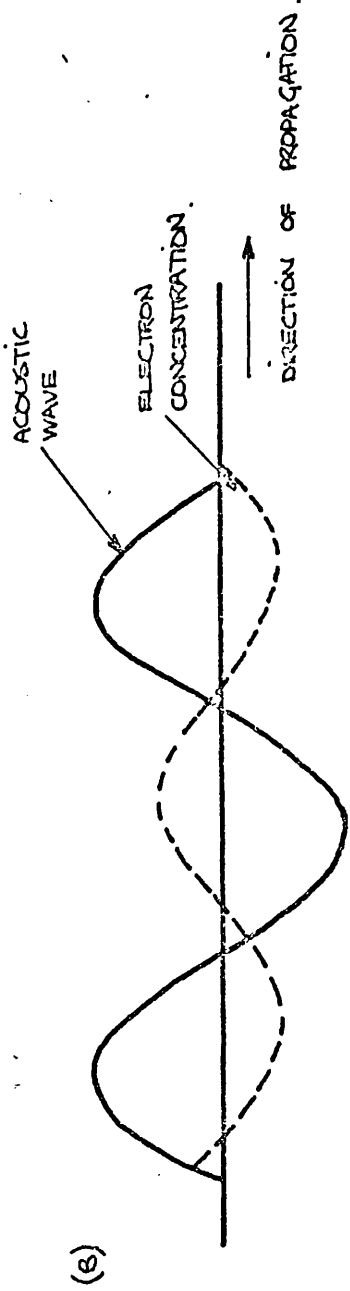
It may be shown (BARDEEN & SHOCKLEY (1950), WHITFIELD (1961)) that the influence of an acoustic wave on the energy of a current carrier may be expressed simply when the acoustic wavelength is long compared to the interatomic spacing of the material and the

carrier energy is low. In such a case it is found that the change in the carrier energy is proportional to the deformation or strain, for small strains. The assumptions of long wavelength, low energy and small strain, will always be justified in the present work. The constant of proportionality in the above relation is called the deformation potential. The gradient of the acoustically induced change in the potential of the carrier is equivalent to a periodically varying field in the direction of acoustic propagation. Thus it can be seen that the acoustic wave will tend to drive carriers through the crystal.

The ratio of the energy relaxation time of the carriers to the period of the acoustic wave has a very marked influence on the strength of the wave-carrier interaction. Consider the travelling periodic potential set up by an acoustic wave propagating through an n-type germanium crystal. The conduction electrons will tend to accumulate at the minima of the potential, in an attempt to reduce the internal energy of the crystal. If the energy relaxation time of the electrons is short compared to the period of the acoustic wave, they will attain an almost exact equilibrium and the electron density at any point will oscillate with the acoustic wave. At the other extreme, if the relaxation time is long compared to the acoustic period the electrons will be almost unaffected by the wave, and electron concentration will remain virtually uniform. In both cases the average net force on the electrons caused by the wave will be very small. However, in the case where the relaxation time is of the same order as the period of the wave, the electrons are affected by the wave



ASSESSMENT OF DRIFT FIELD - ACOUSTIC ATTENUATION.



DRIFT FIELD SUCH THAT $v_d > v_s$ - ACOUSTIC AMPLIFICATION.

Figure(2.1) WAVE - PARTICLE DRAG

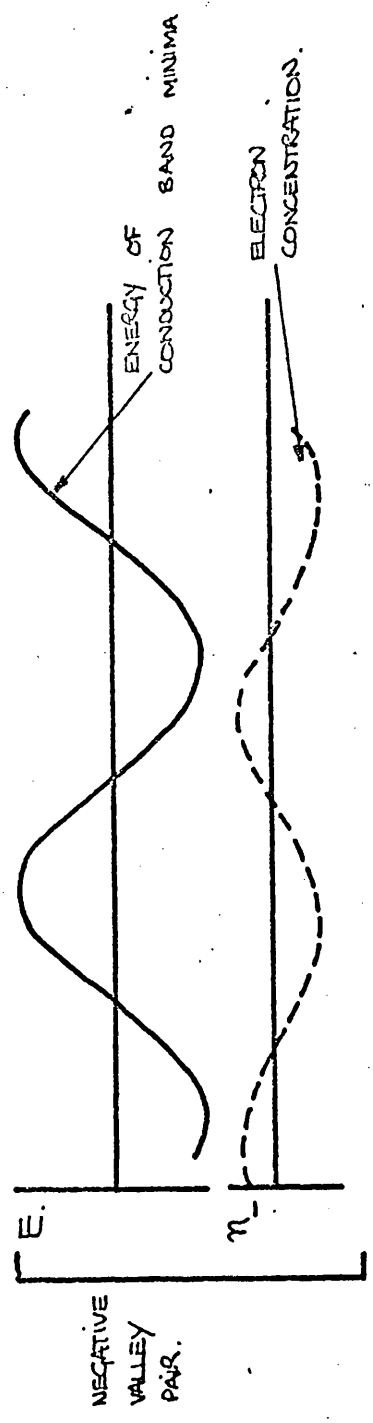
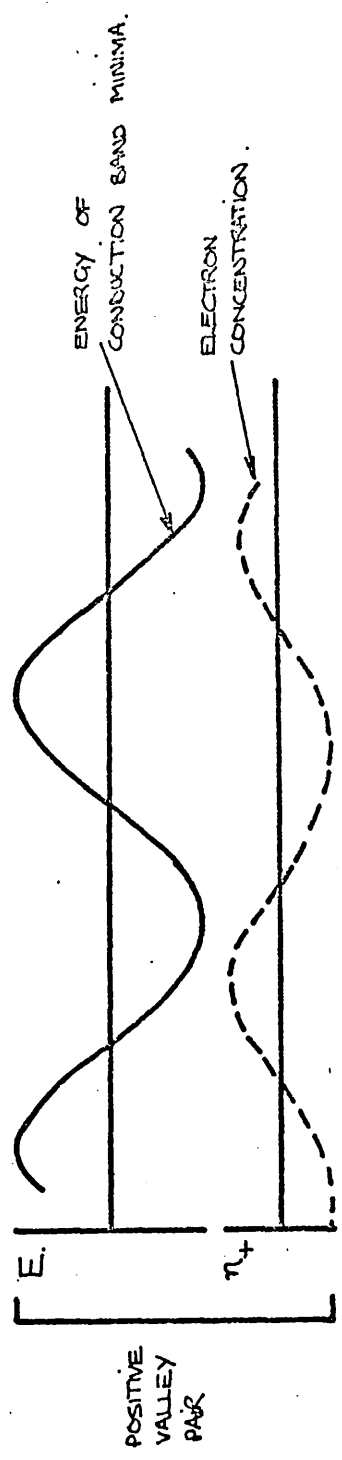
It is obvious from the previous discussion that the existence of non-uniform electron concentrations is essential to the attainment of acoustic amplification. However, the accumulation of such electron bunches would violate local charge neutrality, so that fields would be set up which would tend to disperse the electron bunches. This would result in a decrease in the acoustic amplification.

WEINREICH, SANDERS & WHITE (1959) have pointed out that this 'debunching' effect can in some circumstances be avoided. In semiconductors like germanium, with a multi-valley conduction band; certain acoustic waves destroy the degeneracy of the equivalent valleys (here the term degeneracy is used in its quantum mechanical sense, not as in Chapter 3). That is the effect of the acoustic wave on the Band structure of germanium, is to increase the energy of one or more of the four valleys and to decrease the energy of the others. This non-equivalent valley movement may be accompanied by a common energy shift of all the valleys. The effect of strain on the band structure of a multi-valley semiconductor is considered in detail by KEYES (1960). In certain directions of high symmetry, an appropriate acoustic wave divides the valleys into two pairs. The energy of one pair is increased by the strain and the energy of other decreased by the same amount. Such strains result in germanium in the following cases. Firstly from the propagation of a shear wave along a $\langle 100 \rangle$ direction and polarised in $\langle 010 \rangle$ direction. Secondly, from the propagation of a longitudinal wave along a $\langle 110 \rangle$ direction. These are the two waves of principal concern in this work. If such a wave propagates through an n-type germanium crystal

the electrons will tend to bunch on the forward slope of the wave in each individual valley. However, the relative energy shifts of the valley pairs is equal and opposite under the influence of a constant strain. Thus in the presence of an appropriate acoustic wave the energy shift of the different valley pairs will be in antiphase. Therefore the spacial distribution of the total electron concentration will be uniform, and no space charge fields will be set up. The above argument is illustrated in Figure 2.2. There is of course a net force on the electrons in each valley caused by the acoustic wave, and consequently a total net force on all the electrons.

The effectiveness of this method of eliminating debunching has been demonstrated experimentally by POMERANTZ, KEYES AND SEIDEN (1962). They propagated five acoustic modes in both lightly and heavily doped n-type germanium, at a frequency of 8.9 GHz at 4.2°K. All the modes propagated without significant attenuation in the lightly doped material. However, in the heavily doped material, those modes having an elastic constant (ρv_s^2) containing the coefficient C_{44} were strongly attenuated. In germanium, the modes for which the elastic constant contains C_{44} , are those which produce shear strains that remove the degeneracy of the valleys KEYES (1961). The lifting on the degeneracy of the valleys by the acoustic wave permits bunching without producing space charge, for sufficiently symmetrical directions. This leads in heavily doped material to substantial wave-particle drag and consequent attenuation of the acoustic wave. Those modes where the elastic constant does not contain C_{44} do not remove the valley degeneracy. Therefore any bunching is strongly opposed by mutual repulsion of the electrons, and no significant wave-particle drag or consequent acoustic attenuation results.

→ DIRECTION OF ACOUSTIC PROPAGATION.



Figure(2.2) SPACE CHARGE CANCELLATION IN A MULTI-VALLEY SEMICONDUCTOR.

It is interesting to note that in n-type silicon, as a result of the difference in the number and orientation of the valleys, the elastic coefficient which is sensitive to the electron concentration is different. In n-type silicon the coefficient, the presence of which in the elastic constant results in the corresponding acoustic wave lifting the degeneracy of the valleys is $\frac{1}{2}(C_{11} - C_{12})$ not C_{44} CSAVINSKY & EINSBRUCH (1963).

2.3 Calculation of the gain of a deformation potential amplifier

The theoretical methods of treating deformation potential amplification can be divided into two classes, depending whether the diffusion-mobility approximation is used or the relevant Boltzmann equation is solved. The first method is an extension of the work of WEINREICH (1957), WEINREICH, SANDERS & WHITE (1959) and GUREVICH & EFROS (1963) on acoustic attenuation in semiconductors. A treatment based on this method is given in the present work. No previous account appears to have been published, although POMERANTZ (1964) quotes an expression for the amplification in the case of a particular acoustic mode, obtained using this method. The papers using a Boltzmann equation treatment can be divided into two groups. The first SPECTOR (1962)(1965) ECKSTEIN (1963), employs an extension of a method developed to treat the problem of acoustic attenuation in metals. The second is due to GANTSEVICH & GUREVICH (1967) (1969a) (1969b). In the two groups of papers using methods based on a Boltzmann equation different results for the gain of a deformation potential amplifier are obtained. In the first group of papers

the effect of electron heating on the gain is not included. This omission leads to a serious overestimate of the gain under the experimental conditions described in Chapter 4. A less serious objection to the first group of papers is that they assume degenerate statistics for the electrons, whereas it is shown in Chapter 3 that under the experimental conditions of interest this assumption is not valid. The papers of Gantsevich and Gurevich take account of both of these points.

The Boltzmann equation approach is valid for all acoustic frequencies, whereas the diffusion-mobility approach is only valid when $\omega\tau \ll 1$ (where ω relates to the acoustic wave and τ is the electron momentum relaxation time). The value of τ can be obtained from the measured values of mobility (μ) given in Chapter 3, by using the approximate relation $\mu = \frac{e}{m^*} \tau$ (where e is the electronic charge and m^* is the effective mass of the electron). The amplifier experiments were conducted at a frequency of 9 GHz. Thus the corresponding value of $\omega\tau$ is less than 0.1. The approximation would therefore appear to be valid. An account is given below of the derivation of an expression for the gain of a deformation potential amplifier. The derivation makes use of the diffusion-mobility approximation.

Consider an n-type germanium crystal, to which an electric field (E) is applied along the direction in which an acoustic wave is propagating. The acoustic wave is assumed to be one of the waves discussed previously, which lift the degeneracy of the valleys. Thus space charge effects may be neglected.

The particle current density can be expressed as the sum of three terms; the drift caused by the electric field, the diffusion resulting from the bunching of carriers and the wave particle drag.

$$j_{\pm} = \underbrace{n_{\pm}\mu E}_{\text{DRIFT}} - D \left[\underbrace{\frac{\partial n_{\pm}}{\partial x}}_{\text{DIFFUSION}} \pm \underbrace{\frac{q_{\pm} n_{\pm}}{k_{\pm}} \cdot \frac{\partial \Phi}{\partial x}}_{\text{DRAG}} \right] \quad (2.1)$$

Where the suffices \pm refer to the different valley pairs, j_{\pm} represents the flux of particles rather than the conventional current density, μ is the mobility, D the diffusion coefficient, Φ^2 is the acoustic energy density and q_{\pm} the acoustic charge.

q_{\pm} is defined so that $\delta v_i = q_i \Phi$ where δv_i is the charge in energy of the i^{th} valley caused by the wave. From this definition and that of the deformation potential given previously, it can be seen that the two are related by an expression of the form $q_i = E_i / \sqrt{c}$; where E_i is the deformation potential of the i^{th} valley and c is the relevant elastic constant.

The principle of the conservation of particles can be written in the form

$$\frac{\partial n_{\pm}}{\partial t} + \frac{\partial j_{\pm}}{\partial x} = \pm R \quad (2.2)$$

where R is the intervalley scattering rate / unit volume.

During the measurements the amplitude of the acoustic wave was such that $q_{\pm} \Phi \ll k_B T$. It will be shown in Chapter 3 that the electron concentration was small enough to justify the use of Maxwell-Boltzmann statistics.

If a constant stress were applied to the specimen, then the electron distribution would relax until the concentrations in the valley pairs were given by

$$n = n_0 \left(1 \mp \frac{q\bar{\Phi}}{k_B T} \right) \quad (2.3)$$

where n_0 is the value of n_+ or n_- in an undeformed crystal.

The intervalley transfer rate is controlled by the amount by which the instantaneous difference in concentrations ($n_+ - n_-$) differs from the equilibrium (or constant strain) difference ($-2n_0 q\bar{\Phi}/k_B T$).

$$\text{i.e. } R = -\frac{2}{3\tau_{ix}} \left[(n_+ - n_-) + 2n_0 \frac{q\bar{\Phi}}{k_B T} \right] \quad (2.4)$$

where τ_{ix} is the intervalley relaxation time. The factor $2/3$ is included to take account of the fact that only two intervalley transitions in three are between valleys of different pair.

Assuming a sinusoidal acoustic wave

$$n_{\pm} = n_0 + n'_{\pm} e^{i(kx - \omega t)} \quad (2.5)$$

where $n_0 \gg n'_{\pm}$ as $\frac{q\bar{\Phi}}{k_B T} \ll 1$

i.e. this treatment is a linear one.

On substituting from equation (2.5) into equation (2.1), and from equations (2.5) and (2.4) into equation (2.2), and dropping terms in $(n'_{\pm})^2$; two equations in n'_{\pm} are obtained.

Eliminating j_{\pm} between them yields

$$n_{\pm}' = \pm n_0 \left[\frac{q\Phi_0}{k_B T} \cdot \frac{1}{1 + i\omega\tau_R(1-\beta)} \right] \quad (2.6)$$

where $\Phi = \Phi_0 e^{i(kx - \omega t)}$

and the following substitutions have been made,

$$\frac{1}{\tau_R} = k^2 D + \frac{4}{3\tau_{iv}} \quad (2.7)$$

(i.e. the distribution may relax both by intervalley scattering and diffusion)

and $\beta = \frac{\mu E}{v_s}$

where v_s is the velocity of sound.

Substituting from equation (2.6) into equation (2.5), the expression for n_{\pm} becomes

$$n_{\pm} = n_0 \left[1 \pm \frac{q\Phi_0}{k_B T} A e^{i(kx - \omega t)} \right] \quad (2.8)$$

where $A = \frac{1}{1 + i\omega\tau_R(1-\beta)}$

Substituting from equation (2.8) into equation (2.1), the expression for j_{\pm} becomes

$$j_{\pm} = n_0 \left[1 \pm \frac{q\Phi_0}{k_B T} A e^{i(kx - \omega t)} \right] \left[\mu E - ik \right] \frac{q\Phi_0}{k_B T} e^{i(kx - \omega t)} \quad (2.9)$$

The acousto electric current density is the time average of this instantaneous current density over the period of the acoustic wave, less the component arising from drift caused by the applied field.

$$\text{i.e. } \bar{j}_{ac.} = \langle \text{Re}(j_{\pm} - j_{drift}) \rangle \quad (2.10)$$

where $\langle \dots \rangle$ represents the average over a period of the acoustic wave.

The factor 2 is included to account for the contribution from both valley pairs.

Substituting from equation (2.9) into equation (2.10), and performing the relevant operations yields

$$\bar{J}_{ae} = \frac{n_0 D}{v_s} \left(\frac{q \Phi_0}{k_B T} \right)^2 \frac{\omega^2 \tau_R (1-\beta)}{1 + \omega^2 \tau_R^2 (1-\beta)^2} \quad (2.11)$$

But WEINREICH (1957) has shown that the acoustic attenuation coefficient (Γ) and the acousto-electric field (E_{ae}) are related as follows:

$$\Gamma = \frac{ne v_s E_{ae}}{S} \quad (2.12)$$

where S is the acoustic power density.

The validity of this expression when an electric field is applied to the semiconductor has been questioned. However, ECKSTEIN (1964) has carefully investigated the situation and finds its use justified. As Φ^2 is the acoustic energy density, it follows that it is related to the acoustic power density by the expression

$$S = v_s \langle \Phi^2 \rangle = \frac{1}{2} v_s \Phi_0^2 \quad (2.13)$$

where $\langle \Phi^2 \rangle$ represents the average of Φ^2 taken over a period of the wave.

From equations (2.12) and (2.13)

$$\Gamma = \frac{2ne E_{ae}}{\Phi_0^2} \quad (2.14)$$

but from the definitions of current and mobility

$$\bar{J}_{ae} = n\mu E_{ae} \quad (2.15)$$

Thus from equations (2.14) and (2.15)

$$\Gamma = \frac{2e\bar{J}_{ae}}{\mu\bar{\Phi}_0^2} \quad (2.16)$$

Substituting in equation (2.16) from equation (2.11) yields

$$\Gamma = \frac{ne\bar{d}}{\mu\nu_s} \left(\frac{q}{k_B T}\right)^2 \frac{\omega^2 r_R (1-\beta)}{1 + \omega^2 r_R^2 (1-\beta)^2} \quad (2.17)$$

where use has been made of the fact that $n = 2n_0$.

If $\beta > 1$ i.e. $\mu E > \nu_s$, then the value of Γ is negative, i.e. gain occurs. This result is in agreement with the qualitative conclusion reached in Section (2.1).

Equation (2.17) is a general expression, for the two modes of particular interest the following substitutions can be made.

	$\rho\nu_s^2$	<u>Acoustic Charge</u>
Shear wave along $\langle 100 \rangle$ polarised in $\langle 010 \rangle$ C_{44}		$\frac{E_u}{C_{44}}$
Longitudinal wave along $\langle 110 \rangle$	$\frac{1}{2}(C_{11} + C_{12} + 2C_{44})$	$\frac{E_d + \frac{1}{3}E_u}{\sqrt{\frac{1}{2}(C_{11} + C_{12} + 2C_{44})}}$

The expressions for the acoustic charge are taken from the work of HERRING & VOGT (1956). Where E_d and E_u are the deformation potentials as defined by Herring & Vogt.

Using these expressions together with the Einstein relation

$$d = \frac{k_B T}{e} \mu$$

equation (2.17) becomes for a shear wave propagating along a $\langle 100 \rangle$ direction and polarised in $\langle 010 \rangle$ direction.

$$\Gamma = \frac{n}{9v_s^3 \rho k_B T} \cdot E_u^2 \frac{\omega^2 \tau_c (1-\beta)}{1 + \omega^2 \tau_c^2 (1-\beta)^2} \quad (2.18)$$

and for the longitudinal wave propagating along a $\langle 110 \rangle$ direction

$$\Gamma = \frac{n}{v_s^3 \rho k_B T} \left(E_L + \frac{1}{3} E_u \right)^2 \frac{\omega^2 \tau_c (1-\beta)}{1 + \omega^2 \tau_c^2 (1-\beta)^2} \quad (2.19)$$

The above derivation neglects the possibility of 'electron heating' by the applied field. This effect which is described in section (3.7), is found to be very marked under the conditions of the present experiments. It leads to a decrease in the gains predicted by a factor of more than ten as compared to equations (2.18) and (2.19). Thus it was considered essential to carry out a series of measurements to determine the electron temperatures. A description of these measurements and their interpretation is given in Chapter 3. The effect of electron heating on the performance of the deformation potential amplifier is considered in Chapter 4.

Chapter 3. HOT ELECTRON HALL MEASUREMENTS

3.1 Introduction

It will be seen in Chapter 4 that the electron temperature has a very significant influence on the gain of a deformation potential amplifier. Thus it is of considerable importance to determine this temperature as accurately as possible, in order to assess the device potential of the amplifier and to compare experimental results with theoretical predictions.

Because of its nature, it is not possible to measure the electron temperature directly. The basis of the method used in its determination was a comparison of the measured hot electron or high field Hall mobility with an expression given by MANSFIELD (1956), for the ionised impurity limited mobility. In this theoretical expression the only unknown parameters were the electron concentration, which was determined from the Hall coefficient measurements; and the electron temperature. It should be pointed out that this method could only be used because the mobility was controlled by two similar carrier momentum relaxation processes, so that the ionised impurity limited contribution to the measured mobility could be isolated.

In addition to the electron temperature, two other quantities which depend on the particular specimen appear in the expression for the gain of a deformation potential amplifier. These quantities are the electron concentration and the electron mobility.

The values of both of these quantities can be obtained from the hot electron Hall measurements.

The layout of the chapter is outlined below. Section (3.2) is a brief introduction to the Hall effect. The apparatus used in the measurements is described in Section (3.3). Particular attention is paid to the thermometer. The method of preparing the dumb-bell shaped specimens is described in Section (3.4); the necessity for chemical cleanliness being emphasised. Various aspects of the methods of measurement are discussed in Section (3.5). The properties of the contacts made to the specimens were investigated with special care. The experimental results are presented in Section (3.6), and an explanation of the unexpected shape of the Hall mobility against electric field curves is advanced. The electron temperature approximation is shown in Section (3.7) to be valid in the present case. The same section contains the calculations of electron temperature. Various possible objections to the method of calculation are considered, but are not found to be justified.

3.2 The Hall Effect

If an electric and a weak magnetic field are orthogonally applied to an isothermal conductor, an electric field appears at right angles to both. This effect is called the Hall effect after its' discoverer (HALL (1879)). The origin of this Hall field has been discussed by many authors including PUTLEY (1960).

A Hall coefficient may be defined by the relation,

$$E_H = R_H B j. \quad (3.1)$$

Where R_H is the Hall coefficient, E_H the Hall field, B the magnetic induction and j the current density.

Numerous theoretical treatments of the Hall effect have been given for a wide range of conditions. That given by PAIGE (1964) is in a form suitable for the case of germanium. The most important results of these treatments are those which relate the Hall coefficient to the carrier concentration and the carrier mobility. These relations have well known forms.

$$\text{Firstly} \quad |R_H| = \frac{\alpha}{ne}. \quad (3.2)$$

Where α is dimensionless and depends on the energy distribution of the carriers and the band structure. The value of α can only rarely be obtained analytically, however it appears to lie between 1 and 2 in all conditions.

$$\text{And secondly} \quad \mu = |R_H| \sigma \quad (3.3)$$

Where σ is the conductivity. This mobility is called the Hall mobility and is equal to α times the drift mobility.

3.3 Apparatus

The cryostat used in the Hall measurements employed a conventional pair of glass dewars, the outer for liquid nitrogen

and the inner for liquid helium. At the bottom of each of these was a narrower 'tail' section so that they could be accommodated between the polefaces of an electromagnet. Inside the glass dewars was a metal dewar which was used to control the specimen temperature. This metal dewar is sketched in Figure (3.1). It consisted of a pair of concentric cylindrical metal cans. The upper sections of these cans were of thin walled, stainless steel tube, to reduce the heat leak from the top of the assembly. The lower sections were of brass tube 0.020 inches thick, which formed an approximately isothermal enclosure. The space between the cans and that inside the inner can, could be separately pumped through standard vacuum connectors. A heater coil was bifilar wound on the brass section of the inner can. In order to reduce the possibility of 50 Hz pick-up in the measuring circuit, a d.c. supply was provided for the heater coil.

The method of operating the cryostat was to pump out both metal cans, and then refill them with helium gas from a cylinder. The apparatus was then filled with liquid helium, and the specimen temperature checked. The method of filling the apparatus with liquid helium was the standard one described by WHITE (1961). A series of measurements were then carried out at 4.2°K . If measurements were to be made at a higher temperature the space between the metal cans was pumped with a diffusion pump. The pump reduced the pressure in the space between the cans to about

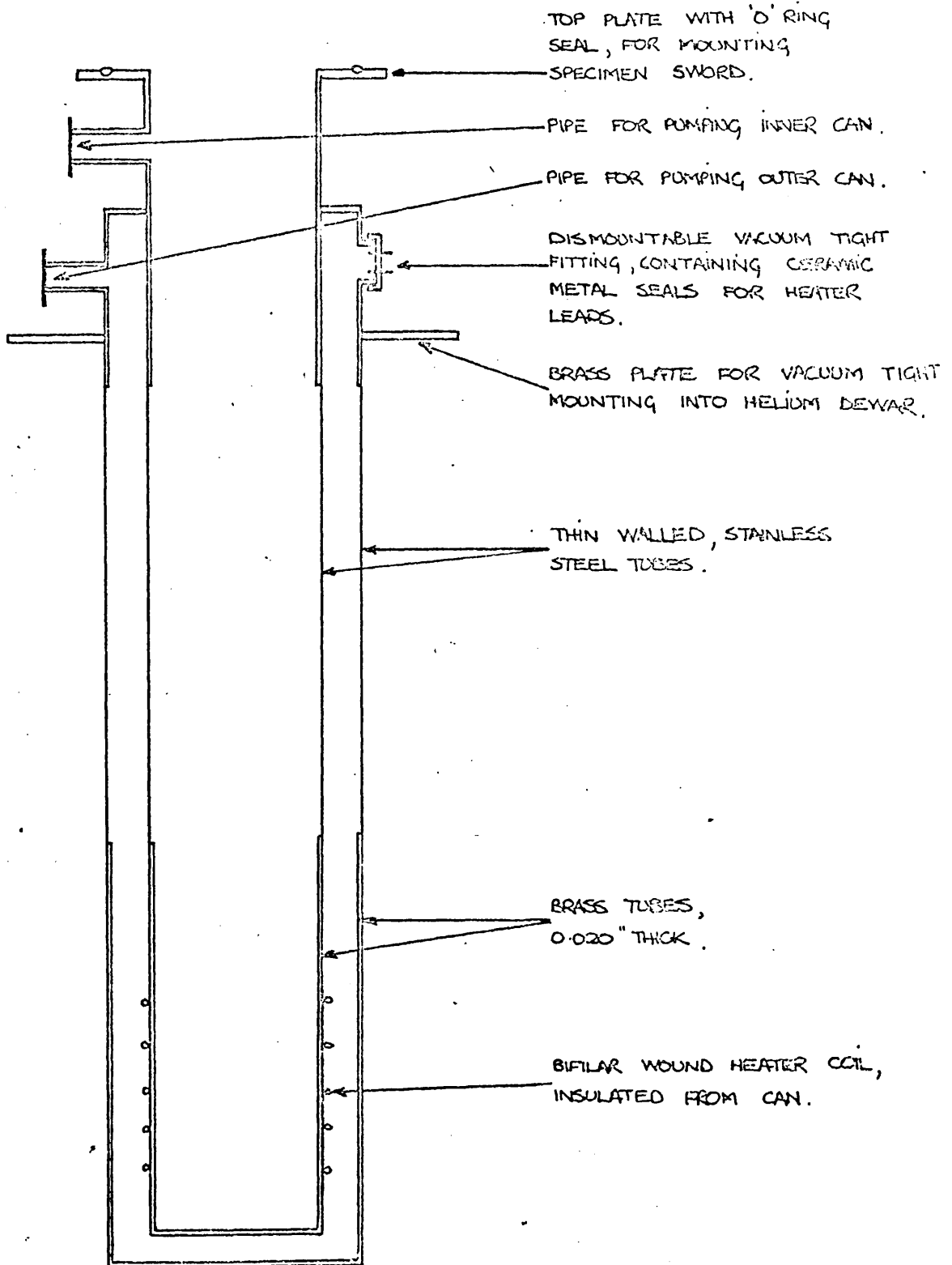


Figure (3.1) TEMPERATURE CONTROL ARRANGEMENT FOR HALL APPARATUS.

10^{-4} torr a lower pressure would have resulted in the heat flow from the top of the cryostat significantly heating the specimen. The temperature was controlled by passing a small current through the heater coil, so that the heating effect of this current just balanced the heat leak across the space between the cans at the required temperature. The temperature was indicated by a platinum resistance thermometer placed close to the specimen. The required temperature was maintained by making small manual corrections to the heater current.

The assembly or sword on which the specimen was mounted, fitted into the metal dewar with a vacuum tight seal at the top. This sword is illustrated in Figure (3.2). The specimen was attached by fine gold wires to six solder pins set into a P.T.F.E. plate. Also attached to the plate was the platinum resistance thermometer, which was placed as close as possible to the specimen. A removable cap was fitted over the specimen and thermometer to protect them while the sword was inserted into the metal dewar. The P.T.F.E. plate was attached to a brass top plate by a coaxial line. This line which transmitted the current pulse to the specimen; consisted of two concentric, thin walled, stainless steel tubes, separated by P.T.F.E. The dimensions were chosen to give a characteristic impedance of 50 ohms. The PTFE dielectric was required to prevent the breakdown of the line by the applied voltage pulse, which was found to occur when it was absent. The

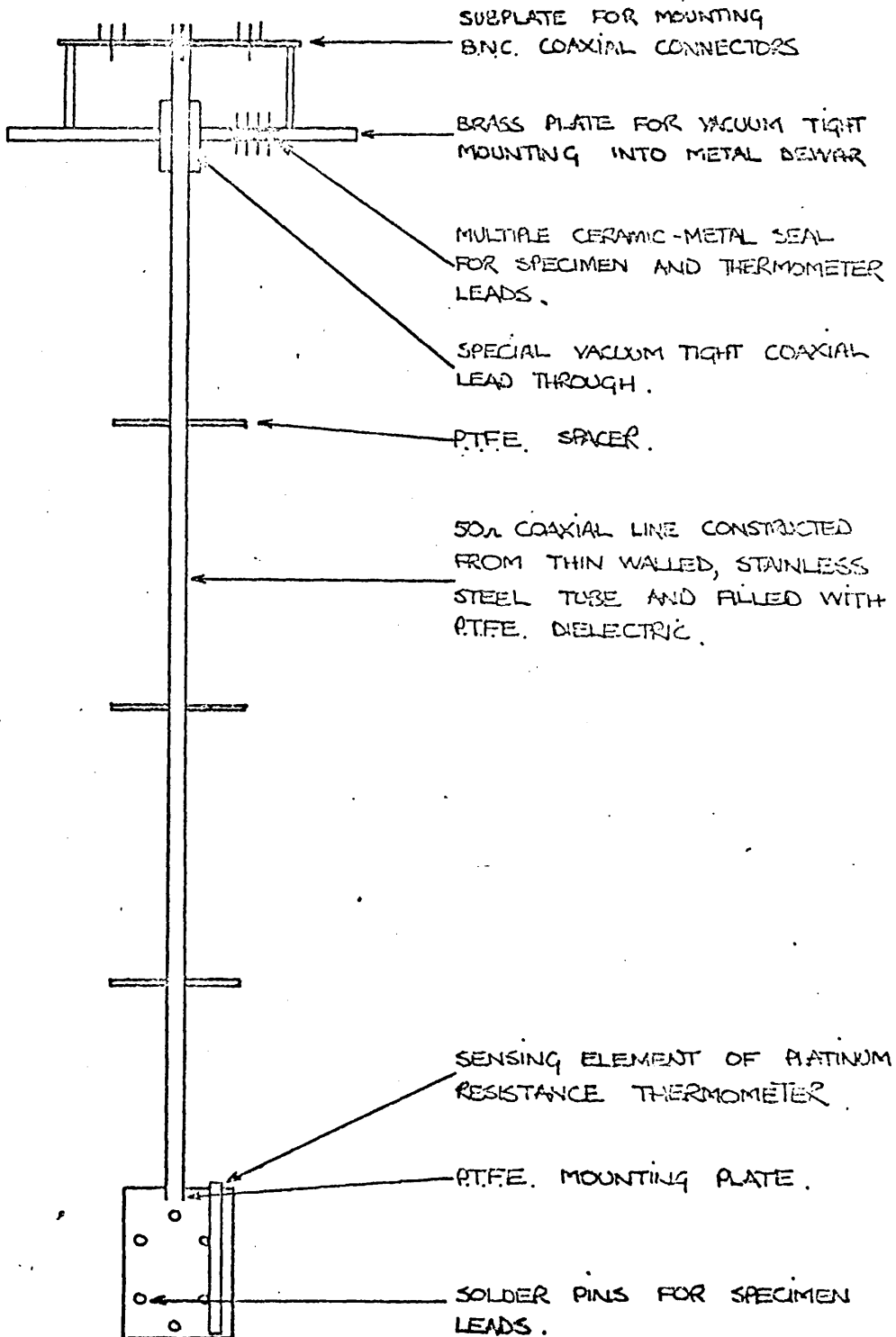


Figure (3.2) HALL APPARATUS SPECIMEN SWORD

coaxial line was connected to solder pins 1 and 6. (See Figure (3.3)). The pins 2 to 5 and the four leads of the resistance thermometer, were connected to the top plate by lengths of 40 s.w.g. 'Eureka' wire. These leads were separated from each other and the coaxial line, by a series of PTFE spacers attached to the coaxial line. The leads passed through the top plate via ceramic-metal vacuum tight lead throughs. A special vacuum tight lead through was devised for the coaxial line. Connection to the external circuits was made by way of nine B.N.C. coaxial connectors mounted on a sub-plate above the top plate.

The coaxial line was not principally used as a transmission line, because the length of the line was about $\frac{1}{30}$ th of the wavelength of the highest significant frequency in the Fourier synthesis of the applied pulse. As a result matching resistors could be satisfactorily placed at the top of the cryostat, rather than close to the specimen inside the cryostat. The main reason for the coaxial nature of this line was that this geometry served to severely limit pickup. The potentially troublesome pickup was that on the leads from the potentiometric specimen contacts, caused by the current pulse applied to contacts 1 and 6. The magnitude of this pickup was checked by soldering a 10 ohm resistor between solder pins 1 and 6, and applying a 100 volt pulse. The pickup voltage observed across a 10 ohm resistor soldered between solder pins 2 and 3,

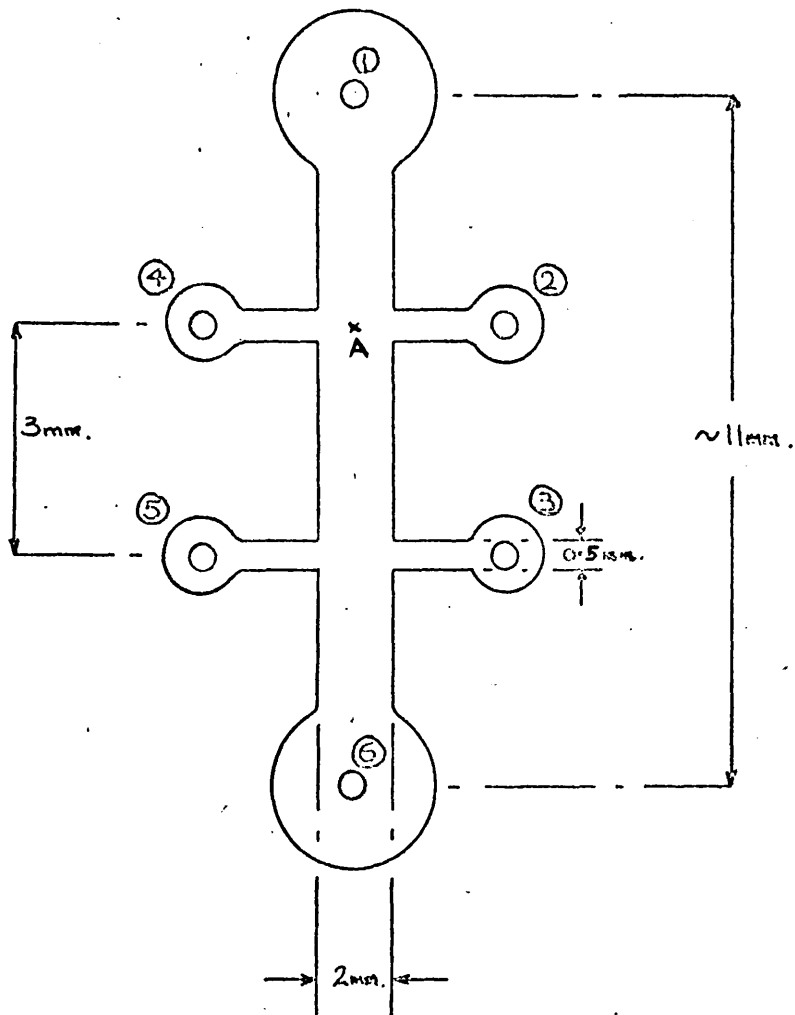


Figure (3.3) DUMB-BELL SHAPED HALL SPECIMEN.

was about 10 millivolts. As the smallest voltage measured during any run was greater than one volt, this pickup was neglected.

Although the number of high field Hall measurements made at temperatures other than 4.2°K was small, it is convenient at this point to discuss the thermometer used. The subject of temperature measurement is discussed further in Chapter 6, in connection with the low temperature acoustic attenuation measurements. In these measurements the accuracy of the measurement of temperature was of great importance.

A number of possible types of thermometer were considered. A platinum resistance thermometer was chosen. BARBER (1955) has shown that measurements can be made with a platinum resistance thermometer to an accuracy of $\pm 0.001^{\circ}\text{K}$ at 20°K , provided the sensing element is constructed of sufficiently pure platinum wire mounted in a strain free manner. In the same investigation it was shown that the long-term stability of such sensing elements is very good.

The elements used were of the type E.109 made by the Rosemont Engineering Company. These elements are mounted in a strain free manner. The calibration of the elements was carried out by the manufacturer using standards traceable to those of the U.S.A. National Bureau of Standards. The interpolation relation used was very similar to that

recommended by WHITE (1961).

The current through the sensing element was measured to an accuracy of $\pm 0.5\%$. Care was taken to ensure that the power dissipation in the element was very small. The voltage across the element was measured with a potentiometer to an accuracy of $\pm 10\mu\text{V}$. The measuring circuit made use of the normal four lead arrangement to eliminate the effect of lead resistance. This precaution was very necessary because element resistances of as low as 0.1 ohm were measured.

The sensitivity of a platinum resistance sensing element is known to decrease at temperatures below 20°K . In the same range of temperatures the resistance of a sensing element is only a small fraction of its room temperature value, so that at these temperatures a greater precision is required of the resistance measuring circuit in order to obtain the same thermometer sensitivity. The combined result of these two effects on the present work was that 15°K was the lowest temperature at which measurements could be made to an accuracy of $\pm 1\%$ or better. It was found that apart from those made at 4.2°K , no measurements were made at temperatures of less than 15°K .

Cold working of a sensing element will cause a change in its residual resistance, and thus disturb the calibration of the element at low temperatures. In order to ensure that the elements had not been cold worked as a result of mechanical

abuse, the residual resistance was checked at 4.2°K before each set of measurements.

Two pieces of electronic equipment were specifically constructed for the Hall measurements these were a reversible magnet power supply and a high current pulse generator.

The magnet power supply was a standard 6A d.c. supply, which was used in conjunction with a heavy duty reversing switch. A high power diode was connected in parallel between the power supply and reversing switch. This was incorporated to reduce the large back e.m.f. when the current through the power supply was reversed. The diode was connected so that it was reverse biased below breakdown when the supply was delivering a steady current, and thus it passed no appreciable current. However when the current through the magnet was reversed a large back e.m.f. would normally have been developed. However this e.m.f. caused the diode to become forward biased and pass current. The steady current through the magnet was measured to an accuracy of 0.5%.

The pulse generator was required to provide current pulses of about 10A in amplitude and $0.5\mu\text{sec}$ in duration, with a P.R.F. of 100 Hz. It was decided to use the delay line type circuit, with a Type 4C35 hydrogen thyatron as switch. This circuit was able to provide the required combination of a fast rise time and large pulse amplitude. All aspects of the design of this type of pulse generator have been extensively discussed

by GLASGOE and LEBACQZ (1948). A 50 ohm cable was used as the delay line. The specimen resistance was about 10 ohms so that it was necessary to use a series resistor to match the line. It was found that a flat topped pulse was not produced unless the delay cable was uniformly wound on a large drum. The rise time of the pulse was about 50n sec. An unusual feature of this particular circuit was the facility to switch the polarity of the pulse; this was achieved by switching the delay cable between the anode and cathode leads of the thyatron.

3.4 Specimen Preparation

The material on which the Hall measurements were made, and from which the deformation potential amplifier was constructed, was arsenic doped germanium. The crystals were grown by the Holboken Company using the Czochralski method. The germanium was in the form of two single crystals grown in $\langle 100 \rangle$ and $\langle 111 \rangle$ directions, each having a resistivity of approximately 0.2 ohm cm at room temperature. Four point probe resistivity measurements VALDES (1954) were made by the crystal grower at regular intervals over 10 cm lengths of the crystals. These measurements showed a resistivity variation throughout the whole length of less than 10% in both cases.

The first stage in preparing a specimen was to cut a piece of crystal about 1.5 cm in length using a diamond impregnated cutting wheel. Care was taken to ensure that the wheels were free from chips and cracks, in order to reduce

cutting damage. The piece of crystal was mounted on a goniometer and one of the cut surfaces orientated by the X-ray 'back reflection laue' technique CULLITY (1956). This was necessary as the actual growth direction of a Czochralski grown crystal is very rarely accurately parallel to the nominal growth direction (i.e. the orientation of the seed crystal). The goniometer was of a special design which permitted it to be transferred from the X-ray machine to the cutting machine without affecting the mounting of the piece of crystal. After cutting, the crystal was returned to the X-ray machine to check that the freshly cut faces had the required orientation.

A slice about 1 mm thick was then cut perpendicular to the orientated faces of the block of germanium, leaving two parallel 1 mm wide reference faces on the slice. A specimen was ultrasonically drilled from the slice using a dumb-bell shaped tool. A specially developed jig made it possible to align the axis of the dumb-bell shaped tool perpendicular to the reference faces of the slice. Thus the specimen was cut so that its axis was parallel to one of the two required crystallographic directions. The ultrasonic drilling was carried out slowly to minimise the mechanical damage to the specimen. It was found that if an attempt was made to drill through the whole thickness of a slice, it usually resulted in breaking the specimen. However if the drilling was stopped

at a point about half way through the slice, it was found to be possible to turn the slice and lap away the remaining material, leaving a complete specimen. In order to determine the point at which drilling should be stopped, the movement of the drilling head was monitored with a clock gauge.

To protect the fragile specimen during the removal of excess material from the slice, the drilled surface of the slice was waxed to a glass plate. Four additional pieces of germanium each 0.5 mm thick were waxed to each corner of the glass plate, and the whole lapped on slurries of carborundum power and water until the undrilled part of the slice had been removed. The additional pieces of germanium were used to ensure that the final specimen was of approximately constant thickness. Any serious non-uniformity in the thickness of a specimen would have made the interpretation of the measurements difficult.

After it had been removed from the glass plate, the specimen was thoroughly degreased. The specimen was then etched in the standard polishing etch C.P.4.A. (McKELVEY and LONGINI (1954)), which was prepared immediately before use on each occasion. The etching was continued until a mirror finish showing no mechanical damage was obtained. Great care was taken to ensure chemical cleanliness throughout the etching process, and as a result a good mirror finish was

obtained after each etch. Such a finish appeared to be a prerequisite of good alloyed contacts.

The material used in preparing contacts was an alloy of lead containing one atom percent of antimony. The contacts were prepared by an alloying process. The alloying tube was of high purity silica and was periodically cleaned. The gas passed through the tube during alloying was a mixture of nitrogen and hydrogen in the ratio 3 : 1. A wash-bottle containing water was placed at the end of the tube. The wash-bottle not only prevented air from being 'sucked back' into the alloying tube, but also acted as a flow meter for the gas flow. The specimen, alloying tube and alloying block, were carefully degreased before alloying. The lead alloy was cleaned with a selvite cloth to remove the film which formed on it, on exposure to air (no etch suitable for this purpose was found). Pieces of the alloy were placed on each of the six arms of the specimen, which was itself placed on the high purity graphite alloying block. The whole was then carefully placed in the tube. The temperature was measured with a platinum/platinum 13% rhodium thermocouple, the hot junction of which was inserted into a hole in the graphite block just below the specimen. The thermal e.m.f. was measured with a valve voltmeter. A small electric furnace well lagged with asbestos wool, was used to heat the specimens.

The power for the furnace was drawn from the mains and was controlled by a 'variac'. The furnace was heated to 560°C . The furnace was then switched off and it cooled to 100°C in approximately one and a half hours, at which point the specimen was removed. Throughout the alloying a slow flow of the reducing nitrogen/hydrogen mixture was maintained through the tube. The slow rate of cooling resulted in a slow rate of solidification of the germanium-lead-antimony alloy below each lead-antimony pellet. This is desirable for the formation of good recrystallised tertiary layers at each contact. There is strong evidence that the formation of such layers is essential for the production of good contacts (DALE 1966).

Fine gold wires were soldered to the alloyed pellets with indium. These wires were used to attach the specimen to the solder pins of the sword described in the previous section.

3.5 Measurement Technique

The shape of the specimens on which measurements were made is shown in Figure (3.3). Contacts 1 and 6 (see Figure (3.3)) are the current carrying contacts. The resistivity voltage would be measured between contacts 2 and 3 or 4 and 5, the Hall voltage between contacts 2 and 4 or 3 and 5.

The ratio of the distance between the current carrying contacts to their diameter was approximately 10; so that from the work of ISENBERG, RUSSEL and GREENE (1948) it can be seen that the tendency of the contacts to short out the Hall field would be negligible.

Carriers flowing between contacts 1 and 6 experience a change in the cross-section of the specimen at point A (see Figure (3.3)), which is precisely the point at which the Hall field is measured (if contacts 2 and 4 are used). This increase in the effective cross-section causes a decrease in the current density, which introduces an error into the measurement of the Hall coefficient. For this reason the width of the side arms was reduced to the minimum that could be handled without breakage. The influence of the side arms on the current density can be investigated by analogue techniques, or by the use of a conformal transformation analysis. PUTLEY (1967) has found that for the geometry of the present specimens the decrease in the current density is about 3%, which is less than the probable error caused by specimen inhomogeneity.

The Hall specimen shape is a particularly suitable one for testing contact behaviour. Good contacts are particularly important in the case of the deformation potential amplifier when current pulses of the order of 50A are passed at liquid helium temperatures. Contact phenomena may effect the performance of an amplifier in two ways. Firstly, high

resistance contacts may drop an appreciable fraction of the applied voltage, so that the voltage across the amplifying region may be less than the voltage measured between the contacts. This is particularly likely when as in the present case, the amplifier resistance is only a few ohms. Secondly injection of carriers at the contacts may lead to a change in carrier concentration in the device, and possibly to non-uniform carrier densities.

The current-voltage characteristics of two specimens were checked for low applied fields at 4.2°K . The characteristics were found to be accurately linear, and to be unchanged on reversing the direction of the applied field. At fields in excess of the impact ionisation threshold field; the resistance of the specimen was found to be independent of the direction of the applied field. The linearity of the current-voltage characteristics could not be checked at high fields, because of the non-linear electrical properties of the germanium at these fields, caused by impact ionisation and electron heating. The high field measurements were made by a pulsed method. The use of an oscilloscope reduced the precision of these measurements. The above results strongly suggest that the contacts were ohmic and non-injecting.

The ratio of the voltage between contacts 2 and 3 to the voltage between contacts 1 and 6, was checked both at high and low fields for both specimens. This ratio was found to agree well with the ratio of the distance between the side arms

to the distance between contacts 1 and 6. It was thus concluded that the resistances of contacts 1 and 6 were small compared to the total resistance between these contacts.

The first measurements were designed to check the carrier type of the material. This was done by checking the sign of the change in the voltage between contacts 2 and 4 when the magnetic field was reversed. If the direction of current flow in the specimen and the direction of the magnetic field with respect to the specimen are known, then it is possible to determine the carrier type in the manner indicated by PUTLEY (1960). The specimens were found to be n-type as expected.

Initial measurements of resistivity and Hall coefficient were made at room temperature, to check the information supplied by the crystal grower. The resistivity measurements were made in two ways, and as a result an 'electrical' value of the ratio of the distance between the side arms to the cross-sectional area of the specimen was obtained. The first method was the conventional one of measuring the current through the specimen and the voltage between contacts 2 and 3, to obtain the resistance (R) between the side arms. The distance between the side arms (l) and the width of the specimen (w) were measured with a travelling microscope, and the specimen thickness (t) with a clock gauge. With this information the resistivity was found from the relation.

$$R = \frac{\rho l}{wt}$$

(3.4)

The second method was that described by VAN DER PAUW (1958) which is applicable to laminar specimens of any shape. Using the value of resistivity given by van der Pauw's method and the value of resistance measured by the first method, the value of the ratio $\frac{1}{\omega t}$ can be found from Equation (3.4). This value of the ratio differed from that measured conventionally by about 5%, presumably because of the irregularities in the specimen shape visible under the travelling microscope. The values of resistivity were in good agreement with the four point probe measurements made by the crystal grower.

Equation (3.1) may be rewritten assuming the permeability of germanium is unity, as

$$V_H = \frac{R_H H I}{t} \quad (3.5)$$

Where V_H is the Hall voltage, H the magnetic field, I the current and t the specimen thickness. If V_H, H, I and t are measured, R_H may be found from Equation (3.5). This procedure was carried out on a specimen from each of the two crystals, and values of R_H obtained. A more significant quantity than the Hall coefficient in checking the quality of the material is the Hall mobility. This parameter can be obtained from Equation (3.3) namely

$$\mu_H = \frac{|R_H|}{\rho}$$

If as in the present case R_H and ρ are known, then μ_H can be

found. The Hall mobility for the two specimens was almost equal having the values $3,300 \text{ cm}^2/\text{V sec}$ for $\langle 100 \rangle$ specimen and $3,400 \text{ cm}^2/\text{V sec}$ for $\langle 110 \rangle$ specimen, ⁱⁿ ~~in~~ agreement with the measurements of DEBYE and CONWELL (1954).

The above description of the room temperature measurements takes no account of the various spurious voltages which may appear simultaneously with the resistivity and Hall voltages. The origin of these voltages has been discussed by PUTLEY (1960). Putley has also given the justification for the measurement procedure described below, which was adopted in order to eliminate the effects of all the spurious voltages except the Ettingshausen voltage. Under the conditions of the experiments the Ettingshausen voltages were expected to be negligibly small, and as a result were neglected. When measuring the resistivity, the voltage and current were measured; and then the direction of the current was reversed and the measurements repeated. The average values of voltage and current were used in calculating the resistivity. During the Hall coefficient measurements the directions of both the current and magnetic field were reversed. The average values of voltage and current were used in calculating the Hall coefficient.

Most of the experimental work was carried out at temperatures of 20°K or less. The measurements carried out at these temperatures were made in the same general manner as those described previously, but certain of the techniques differed from those used in the room temperature measurements. The main difference was that the low temperature measurements were made by pulsed methods.

This approach was necessary because the result of applying a field of 200 Volts/cm to the specimens would have been to dissipate 2kW in them. As a result of the small size and low specific heat of the specimens, such a power dissipation would have lead to very large increases in the specimen temperature. The pulses were of 0.5 μ sec duration with a repetition frequency of 100 Hz. The measurements were made with a dual beam oscilloscope. The Hall and resistivity voltages were measured with a differential input unit, because one of the current carrying contacts (1 and 6) was earthed through the pulse generator. Care was taken to ensure that the common mode rejection ratio of the differential unit was adequate when used with 0.5 μ sec pulses. The amplitudes of the current pulses through the specimen were measured with a current monitor which operated in a manner similar to a current transformer. The output of the current monitor and the amplitude of the applied voltage pulse could be displayed on the second beam of the oscilloscope.

The magnetic field produced by the electromagnet was initially calibrated as a function of the current through it, using a proton resonance magnetometer. The current through the magnet was measured during a run to an accuracy of 0.5%.

3.6 Results

Measurements were made on specimens with $\langle 100 \rangle$ or $\langle 110 \rangle$ axes at 4.2 $^{\circ}$ K and 20 $^{\circ}$ K. The results at the two temperatures differed by less than 5% in both cases. A further $\langle 100 \rangle$ specimen was measured, the results in this case agreed with

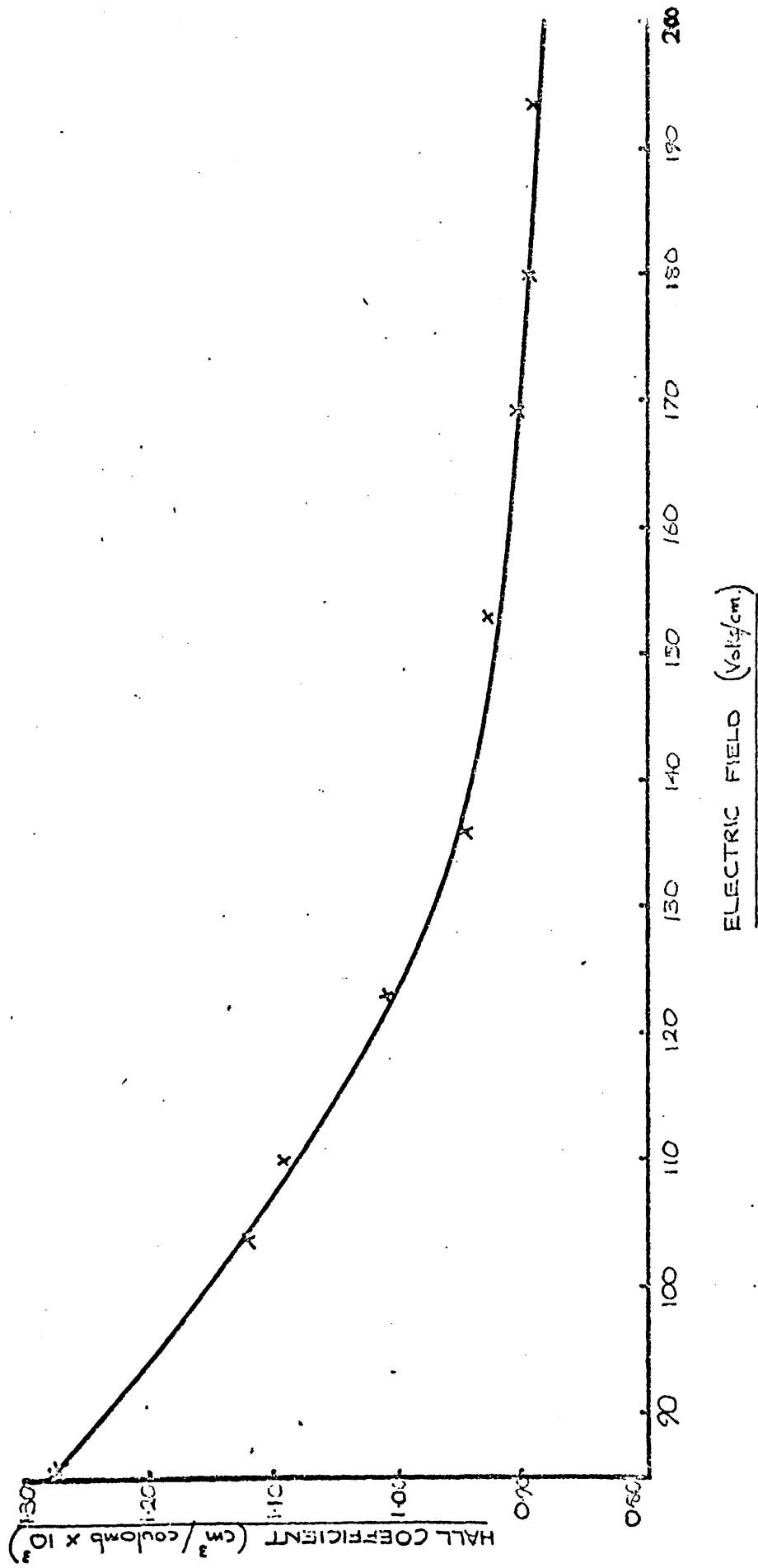
those for the first $\langle 100 \rangle$ specimen to within 5%. The results were obtained from the experimental data in the manner described in Section (3.5).

The results are plotted as a function of applied field for the initial $\langle 100 \rangle$ specimen in Figures (3.5) and (3.6), and for the $\langle 110 \rangle$ specimen in Figures (3.7) and (3.8).

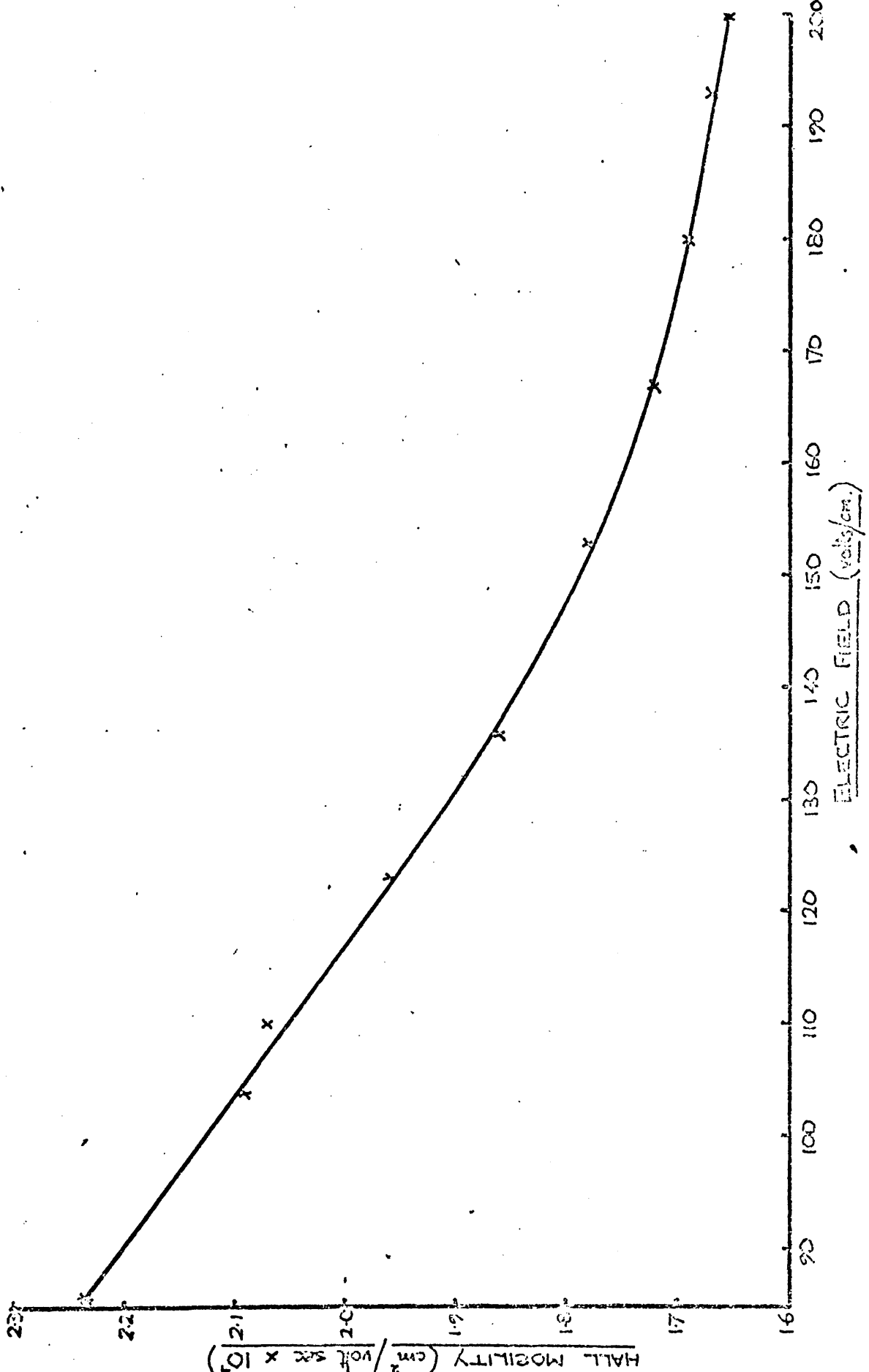
The impact ionisation breakdown field was found to be 50V/cm in the $\langle 110 \rangle$ specimen, in good agreement with the results of SCALAR and BURNSTEIN (1956). The breakdown field was rather higher in the $\langle 110 \rangle$ specimen.

The shape of the Hall coefficient against field curves show that in both cases the carrier concentration continues to rise with increasing field throughout the measured range. This residual impact ionisation appears to be nearing completion at fields about three times the breakdown field. At first sight the mobility against field curves are rather surprising. It is usual for the mobility to increase with field when ionised impurity scattering is dominant, as may reasonably be assumed in the present case. However the increasing carrier concentration with field shown in the Hall coefficient curves, means that the number of ionised impurities is also increasing with the field. This increase will result in increased scattering, and a consequent drop in the mobility. It would therefore appear that within the measured range of field, the effect of the increasing concentration of scattering centres on the mobility is greater

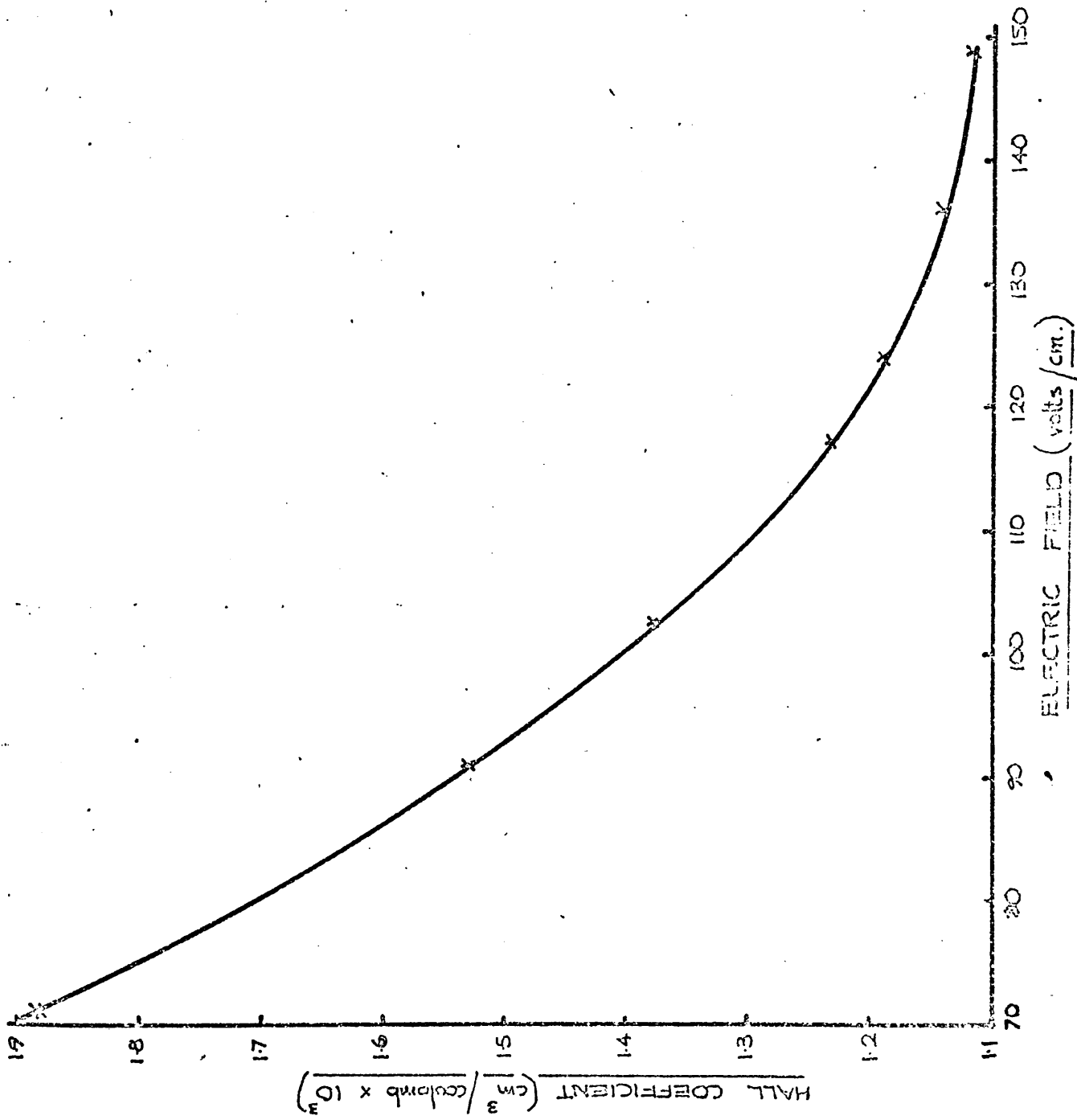
Figure(3.5) HALL COEFFICIENT AS A FUNCTION OF ELECTRIC FIELD ALONG A $\langle 100 \rangle$ DIRECTION IN GERMANIUM AT 4.2°K.



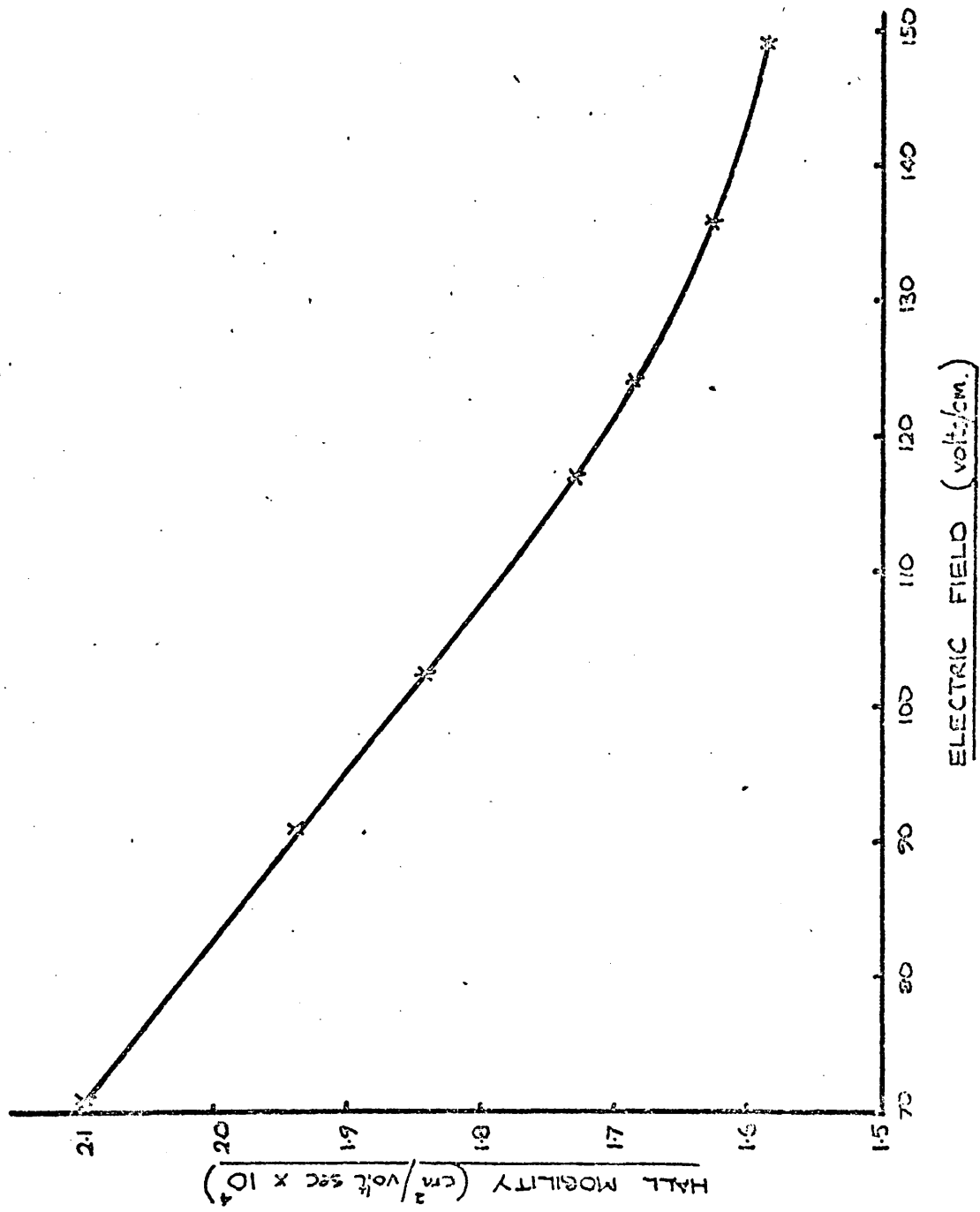
Figure(3.6) HALL MOBILITY AS A FUNCTION OF ELECTRIC FIELD ALONG A $\langle 100 \rangle$ DIRECTION IN GERMANIUM AT 4.2°K.



Figure(37) HALL COEFFICIENT AS A FUNCTION OF ELECTRIC FIELD ALONG A $\langle 110 \rangle$ DIRECTION IN GERMANIUM AT 4.2°K.



Figure(3.8) HALL MOBILITY AS A FUNCTION OF ELECTRIC FIELD ALONG A $\langle 110 \rangle$ DIRECTION IN GERMANIUM AT 4.2°K.



than the effect of the decrease in the scattering cross-section of each centre.

Measurements of the Hall mobility as a function of magnetic field were made in the range 0 to 5000 ~~gauss~~^{gauss}. No change in the mobility was observed. This experimentally verifies the prediction made on the basis of the measured mobilities of the two specimens, that a magnetic field of 2150 ~~gauss~~^{gauss} is less than the threshold field for quantum effects. The results shown in Figures (3.5) and (3.7) were obtained at a magnetic field of 2150 gauss.

3.7 Calculation of Electron Temperature

The objective of this section is to obtain estimates of the 'electron temperature' under the conditions of the experiments described in the previous sections. These estimates will be obtained from an analysis of the experimental data presented in Section (3.6).

If the current carriers in a solid receive energy from an electric field at a greater rate than they are able to lose it to the lattice, then the average carrier energy increases. However provided the applied field is less than the dielectric breakdown field a new steady state will be reached, because as the carrier energy increases the rate of loss of energy to the lattice will also increase until the carriers are gaining and losing energy at the same rate. But in this condition the average energy of the carriers is higher than it would be

if they were in thermal equilibrium with the lattice, and they are said to be 'hot'. The conditions under which the energy distribution of the carriers can be characterised by an 'electron temperature' have been considered by FRÖLICH and PARANJAPÉ (1956) and by STRATTON (1957). Physically these conditions amount to the requirement that the rate of energy interchange by electron-electron collisions should be greater than the rate of loss of energy by the electrons to the lattice. This requirement has the effect of setting a minimum electron concentration, which is a function of the experimental conditions, below which an electron temperature cannot be defined. Stratton has an expression for this minimum electron concentration. On substituting in this expression the appropriate values, the minimum electron concentration was found to be $\sim 10^9 T_e^2 / \text{cc}$ (where T_e is the electron temperature). It is shown later in this section that a typical value of the electron temperature is 50°K . Assuming this value the minimum electron concentration is $\sim 3 \times 10^{12} / \text{cc}$, which is much less than the measured concentration of $\sim 10^{16} / \text{cc}$. Thus the electron temperature approximation would seem to be valid.

Before starting to estimate the electron temperature it is desirable to determine the degree of degeneracy of the carriers under the conditions of the experiments, as this has a significant effect on the expressions used later to estimate the electron temperature. In this context the term non-

degeneracy indicates the accuracy with which the Fermi-Dirac distribution may be replaced by the Maxwell-Boltzmann one.

Assuming a Fermi-Dirac distribution of carrier energies FOWLER (1936) and a band structure in which the constant energy surfaces in k -space are spherical, it is possible to derive in a straightforward manner an expression for the carrier concentration. This expression can be written.

$$n = 4\pi \left[\frac{2m^*k_B T}{h^2} \right]^{3/2} \int_0^{\infty} \frac{\epsilon^{1/2}}{1 + \exp(\epsilon - \eta)} d\epsilon \quad (3.10)$$

Where m^* is the effective mass of a carrier and h is ~~Planck's~~ ^{Planck's} constant : ϵ and η are defined as $\epsilon = \frac{\mathcal{E}}{k_B T}$ and $\eta = \frac{\phi}{k_B T}$, where \mathcal{E} is the carrier energy and ϕ is the Fermi level or electrochemical potential. The integral is well known and is called the Fermi-Dirac integral of order one half ($F_{1/2}(\eta)$).

If instead of assuming a Fermi-Dirac distribution a Maxwell-Boltzmann one is assumed, then an expression for the carrier concentration can be derived in the same manner as that above. The expression in this case is

$$n = 4\pi \left[\frac{2m^*k_B T}{h^2} \right]^{3/2} \frac{\pi^{1/2}}{2} \exp \eta \quad (3.11)$$

In determining the conditions under which equation (3.10) may be replaced by Equation (3.11) the important factor is the ratio

$$\frac{F_{1/2}(\eta)}{\frac{\pi^{1/2}}{2} \exp \eta}$$

From the tabulated values of $F_{1/2}(\eta)$ given by McDOUGALL and STONER (1938), it is found that the ratio is 1.05 if $\eta = -2$.

Without knowing the value of the electron temperature it is not possible to estimate the degeneracy of the system. However if the assumption is made that the system is non-degenerate, it is possible to check this assumption after the electron temperature has been estimated.

Values of the electron temperature may be deduced from the Hall measurements. This may be done by comparing the experimentally determined values with a theoretical expression for the mobility which contains the electron temperature.

It is necessary to make two assumptions at the start of the calculation which will be justified later. The first is that the mobility is limited by a combination of ionised impurity scattering and electron-electron scattering. The second mentioned previously, is that non-degenerate statistics are applicable to the experimental conditions.

It will be seen later to be sufficient to determine the electron temperature for the two crystallographic directions, at a single representative value of the electric field. The

field of 120V/cm was chosen. This was the highest used in the amplifier experiment.

At this field the experimental values of Hall coefficient and mobility are listed below.

<u>Direction</u>	<u>Hall Coefficient</u>	<u>Hall Mobility</u>
$\langle 100 \rangle$	$1.0 \times 10^3 \text{ cm}^3/\text{coulomb}$	$2.0 \times 10^4 \text{ cm}^2/\text{V. sec}$
$\langle 110 \rangle$	$1.2 \times 10^3 \text{ cm}^3/\text{coulomb}$	$1.7 \times 10^4 \text{ cm}^2/\text{V. sec}$

If the value of the quantity α is known, the electron concentration can be obtained by substituting the above values of Hall coefficient into Equation (3.2). BLATT (1957a) has found the value of $\alpha = 1.65$ for the conditions under consideration. It is interesting to note that even though Blatt assumed a simple band structure, it was necessary to resort to numerical methods to obtain values of α .

The result of the substitution is

$$\langle 100 \rangle \quad n = 1.0 \times 10^{16}/\text{cc}$$

$$\langle 110 \rangle \quad n = 8.6 \times 10^{15}/\text{cc}$$

The theoretical expression for the mobility, with which the experimental values will be compared, is an expression for the drift mobility. But the Hall mobility was measured. However, the two types of mobility are related by the expression.

$$\mu_H = \alpha \mu_D.$$

When the mobility is limited by a combination of ionised impurity and electron-electron scattering, it has been shown

by McLEAN and PAIGE (1960) that the effect of electron-electron scattering is to reduce the ionised impurity limited mobility by a factor of 0.58. This result assumes that the concentrations of ionised impurities and electrons are equal, which is virtually the case when the field is 120V/cm.

Taking account of these two points the values of the ionised impurity limited drift mobility for a field of 120Volts/cm are

$$\begin{aligned} \langle 100 \rangle \quad \mu_D &= 2.1 \times 10^4 \text{ cm}^2 / \text{Volt sec.} \\ \langle 110 \rangle \quad \mu_D &= 1.8 \times 10^4 \text{ cm}^2 / \text{Volt sec.} \end{aligned}$$

An expression for the ionised impurity limited mobility for the case of non-degenerate statistics has been given by MANSFIELD (1956). The same result has been derived, by somewhat different methods, by BROOKS (1951) and DINGLE (1955).

The relevant equations from Mansfield's paper are

$$\mu = \frac{2^{7/2} \chi^2 (k_B T_e)^{3/2}}{N \pi^{3/2} (m^*)^{1/2} e^3 f(x)} \tag{3.13}$$

Where N is the concentration of ionised impurities, χ is the dielectric constant.

And
$$f(x) = \ln(1+x) - \frac{x}{1+x} \tag{3.14}$$

where
$$\chi = \frac{24\pi m^* \chi (k_B T_e)^2}{h^2 n e^2} \tag{3.15}$$

where n is the carrier concentration.

Substituting into Equation (3.15) the experimental values of carrier concentration and the values $m^* = 0.22m$ (where m is the electron mass) given by LEVINGER and FRANKL (1961) for the density of states effective mass, $\chi = 16$ given by BRIGGS (1950); the resulting values of α are

$$\begin{aligned} \langle 100 \rangle \quad \alpha &= (5.9 \times 10^{-2}) T_e^2 \\ \langle 110 \rangle \quad \alpha &= (6.9 \times 10^{-2}) T_e^2. \end{aligned}$$

Equation (3.13) becomes when the appropriate values of mobility are substituted.

$$\begin{aligned} \langle 100 \rangle \quad \ln [(5.9 \times 10^{-2}) T_e^2] - 1 &= (1.1 \times 10^{-2}) T_e^{3/2} \\ \langle 110 \rangle \quad \ln [(6.9 \times 10^{-2}) T_e^2] - 1 &= (1.3 \times 10^{-2}) T_e^{3/2} \end{aligned}$$

These equations have solutions

$$\underline{T_e = 55^\circ\text{K}} \text{ for } \langle 100 \rangle \text{ case, and } \underline{T_e = 45^\circ\text{K}} \text{ for } \langle 110 \rangle \text{ case.}$$

These electron temperatures may now be used to check the validity of the assumptions made in deriving them. The validity of the non-degeneracy approximation can be checked by substituting $T = 45^\circ\text{K}$ and $\eta = -2$ into Equation (3.12). The limiting value of electron concentration, i.e. that concentration above which a significant ($\sim 5\%$) deviation from non-degeneracy occurs, is found to be $3.5 \times 10^{16}/\text{cc}$. As the measured electron concentration was $86 \times 10^{15}/\text{cc}$, the assumption is seen to be justified for the $\langle 110 \rangle$ specimen. For the $\langle 100 \rangle$ specimen the situation is similar.

In order to justify the assumption that the dominant scattering mechanisms were a combination of ionised impurity and electron-electron scattering, it is necessary to consider the alternative mechanisms by which relaxation of the distribution of electron momentum might occur and show that their influence may be neglected.

The dislocation density, measured by an etch pit count, was $4000/\text{cm}^2$ in both crystals. Thus the effect of dislocation scattering can be neglected BARDSLEY (1960). Another mechanism involving impurities is scattering by neutral impurities, this will not be significant because the concentration of neutral impurities would be small as a result of impact ionisation. Further ERGINSOY (1950) has shown that a neutral impurity scattering cross-section is small compared with that of an ionised or charged impurity. Scattering by thermal phonons is a possible mechanism, which can take several forms. Piezoelectric lattice scattering is not possible as germanium is not piezoelectric. Optical phonon scattering may be neglected because of the very low density of these phonons, at the low lattice temperatures of the experiments, resulting from their high energies PAIGE (1964). Acoustic phonon scattering however cannot be neglected at first sight.

The method of BARDEEN and SHOCKLEY (1950) can be used to estimate the acoustic phonon limited mobility. A simple extension of this method is needed to take account of electron heating. The derivation

of the expression for the lattice limited mobility is given in the appendix to their paper. If the electron temperature (T_e) is greater than the lattice temperature (T_L), the necessary modifications are as follows. The Equation (A.29) remains the same as it refers to the phonons, namely

$$|a_k|^2 = \frac{k_B T_L}{2 M k^2 v}$$

As a result the expression for the mean free path remains the same, namely

$$\frac{1}{\ell} = \frac{(m^*)^2 E^2 k_B T_L}{\pi \hbar^4 c_{ij}}$$

But Equation (A.39) refers to the electrons and must be altered to

$$\mu = \frac{4 e \ell}{3 (2\pi m^* k_B T_e)^{1/2}}$$

Thus combining the last two equations the modified expression for the mobility is obtained as

$$\mu = \frac{2 (2\pi)^{1/2} e \hbar^4 c_{ij}}{3 (m^*)^{3/2} k_B^{3/2} T_L T_e^{1/2} E^2}$$

Where C_{ij} is the appropriate elastic constant and E is the appropriate deformation potential coefficient.

The previously determined values of electron temperature were substituted into the above expression, together with values of elastic constant taken from the work of McSKIMMIN (1953)

and of deformation potential taken from the paper of HERRING and VOGT (1956). The results were $\mu = 8 \times 10^5 \text{ cm}^2/\text{V. sec}$ for the $\langle 100 \rangle$ directions and $\mu = 9 \times 10^5 \text{ cm}^2/\text{V. sec}$ for the $\langle 110 \rangle$ directions.

These predicted values are about forty times as large as the measured ones, so that the assumption concerning the dominant scattering mechanism appears to be correct.

In deriving the expression for the ionised impurity limited mobility used above, the Born scattering approximation was employed. This was necessary in order to obtain a simple analytical result. The role of this approximation is seen more clearly in the paper by MOTT (1936), on which Mansfield's work is based. A discussion of the conditions under which this approximation is valuable has been given by SCHIFF (1955), from this it can be seen that the approximation is likely to lead to serious errors at low temperatures. The matter has been investigated by BLATT (1957b) using the partial wave approach. Analytical results are not obtained, but the numerical analysis shows that for conditions similar to those of the present experiments an error of less than 5% is introduced by the use of the Born approximation at temperatures above 40°K . The electron temperature is the relevant one in this context; thus this approximation does not lead to a significant error in the Mansfield expression, for the conditions of the experiments under discussion.

Throughout this chapter it has been assumed that the constant energy surfaces in k -space are spherical for the conduction band of germanium. In fact it is well known that, at least near the individual minima of the conduction band these surfaces are elliptical in section. The cyclotron resonance experiments of LEVINGER and FRANKL (1961) show that the ratio of the major to the minor axes of these ellipses is 19 : 1. It would therefore appear that neglecting this anisotropy by the use of a scalar effective mass would lead to gross errors. This is not the case as the momentum relaxation time is also anisotropic. HAM (1955) has estimated this anisotropy to be about 1 : 12. Thus the mobility which is a function of the ratio τ/m^* only has an anisotropy of about 1 : 1.5

A further uncertainty in these measurements is the effect of Joule heating. This can be considered in two categories. The first is the average effect over a long period. Changing the pulse repetition frequency is sufficient to test for the effects of long term heating. When the repetition rate was increased from 30/sec to 300/sec no changes in the Hall measurements were noted, so it was assumed that the effects of long term heating were negligible. The second category of heating effects is the heating during the application of a single field pulse. Because of the short pulse length this will be largely adiabatic. The influence of this type of heating is estimated below. Consider unit volume of germanium.

The rate of heating by the electric field is given by

$$\frac{\sigma E^2}{J}$$

Where σ is the electrical conductivity, and J is the mechanical equivalent of heat.

Assuming no loss of heat to the surroundings the rate of increase of temperature will be given by

$$\frac{\sigma E^2}{J} = \rho C_v \frac{dT}{dt} \quad (3.16)$$

where ρ is the density, and C_v the specific heat at constant volume. Debye has shown that at low temperatures the specific heat has the form

$$C_v = AT^3 \quad (3.17)$$

Where A is a constant for a given material. (WILSON (1953) discusses this relation.) Thus from Equations (3.16) and (3.17) the rate of change of temperature is given by

$$\frac{dT}{dt} = \frac{\sigma E^2}{\rho J A} \cdot \frac{1}{T^3},$$

thus

$$\frac{dt}{dT} = \frac{\rho J A}{\sigma E^2} \cdot T^3.$$

Integrating with respect to T yields

$$\Delta t = \frac{\rho J A}{4\sigma E^2} (T_1^4 - T_0^4) \quad (3.18)$$

Where T_0 and T_1 are the temperatures at the beginning and end of the pulse, and Δt is the pulse length.

From the experimental data of HILL and PARKINSON (1952), the value of the constant A in Equation (3.17) is found to be

$$A = 3.8 \times 10^7 \text{ cal/cm}^3 / \text{gm}(\text{°K})^3.$$

From Equation (3.18) using the measured electrical conductivity and taking the field to be 120V/cm, the following results are obtained,

$$\text{For a pulse length of } 0.5\mu\text{sec} \quad T_1 = 16^\circ\text{K}$$

$$\text{For a pulse length of } 2\mu\text{sec} \quad T_1 = 23^\circ\text{K} \text{ (This was the pulse length used in the amplifier experiment).}$$

These final temperatures are not large enough to invalidate the use of the form of Cv given in Equation (3.17). Because these final temperatures are less than the electron temperatures, the estimates of the electron temperature are unaffected. These temperatures do not reduce the predicted lattice mobilities sufficiently to effect the conclusion regarding the dominant scattering mechanism.

It has been indicated previously that the mobility of electrons in a given valley in germanium is not isotropic. A valley being that region of k-space surrounding one of the energy minima in the conduction band. It is known that the four valleys are symmetrical about the $\langle 111 \rangle$ directions (BROOKS (1955)). Therefore if an electric field is applied in an arbitrary direction, the electrons will have a different mobility in each of the valleys.

However the position is simplified in directions of high symmetry. If the field is applied in one of the $\langle 100 \rangle$ directions, then the electrons in all four valleys have the same mobility. In the case of the $\langle 110 \rangle$ directions the valleys are divided into two pairs.

The rate at which an electron gains energy from an electric field E is given by the expression $e\mu E^2$. Therefore the difference in mobility of the valley pairs when the field is applied along one of the $\langle 110 \rangle$ directions, will lead to a difference in the rate of energy gain of the electrons in the valley pairs. This in turn will lead to a difference in the electron temperatures.

In the $\langle 110 \rangle$ case, this argument appears to cast serious doubt on the assumption, on which the estimate of electron temperature was based, that the energy distribution of the carriers could be represented a Maxwellian distribution centred at a single electron temperature. However the pairs of valleys are able to exchange carriers and their energy as a result of intervalley scattering, and carrier energy by means of electron-electron scattering. So that the validity of the assumption concerning the distribution, depends on whether the rate of exchange of energy between the electrons in the different pairs of valleys is sufficiently rapid to reduce the temperature difference between them to a small fraction of the temperature of either.

The rate at which a high energy carrier loses energy to an assembly of lower energy carriers via carrier-carrier scattering, has been considered by several authors. The method of HEARN (1965) is useful in the present context.

It is first necessary to find the value of the quantity n_λ . This can be done by substituting the experimental values of electron concentration and temperature into Hearn's equation (11), namely

$$n_\lambda = \frac{9 \times 10^{-14} n_1}{\psi K T_e^2}$$

Where ψ is the ratio of the effective mass to the rest mass of an electron; and n_1 is the concentration of electrons in the cooler pair of valleys, i.e. half the total electron concentration if population transfer is neglected. WEINREICH, SANDERS and WHITE (1959) have shown that, for material of the impurity concentration used in the present measurement, the variation of intervalley scattering rate with temperature is small. Therefore the population transfer will be very small.

The result of the substitution is $n_\lambda = 0.1$

The next step is to use this value of n_λ in conjunction with a suitable value of the electron temperature difference between the valley pairs (ΔT_e), to find the rate of loss of energy by one of the electrons in the hotter valleys as a result of electron-electron collisions (W). This quantity can be obtained from Hearn's equations (3) and (4). A graphical solution of these equations is given in Figure (1) of the paper.

From this figure, for the case $n_\lambda = 0.1$, $\Delta T_e = 0.02 T_e$, it is found that $\frac{W}{kT_e} = 1.0 \times 10^{-2}$

The definition of σ is given in Equation (7) as

$$\sigma = \frac{1.3 \times 10^{-15}}{X^2 \psi^{1/2} T_e^{1/2}} ,$$

therefore

$$W = \frac{(1.0 \times 10^{-2})(1.3 \times 10^{-15}) n_1}{X^2 \psi^{1/2} T_e^{1/2}} ,$$

that is

$$W = 8 \times 10^{-5} \text{ eVgs/sec.}$$

This means that each carrier in the hotter valleys would lose energy to the carriers in the cooler valleys at the above rate as a result of electron-electron scattering, if the temperature difference was 2% of the temperature of the cooler valleys.

The rate at which a carrier gains energy from the electric field is given by $e\mu E^2$.

As was mentioned previously the maximum anisotropy in the mobility in a valley when ionised impurity scattering is dominant, is about 1.5 : 1. Let us assume that this is the ratio of the mobilities in the two pairs of valleys when an electric field is applied along one of the $\langle 110 \rangle$ directions. This assumption introduces an error, but this is not significant as it will lead to an over-estimate of the differential heating.

Thus the rate of heating of the carriers in the hotter valleys will be

$$\frac{1}{3} e\mu E^2$$

larger than the rate of gain of energy of the carriers in the cooler

valleys.

In deducing the rate of loss of energy by the hotter carriers it was assumed that $T_e = 45^\circ\text{K}$, the corresponding field is 120V/cm.

Therefore the excess heating rate of the higher mobility carriers (W') is

$$W' = 8 \times 10^{-5} \text{ ergs/sec.}$$

So that electron-electron scattering limits the ratio of the temperatures of the two valley pairs to about 1.02. Thus it is apparent that when the electric field is applied along one of the $\langle 110 \rangle$ directions the energy distribution of the electrons can be represented by a simple Maxwellian distribution to a good approximation. The above method is open to criticism in that it attempts to find an equilibrium condition without considering all the processes involved in establishing it, particularly the loss of energy by the carriers to the lattice. The point is not very important however as only an approximate estimate of the temperature ratio is needed.

In this section it has been found possible to obtain estimates of the electron temperature under the operating conditions of a deformation potential amplifier. The estimates have been made by an unusual method. The method was to compare experimental values of the electron mobility with a theoretical expression for the ionised impurity limited mobility, in which the only

undetermined parameter was the electron temperature. A critical assumption in this method was that the dominant scattering mechanisms were ionised impurity and electron-electron scattering. McLEAN and PAIGE (1960) have shown that the individual contributions to the total scattering caused by this combination of mechanisms can be separated under suitable conditions. The contributions to the total scattering arising from other mechanisms like acoustic phonon scattering have been shown to be negligible, thus justifying the assumption concerning the dominant scattering mechanisms. A number of possible objections to the method were considered. It was shown that neither the breakdown of the Born scattering approximation at low temperatures or the effect of Joule heating by the applied field, introduced a significant error. An objection peculiar to the measurements made with the applied field along a $\langle 110 \rangle$ direction was the differential heating of the electrons in different valleys arising from the anisotropy in the mobility. However it was shown that the rate of energy redistribution by electron-electron collisions was sufficiently rapid to effectively remove any temperature differences between valleys.

The results obtained in this section appear to be the first quantitative data on the electron temperature under the operating conditions of a deformation potential amplifier. Using these results it will be shown in Chapter 4 to be possible

to make quantitative predictions concerning the gain of such an amplifier. It is interesting to note that the author has not been able to discover a previous report of this method of determining electron temperature. The high field measurements are also interesting because they add to the very small number of hot electron measurements at low temperatures which have been reported.

4.1 Introduction

This chapter is concerned with experimental work on the deformation potential amplifier, and with the interpretation of this work. The organisation of the Chapter is as follows. Section (4.2) contains a description of the apparatus used and of the preparation of the germanium amplifier rods. Various aspects of both longitudinal wave and shear wave transducers are discussed in Section (4.3), in relation to their use in amplifiers. The method of measuring the gain of an amplifier is described in Section (4.4). The results obtained with longitudinal mode amplifiers are presented in Section (4.5). In section (4.6) an explanation is advanced of the direction dependence of the results presented in the previous section. Also in section (4.6) the theory of the amplifier set out in Chapter 2 is extended to take account of electron heating by the applied field. Calculations of the gain are made on the basis of this extended model, which are compared with the experimental results. Section (4.7) contains a discussion of the deformation potential amplifier as an electronic device, in the light of the work described in the rest of the chapter.

4.2 Apparatus and Amplifier rods

A microwave system was developed to measure the change in insertion loss of a deformation potential amplifier as a function of electric field. This system, operated in the frequency range 8.5 to 9.6 GHz, and is described in detail in Chapter 6 in

connection with other measurements. The amplifier experiments were conducted at a frequency of 8.9 GHz. A microwave cavity was used to excite the transducers attached to the end of the amplifier rods.

The measurements were carried out at the boiling point of helium, the amplifier being immersed in liquid helium. The drift field pulse was transmitted to the amplifier via a specially constructed coaxial line. The line consisted of thin walled stainless steel tubes with P.T.F.E. dielectric, similar to that used in the Hall apparatus sword. Stainless steel was used to reduce the heat leak from the top of the cryostat into the liquid helium.

The thyatron-delay line pulse generator used in the Hall measurements, provided the drift field pulses. For the amplifier measurements a 14Ω characteristic impedance delay cable was used. By using this low impedance delay cable, it was possible to produce the 50A pulses required without charging the delay cable to a voltage greater than 1 kV. Thus breakdown problems were avoided. The pulse duration was 2 μ S, and the repetition rate 100 per second. As with the Hall measurements, the specimen impedance ($\sim 2\Omega$) was much less than the impedance of the delay cable; so that a matching resistor was placed at the top of the cryostat.

The amplifier rods were in the form of rectangular bars of germanium, having dimensions 12 x 1.5 x 1.5 mm. The end faces of the rods were polished flat to within one tenth of a wavelength of visible light, and parallel to within about 3 seconds of arc.

The rods were cut after polishing, from pieces of crystal of larger cross-section. This was necessary as no method was found of polishing the end faces of such small cross-section rods to the required flatness and parallelism. The polishing was largely carried out in the Department, the technique has been described by BENNET & WILSON (1966). The contacts were alloyed in the manner described in Section (3.4), and were symmetrically placed on the rods about 8 mm apart. Contacts were made to three of the four sides of the rods, in the form of an incomplete ring. The main error in determining the electric field with such an arrangement of contacts probably arises from their finite width, rather than from the distortion of the lines of current flow resulting from the contacts being made to the sides of the rod. The error in the field determination arising from the latter cause is for the geometry used, of the order of 3% (BERZ (1965)).

4.3 Transducers

A transducer is needed to launch and detect an acoustic wave in germanium. Particular attention was paid to cadmium sulphide evaporated film transducers, as this was considered to be the type of transducer most likely to operate satisfactorily at 9 GHz at 4.2°K.

It has been shown to be possible to deposit crystallographically highly orientated, evaporated, cadmium sulphide films; having a predominantly hexagonal crystal structure. deKLERK & KELLY (1965) and other workers, have shown such films to have a preferred orientation with the c-axis perpendicular to the substrate.

RICHTER (1962) and GIBSON (1966) have considered the behaviour of cadmium sulphide films as transducers. They have shown that if an alternating electric field is applied to such a film, so that the direction of the field is normal to the surface of the film, then a longitudinal acoustic wave is generated.

Such films were prepared for this work both in the Department and at Standard Telecommunications Laboratories Limited. Both the direct evaporation technique described by FOSTER (1964), and the indirect method described by de KIEK & KELLY (1965) were employed. The cadmium sulphide films were evaporated onto gold films, which had been previously evaporated or sputtered onto one end of one of the germanium rods. The cadmium sulphide films were half an acoustic wavelength thick at 9 GHz. The transducers were evaporated after the contacts had been alloyed to the rods, as the heating involved in applying the contacts would have damaged the transducer films. The transducers were excited in the high field region of a re-entrant coaxial cavity HANSEN (1939). The details of these cavities are given in Chapter 6, in connection with other measurements.

The position of the specimen was carefully adjusted so that the transducer was flush with the top of the cavity. With the specimen in this position the gold backing film was expected to act as part of the cavity wall. Thus the transducer experienced the full electric displacement in the cavity, but the germanium rod was screened from the field in the cavity by the gold film.

This screening was necessary because if the end of the germanium rod had been exposed to the electric field in the cavity, it would have been impact ionised and the resulting free carriers would have attenuated the acoustic wave by an unknown amount. Consequently any comparison between theory and experiment would have been very suspect. The gold film also ensured that the field through the transducer was normal to the film, thus preventing the excitation of additional unwanted acoustic modes. The electromagnetic-acoustic ~~conversion~~ ^{conversion} efficiency of the longitudinal transducers was about 0.1%.

Particular interest was taken in shear wave transducers, as it was predicted that shear mode amplifiers would have a larger gain than longitudinal mode ones. However, the position with regard to shear wave transducers was much less satisfactory than with longitudinal wave transducers. In order to appreciate the situation, it is necessary to consider the possible types of shear wave transducer and their modes of operation.

Again cadmium sulphide film transducers appeared to be potentially the most satisfactory. The fact that these films tend to grow with the c-axis perpendicular to the substrate has been mentioned previously. RICHTER (1962) and GIBSON (1966) have shown that if such a film is excited with the electric field applied in the plane of the film (i.e. in the basal plane of the CdS), a shear wave is generated. Using for example the method of LAMB & RICHTER (1966), a field may be applied in the plane of the evaporated film. However, for all normal values of the input microwave power the end

of the germanium rod would be impact ionised, and the resulting low resistivity germanium would short out the transducer.

Richter and Gibson have also shown that if the exciting electric field is applied at an angle of about 38.5° to the 'c' axis of a cadmium sulphide film, strong shear acoustic wave generation should result with no simultaneous longitudinal wave generation. The growth of direct, obliquely evaporated films, has been investigated by FOSTER (1967). This investigation showed that in the initial layers of such films the c-axis is perpendicular to the substrate. However, as the film grows in thickness the orientation of the c-axis is found to tilt until it is pointing in the direction of evaporation. It was found that this tilting of the c-axis was not complete in films less than about $0.5\mu\text{m}$ thick. The actual thickness depended on the substrate. But the thickness of a 9 GHz resonant shear transducer is approximately $0.1\mu\text{m}$, so that such transducers cannot be produced by this method. With the above results in mind, two thick, obliquely evaporated films, resonant at 500 MHz were grown. It was known that the initial layers of directly evaporated films tend to be disordered, and it was hoped that the transduction in these films at 9 GHz would be largely by surface excitation at the free surface of the film. The c-axis being fully tilted at the free surface, it was hoped that a shear wave would be launched. Both films were found to act as satisfactory transducers at 450 MHz, but no acoustic echoes were detected at 9 GHz at 4.2°K .

A new evaporation procedure was developed in the Department with the object of producing efficient shear wave transducers. The method involved obliquely evaporating a sufficiently thick layer of low resistivity cadmium sulphide to ensure that the c-axis was fully tilted at the free surface. Then on top of this low resistivity layer, a high resistivity layer of the appropriate thickness was evaporated. The objective was to arrange that the transduction should occur in the correctly orientated, high resistivity layer. The low resistivity was ensured by depositing the first layer at a low substrate temperature which results in a low resistivity non-stoichiometric film, and further by doping the layer by co-evaporation of cadmium. Shear wave transducers were prepared by this method which operated successfully at frequencies of about 1 GHz at room temperature. However, attempts to produce transducers operating at a frequency of 9 GHz at 4.2°K were not successful.

Simultaneously with the testing of cadmium sulphide film transducers, attention was paid to other types of transducer. The only probable alternatives appeared to be bonded piezo-electric rods and thin ferromagnetic films.

There are well known difficulties associated with making low loss bonds capable of both transmitting X-band acoustic waves and being thermally cycled between room and liquid helium temperatures. These were accentuated by the small cross-sectional area of an amplifier rod, which was a consequence of the high current density required to obtain acoustic amplification. Attempts were made to bond 3 mm diameter X and BC cut quartz rods to pieces of germanium.

Silicone oils of varying viscosity were used as the bonding agent. All the bonds appeared to be capable of thermal cycling, but a marked variation in the transmission loss was observed. Those bonds made to X-cut quartz, that is the ones transmitting longitudinal waves; showed a transmission loss of about 10dB. But all the bonds made to BC cut quartz, that is for shear waves, showed a transmission loss greater than the maximum detectable (about 35dB).

A ferromagnetic film transducer requires a steady magnetic field for its operation. In general this field is of such a value for the generation of 9 GHz phonons, that $\omega_c \tau > 1$ (SEAVEY(1963)). Where ω_c is the cyclotron frequency, and τ is the acoustic phonon momentum relaxation time. Thus the use of these transducers would impair the understanding of the behaviour of the device.

4.4 Measurement Technique

The acoustic gain of an amplifier was determined by measuring the change in insertion loss with applied field. This was done by varying the applied field and adjusting a calibrated attenuator, placed in front of the receiver, to maintain the signal at the receiver constant. The measured changes in attenuation were directly related to the acoustic gain.

In order to make a comparison between theory and experiment the drift velocity (v_d) of the electrons, rather than the applied field is needed. This information was obtained from the relation

$\alpha v_d = \mu_H(E) E$, where μ_H is the Hall mobility and α is the ratio of the Hall and drift mobilities discussed in Chapter 3. Care was taken to ensure that the values of Hall mobility used were those

appropriate to the fields applied.

4.5 Results

Measurements were made on two longitudinal mode amplifiers, the results were almost identical.

The field dependent changes in the insertion loss were small, so that no accurate determination of the variation of these changes with field could be made. Thus measurements were only made at the highest field applied, namely 120V/cm (the current being 50A). The delay between the launching of the acoustic pulse into the bar and the firing of the drift field pulser, was adjusted so that the drift field was applied as the acoustic pulse was travelling away from the transducer. With this delay, the change in insertion loss on applying the field was measured. Firstly a measurement was made when the direction of the field was such that it caused the carriers to drift in the direction of acoustic propagation. Secondly, a measurement was made with the field direction reversed, so that the carriers were drifting in the direction opposite to that of the acoustic pulse. For these two cases the changes in insertion loss on applying the field were 0dB and +4dB respectively. The delay was then increased so that the field was applied as the acoustic pulse was travelling towards the transducer, after being reflected from the end of the rod. With this new delay the above measurements were repeated. When the current and acoustic propagation were in the same direction the change in insertion loss was ± 1 dB. When the field was reversed the change was +3dB. These figures are approximate, the measurement accuracy being about ± 1 dB.

4.6 Comparison of Theory & Experiment

The direction dependent results obtained with the longitudinal mode amplifier are probably susceptible of the following explanation. The changes resulting from reversing the direction of the applied field relative to the direction of acoustic propagation, are predicted in the non-reciprocal nature of the expression for the attenuation (Γ). It can be seen from equation (2.19) that when $\omega\tau \ll 1$, the expression for Γ can be written as

$$\Gamma = A \left(1 - \frac{v_d}{v_s} \right)$$

Where A is independent of the sign of v_d . It will be shown that $|v_d| = 2.2 |v_s|$. Thus if v_d is positive $\Gamma = -1.2A$, whereas if v_d is negative $\Gamma = 3.2A$. The dependence of the measured values on the direction of propagation of the acoustic pulse, may be explained in terms of the mechanism of acoustic attenuation by neutral donors demonstrated by POMERANTZ (1965). Theoretical treatments of the effect have been given by KWOK (1966) and SUZUKI & MIKOSHIBA (1966). The attenuation is caused by neutral donors, so that the mechanism is not effective when the electric field is applied and the donors are impact ionised. Further Pomerantz has shown that the effect does not become significant in arsenic doped germanium until the temperature is raised above 15°K. If the field is applied while the acoustic pulse is travelling towards the transducer, no attenuation is expected. This follows because the temperature of the rod is that of liquid helium as the pulse propagates through unionised material, i.e. when travelling away from the transducer. However, if the field is applied while

the pulse is travelling away from the transducer, then attenuation is expected. This results from the fact that the applied field heats the rod as shown in Chapter 3, and thus the acoustic pulse returns through heated unionised material. The thermal time constant of the rod is expected to be longer than the time interval between echoes.

In order to predict the gain of an amplifier, it is necessary to extend the theory developed in Chapter 2. The theory of the deformation potential amplifier set out in Chapter 2 is based on the assumption that the electron and lattice temperatures are equal. However, in Chapter 3 it was shown that this was not the case for the operating conditions of the amplifier. But equations (2.18) and (2.19) are still valid if the low field values of some of the parameters they contain are replaced by high field ones. This approach is valid if, as was shown in Chapter 3, the definition of an electron temperature is justified.

The important equations from Chapter 2 are reproduced below. They are for a shear wave along a $\langle 100 \rangle$ direction polarised in $\langle 010 \rangle$ direction.

$$\Gamma = \frac{n}{9v_s^3 \rho k_B T_e} E_0^2 \frac{\omega^2 \tau_R (1-\beta)}{1 + \omega^2 \tau_R^2 (1-\beta)^2}$$

and for a longitudinal wave along a $\langle 110 \rangle$ direction.

$$\Gamma = \frac{n}{v_s^3 \rho k_B T_e} (E_L + \frac{1}{3} E_0)^2 \frac{\omega^2 \tau_R (1-\beta)}{1 + \omega^2 \tau_R^2 (1-\beta)^2}$$

where $\frac{1}{\tau_R} = \frac{4}{3\tau_{IV}} + k^2 D$

and $\beta = \frac{v_D}{v_s}$

The effect of electron heating on the expression for the gain is threefold.

- a) the temperature appearing explicitly in the expression is the electron temperature, its value being as found in Chapter 3.
- b) the low field value of τ_{IV} is replaced by the high field one.

This can be done using the results of WEINREICH, SANDERS & WHITE (1959), who measured τ_{IV} as a function of lattice temperature.

The results show a dominant contribution to the scattering rate from impurity intervalley scattering at temperatures below 80°K, for the appropriate impurity concentration. Therefore the value of τ_{IV} does not depend on whether the electrons are in thermal equilibrium with the lattice. In fact the results show that is only weakly dependent on the electron temperature.

- c) the value of the diffusion coefficient (D) is that obtained from the Einstein relation ($D = \frac{k_B T_e}{e} \mu$). Where the mobility is the drift mobility.

The values of the acoustic gain for the two modes of interest may now be calculated, for a field of 120 Volts/cm. Use will be made of the high field forms of equations (2.18) and (2.19),

together with the values of electron temperature from Chapter 3. The measured high field values of electron concentration and mobility are also required. The only undetermined parameter in the expression for the gain is the deformation potential. In the case of the potential E_u a value of about +17ev has been established by several measurements. Some uncertainty exists about the value of the quantity $E_d + \frac{1}{3} E_u$. The reported values are -1.7ev (HERRING & VOGT (1956)) and -2.7ev (FRITZSCHE (1959)). A value of 2.2ev has been assumed in the calculation indicated below. The density and acoustic velocities were taken from the work of M^CSKIMIN (1953). For the longitudinal acoustic mode

$$\beta = 2.2 \quad \text{and} \quad \omega \tau_R (1 - \beta) = 0.12$$

therefore $G_+ = +1.3 \text{ dB/cm}$. (where $G = -\Gamma$).

In order to discuss the effect on the gain of a deformation potential amplifier of reversing the direction of the applied field, it is convenient to define two quantities G_+ and G_- .

G_+ is defined as the gain of an amplifier when the directions of v_d and v_s are the same, G_- is the gain when the directions are opposite. It is simply shown from equations (2.18) and (2.19) that ^{because $\omega \tau_R (1 - \beta) \ll 1$} these two quantities are related as follows

$$G_- = - \frac{(\beta + 1)}{(\beta - 1)} G_+$$

Substituting in this relation, it is found that the longitudinal mode amplifier that $G_- = -3 \text{ dB/cm}$.

For the shear mode

$$\beta = 4.1 \quad \text{and} \quad \omega\tau_R(1-\beta) = 0.09.$$

therefore $G_+ = 20\text{dB/cm}$.

In order to estimate the effect of electron heating, the calculation of the gain for a longitudinal mode amplifier is repeated assuming that $T_e = 4.2^\circ\text{K}$. The result is

$$\beta = 2.2 \quad \text{and} \quad \omega\tau_R(1-\beta) = 0.45$$

therefore $G_+ = 45 \text{ dB/cm}$.

Thus it can be seen that electron heating is expected to have a very large effect on the gain of an amplifier. ~~For the case considered above the predicted reduction is by a factor of 35.~~
A similar reduction is expected for a shear mode amplifier.

It is apparent from the previous discussion that the measured gain of the longitudinal mode amplifier was $\sim +1\text{dB/cm}$ when the directions of the applied field and of the acoustic propagation were the same, and -3dB/cm when the directions were opposed. These results are in good agreement with the predicted ones. The only other piece of experimental data was obtained by POMERANTZ (1964) who measured a gain of 20dB/cm in a shear mode amplifier. This is also in good agreement with the predicted value. It is clear that the values of electron temperature obtained from the hot electron measurements, have made it possible to predict with considerable precision the large reduction in the gain of an amplifier resulting from electron heating. The extent to which precise agreement can be expected between the theoretical

and experimental values for the gain of an amplifier, is not clear for the following reasons. In the case of the longitudinal mode amplifier the measured gain is close to the limit of measurement, and there is some doubt about the precise value of the appropriate deformation potential. In the case of the shear mode amplifier the electrical parameters of the amplifier material are not known precisely, and the effect of the magnetic field applied in order to operate the magnetostrictive shear wave transducers is not entirely clear.

The agreement between the predicted and measured gain at a frequency of 9GHz, suggests that it should be possible to predict with reasonable accuracy the gain of an amplifier in the technologically interesting frequency range of 10 to 100 GHz. A calculation of gain was carried out in the same manner as above. It was found for a shear mode amplifier, that the maximum gain for a field of 120V/cm is expected to be approximately 1000dB/cm. This gain is expected to occur at a frequency of 80 GHz. The factor $\frac{E^2}{v_s^2}$ in the expression for the gain, will again result in the gain of a longitudinal mode amplifier being substantially smaller than that of a shear mode amplifier. As was pointed out in Chapter 2, equations (2.18) and (2.19) are only valid when $\omega\tau \ll 1$. For germanium of the doping used in the present experiments, this condition breaks down for frequencies greater than about 200 GHz. It should be recalled that in deriving equations (2.18) and (2.19) various non-linear terms were neglected, for example in the electron concentration and elasticity. This means that a 1cm.

long shear mode amplifier would not have a gain of 1000dB at 80 GHz, because as the acoustic energy density increased non-linear processes would limit the gain.

4.7 Discussion of the deformation potential amplifier as an electronic device

This study of the deformation potential amplifier was stimulated in part by the potential applications of the device as a low noise microwave amplifier. These potential applications would appear to be at the higher microwave frequencies (10 - 100 GHz). Since the start of this work, the limitation of the potential applications to the higher frequencies has become more apparent as a result of advances in the technology of competitive devices, particularly the parametric amplifier.

A very important property of any amplifier is the gain available from it. The calculations made in this chapter appear to provide the first quantitative estimates of the acoustic gain of a deformation potential amplifier. The predicted acoustic gain is found to be in good agreement with the experimental data, despite the difficulties outlined previously. This agreement between theory and experiment at a frequency of 9 GHz, is considered to lend additional weight to the predictions of the gain available at higher frequencies. It is expected that at the higher microwave frequencies very substantial acoustic gains should be available (e.g. 1000dB/cm at 80 GHz with a field of 120V/cm.) despite the effect of electron heating.

The gain of an electronic amplifier is usually defined in terms of the ratio of the power at the output terminals to the power at the input terminals. It is convenient to refer to this as the terminal gain of the device. In the case of a deformation potential amplifier there are two factors which determine the terminal gain of the amplifier. The first is the acoustic gain. The second is the efficiency of the transducers. As has been mentioned previously, an extensive programme of transducer development was carried out in the Department simultaneously with this work. Although significant developments in the transducer deposition were made; it was found to be very difficult to produce efficient shear wave transducers operating at a frequency of 9 GHz or higher. The same conclusion was reached in other laboratories. The lack of efficient transducers has two important effects on the device. Firstly the terminal gain of the amplifier will be seriously reduced. Secondly the noise figure of the device will be degraded. This degradation results from the fact that the amplified signal will undergo transduction twice, whereas the main component of the noise undergoes only one transduction. The chief source of noise in such an amplifier is the amplified thermal noise. MAY (1965)

In conclusion it may be said that it has been demonstrated that very large acoustic gains may be expected in a deformation potential amplifier at the higher microwave frequencies. However, the problems resulting from the lack of efficient transducers make it unlikely that the mechanism will form the basis of a viable electronic device.

Chapter 5 THEORETICAL ASPECTS OF ACOUSTIC ATTENUATION

MEASUREMENTS AT LOW TEMPERATURES

5.1 Introduction

This chapter is concerned with various aspects of the theoretical background to some measurements which have been made in the temperature range 15-120°K, of the attenuation of microwave frequency acoustic waves in piezoelectric dielectrics. The measurements were made by the well known pulse echo method McSKIMMIN (1964). As the materials of interest were piezoelectric it was convenient to excite the acoustic waves by the surface excitation method. This method has been discussed in detail by a number of authors including JACOBSON (1960) and RICHTER (1966).

In the rest of this chapter no explicit account is taken of the fact that the materials of interest are piezoelectric. It is therefore of interest at this point, to consider the influence of the piezoelectricity on the acoustic propagation. This problem has been studied by KYAME (1949) and reviewed by HUTSON and WHITE (1962). They found that for materials like those which are the subject of the present study, no significant effect is anticipated except the increase in the effective elastic constant resulting from the piezoelectric fields set up by the acoustic wave. This is the well know piezoelectric stiffening effect.

The layout of the chapter is as follows. Section (5.2) deals with those aspects of specimen preparation and geometry which might affect the attenuation measurements, for example the flatness and parallelism of the end surfaces of the specimens. Section (5.3) is concerned with those properties of the material from which specimens are prepared, which could cause attenuation of the acoustic wave in addition to that caused by thermal phonons. Among the possible causes of additional attenuation are lattice imperfections and local strain in the specimens. A treatment of the attenuation caused by thermal phonons is given in Section (5.4). Consideration is given to the selection rules to which the phonon-phonon processes are subject. The type of process most likely to be responsible for the attenuation is shown to be a three phonon process involving two thermal phonons. The selection rules are found to severely limit the type of three phonon process permitted. It is found necessary to consider the effect on the selection rules of the uncertainty in the energy of a thermal phonon, resulting from the finite lifetime of the phonon. It is also found that a discussion of higher order three phonon processes is needed. Section (5.5) contains a short summary of the predicted behaviour of the attenuation arising from three phonon processes.

5.2 Geometric and Surface Effects

It is well known that difficulties may arise, when making acoustic attenuation measurements by the pulse echo method, as a result of diffraction SEKI, GRANATO and TRUPELL (1958) and the

finite cross-section of the specimen REDWOOD (1960). In connection with these effects it is of interest to determine the values of the quantities $\frac{d^2}{\lambda}$ and $\frac{\lambda}{a}$; where λ is the acoustic wavelength, d is the acoustic beam diameter and a is the average transverse dimension of the specimen. These effects will be largest in the present measurements for the 1.0 GHz longitudinal wave in zinc oxide.

For this case $v_s \approx 6 \times 10^5$ cm/sec, $\nu = 1 \times 10^9$ Hz,
 $d = 0.2$ cm, $a = 0.4$ cm.

$\therefore \frac{d^2}{\lambda} \sim 10^2$ cm
 and $\frac{\lambda}{a} \sim 10^{-3}$

Seki, Granato and Truell have given an approximate criterion for estimating the importance of diffraction in attenuation measurements. This ~~c~~ⁿ criterion is that the apparent attenuation caused by diffraction is ~ 1 dB over a length of $\frac{d^2}{\lambda}$. Thus in the present case the apparent attenuation is $\sim 10^{-2}$ dB/cm, which may be neglected. The very small value of the ratio $\frac{\lambda}{a}$ shows that guided wave effects resulting from the finite cross-section of the specimen could be neglected.

The method of detecting the acoustic pulse by means of the inverse piezoelectric effect at the launching surface, requires that the acoustic wave front should be of constant phase. As the end surfaces of the rods were not precisely parallel, a difference in the distance travelled by different parts of the wave front between reflections was anticipated. This difference was expected to lead to a phase difference across the wave front

which would increase with successive reflections. After a number of reflections the phase difference would be approximately 2π and the signal received very small. On further reflection the signal would go through a series of maxima and minima, each maxima being smaller than the previous one. This 'beating' effect would be superimposed on the exponential decay of the echo pattern due to the attenuation of the acoustic pulse. The modification of the echo pattern owing to this effect has been treated in detail by CARR and STRANDBERG (1962) and RICHTER (1966). From an experimental standpoint it would appear to be valuable to estimate approximately the number of the first echo to be extinguished if the lack of parallelism were two seconds of arc. Assuming the end faces to be entirely flat, a very simple geometric argument suggests that the number (n) of the first extinguished echo is given by

$$n \sim \frac{\lambda}{2d\theta}$$

where θ is the angle between the end faces, λ the wavelength and d the beam diameter. (This relation shows the advantage of keeping d as small as possible.)

The 'beating' effect is expected to be most pronounced in the X-band measurements.

Using the values $\nu = 9 \times 10^9$ Hz, $v_s = 6 \times 10^5$ cm/sec, $d = 0.15$ cm, $\theta = 2$ sec or 10^{-5} radians,

$$n = 20.$$

The lack of parallelism of the end faces of the specimens on which measurements were made was about 2-4 seconds of arc. Thus it was anticipated that the 'beating' effect should be observed on the echo pattern. This proved to be so. The manner of obtaining information concerning the attenuation from an echo pattern showing 'beating' is discussed in Chapter 6.

As the end surfaces of the specimens were not flat, the distances travelled between reflections by different parts of the acoustic wave front were expected to be different. In this case the effect on the echo pattern depended on the precise shape of two surfaces. However the effect on the echo pattern was expected to be similar to that described above. The wavelengths of the acoustic waves at 9.0 GHz were close to those of visible light so it was anticipated that a lack of flatness of $\frac{\lambda}{10}$ would cause the same order of disturbance of the echo pattern as a non-parallelism of 3 seconds of arc. The lack of flatness of the end faces of the specimens was found to be about $\frac{\lambda}{10}$.

The end faces of the specimens had some scratches and polishing marks on them. Thus it was expected that some of the acoustic energy would be scattered on reflection, causing a reduction in the amplitude of the coherent beam as compared with that reflected by an ideally smooth surface. This would occur at each reflection and might manifest itself as a contribution to the apparent attenuation.

5.3 Bulk Effects

Imperfections in a crystal will cause a local disturbance of the elastic properties of the crystal, which may scatter a coherent acoustic beam and add to the apparent attenuation in the specimen. Defects in a crystal may take a variety of forms. Possible defects are (a) point defects e.g. vacancies or impurities (substantial or interstitial), (b) line defects in particular dislocations, (c) sheet defects such as twin planes, (d) volume defects i.e. voids or inclusions. An example of the effect of volume defects is given in Chapter 8, in connection with the room temperature attenuation measurements.

As the materials studied were piezoelectric semiconductors it might be expected that they would have contained conduction electrons which would absorb energy from the acoustic wave in a manner analogous with the deformation potential interaction discussed in Chapter 2. The matter is considered in Section 6.5 , where it is shown that as a result of the high resistivity of the specimens the effect can be neglected.

The presence of certain paramagnetic impurities in the specimens could lead to changes in the attenuation of the acoustic wave, as a result of an absorption of acoustic energy or a reduction in the thermal phonon lifetime. The mechanism is considered to be as follows. A phonon, which may be either acoustic or thermal, causes an electronic transition between two energy levels of an impurity atom. The difference in energy of the two levels is approximately equal to the phonon energy.

In general it is expected that the energy levels involved will be degenerate levels which have been split by the crystal field. Such a contribution to the total attenuation appears to have been observed by CICCARELLO and DRANSFELD (1964). To check for the presence of attenuation arising from this mechanism a series of subsidiary experiments were conducted, in which the echo pattern was carefully observed while a magnetic field applied to the specimen was varied. Fields in the range 0-4000 ~~gauss~~^{gauss} were applied, at temperatures of 4.2°K and 20°K. No significant change in the echo pattern was observed in any such experiment, and it was thus concluded that the effect was absent in those specimens on which attenuation measurements were made.

Local strain in a crystal will modify the local elastic properties of the material, but not in general in as abrupt a manner as lattice imperfections. It is envisaged that the principal results of propagating an acoustic wave through a strained specimen will be that the wave front becomes distorted. The variation of phase across the wave front will lead to some cancellation of the signal at the receiving surface of the specimen.

The influence of the effects discussed in the present and the previous section, on the observed echo pattern, will take one of two forms. Firstly, the effects involving signal cancellation at the receiving surface of the specimen i.e. those

due to non-parallelism and lack of flatness of the end surfaces and to local strain. These effects will cause a 'beating' pattern to be superimposed on the exponential decay of the echo pattern caused by the lattice attenuation. Secondly the other effects will simply add to the effect of the lattice attenuation and make the exponential decay more rapid. Owing to the nature of the effects discussed above; sufficient information is not, in general, available to estimate the apparent attenuation resulting from them. However an experimental method used to extract information concerning the attenuation caused by thermal phonons from an echo pattern of the type described above, is explained and discussed in Chapter 6. This method makes use of the fact that the contributions to the total attenuation resulting from the mechanisms described above are at most only weakly temperature dependent, whereas the contribution to the attenuation caused by thermal phonons is, in general, very strongly temperature dependent.

5.4 Attenuation by Thermal Phonons

The attenuation of acoustic waves by thermal phonons in solids, has been discussed by many authors. The problem is complicated by the wide ranges of temperature and acoustic frequency over which measurements have been made. In order to simplify the treatment it is convenient to divide the conditions into three regions.

Such a division is outlined below.

<u>Region</u>	<u>Conditions Pertaining</u>
High Temperature	$\omega\tau_t < 1.$
Intermediate	$\omega\tau_t \gg 1, \hbar\omega \ll k_B T.$
Low Temperature	$\hbar\omega > k_B T.$

Where ω refers to the acoustic wave and τ_t is the thermal phonon relaxation time. At a sufficiently low frequency the intermediate region will not exist as the two conditions will not be simultaneously satisfied. This however was not the case in the frequency range in which measurements were made.

Although three regions have been defined only two of them are of interest in connection with the present measurements.

This is because for a 10 GHz acoustic wave, the condition

$\hbar\omega > k_B T$ gives the maximum temperature of the low temperature region as $\sim 0.5^\circ\text{K}$. At this temperature the attenuation caused by thermal phonons is so small that it cannot be separated from that due to the other effects described in the previous two sections.

The other limit of the intermediate region i.e. $\omega\tau_t \approx 1$ represents the situation where the acoustic wavelength is approximately equal to the thermal phonon mean free path. For temperatures such that $\omega\tau_t < 1$, that is in the high temperature region, the mean free path of the thermal phonons is shorter than the acoustic wavelength. In this case the strain associated with the acoustic wave can be treated as a slowly varying field in which the thermal phonons are moving,

that is the acoustic wave is assumed to interact collectively with the assembly of thermal phonons. On the other hand if the temperature is such that $\omega\tau_t \gg 1$, the mean free path of the thermal phonons is long compared to the acoustic wavelength. In this case the interaction is assumed to take the form of discrete interactions between thermal and acoustic phonons. This is equivalent to saying that the uncertainty in the energy of a thermal phonon as a result of its lifetime τ_t , i.e. $\hbar\omega > \frac{\hbar}{\tau_t}$ is less than the energy of an acoustic phonon ($\hbar\omega$).
or $\omega\tau_t > 1$

It is possible to treat both regions with the same theoretical approach KWOK, MARTIN and MILLER (1965). However this is a microscopic treatment making use of an atomic displacement correlation function and thermodynamic Green's functions. Such an approach is considered to be more complex and less 'direct' in the context of comparing theoretical predictions with experimental results, than treatments employing phenomenological parameters. Consequently it is proposed to adopt the procedure of treating the two regions separately by as simple methods as are realistic. The high temperature region is treated in Chapter 8 in connection with the room temperature measurements.

Before proceeding to investigate the intermediate region it is worthwhile to consider the meaning of the term phonon.

If suitable boundary conditions are assumed, it is possible to analyse a general vibration of a crystal into a sum of vibrations each associated with one of the normal modes PEIERLS (1955). The sum has the form

$$E = \sum_i \left(N_i + \frac{1}{2} \right) \hbar \omega_i + V. \quad (\text{the } N_i \text{ are integers}) \quad (5.1)$$

where the ω_i are the normal modes of the lattice and V is the potential energy. The energy of the i^{th} normal mode may be considered as the energy of N_i phonons each having energy $\hbar \omega_i$ plus a zero point energy $\frac{1}{2} \hbar \omega_i$. When all the normal modes are in thermal equilibrium the probable number (\bar{N}_i) of phonons in the i^{th} mode is given by the Bose-Einstein distribution function

$$\bar{N}_i = \frac{1}{\exp\left(\frac{\hbar \omega_i}{k_B T}\right) - 1} \quad (5.2)$$

Because of the elastic anharmonicity of the crystal the modes are not completely independent. Usually the anharmonicity may be treated as a perturbation on the behaviour of a harmonic lattice. This coupling between modes arising from the anharmonicity, results in interactions between phonons which are often referred to as phonon-phonon processes or phonon collisions.

Because no detailed information concerning the elastic anharmonicity of the materials studied appears to be available, no predictions of the magnitude of the attenuation can be made. For this reason attention was directed to the variation of the attenuation with temperature and frequency. It is assumed

throughout this work that the materials are elastically isotropic.

The sound wave is considered as corresponding to a very large increase in the number of phonons in some modes, to values far greater than the thermal equilibrium values for those modes. As all the excited modes have almost the same wave vector and frequency only one of the modes need be considered.

The object of this section is to consider the manner in which the acoustic phonons are absorbed as a result of interactions with thermal phonons. The lowest order of such a process is one involving three phonons.

The Debye model predicts that below the cut-off energy, the expression for the density of phonon states has the form

$$N(E) = r\omega^2,$$

where r is a constant independent of the phonon energy.

The expression for the distribution function is given in (5.2).

Thus the number of phonons having energies in the range E to $E+dE$ is given by

$$\frac{r\omega^2 dE}{\exp\left(\frac{\hbar\omega}{k_B T}\right) - 1}$$

It is simply shown that this expression is strongly peaked at an energy close to $k_B T$. Even at a frequency of 10 GHz at 10⁰K, the relation $\hbar\omega_l \ll k_B T$ is valid (where the suffix l denotes an acoustic phonon). Therefore in order that an acoustic phonon should be able to interact with the majority of thermal phonons, it is necessary that it should interact with a phonon of much higher energy.

Three phonon processes can be divided into two classes as shown below

$$1 + 2 \rightarrow 3 \quad (a)$$

$$1 \rightarrow 2 + 3 \quad (b)$$

where the numbers represent phonons, which may be either acoustic or thermal. Because the present interest is in acoustic attenuation, the important processes are those in which phonon 1 is an acoustic phonon. The conservation of energy requires that the energies of phonons 2 and 3 in a process belonging to class (b), should be less than that of the acoustic phonon 1. But it has already been noted that most of the thermal phonons have energies greatly in excess of the acoustic phonons of the present experiments, thus processes of class (b) will only occur infrequently and can be neglected as a significant source of attenuation. Processes of class (a) can involve the interaction of an acoustic phonon and a thermal phonon, having an energy of about $k_B T$, and simultaneously conserve energy. This is possible if phonons 2 and 3 are both thermal phonons. Thus the processes of particular interest are those having the form

$$\text{acoustic phonon} + \text{thermal phonon} \rightarrow \text{thermal phonon} \quad (5.3)$$

Any phonon-phonon process must satisfy two selection rules. The first is the conservation of energy, which may be written for a process of the type (5.3)

$$\omega_1 + \omega_2 = \omega_3. \quad (5.4)$$

The second is the crystal momentum selection rule, this can be written.

$$\vec{k}_1 + \vec{k}_2 = \vec{k}_3 + \vec{g} \quad (5.5)$$

where the suffix 1 refers to an acoustic phonon and the suffices 2 and 3 refer to thermal phonons. \vec{g} is a reciprocal lattice vector.

The processes for which $\vec{g} \neq 0$ are termed umklapp processes and require that the initial and final thermal phonons are in different Brillouin zones. Because \vec{k} is small for an acoustic phonon, the value of \vec{k} for the initial thermal phonon must be close to the edge of the Brillouin zone, ~~if~~^{if} an umklapp process is to occur. This means that the initial thermal phonon must have a large energy. But Equation (5.2) shows that at low temperatures the number of these high energy phonons drops exponentially as the temperature decreases. Thus at low temperatures the occurrence of ~~three~~ phonon umklapp processes is rare, and they may be neglected. Therefore it is justified to set $\vec{g} = 0$ in Equation (5.5), so that the selection rule now becomes

$$\vec{k}_1 + \vec{k}_2 = \vec{k}_3. \quad (5.6)$$

The general relation (5.3) describes eight possible processes, depending on the polarisations of the three phonons. Because the material is assumed to be isotropic no distinction is made between different shear polarisations. A consideration of Equation (5.6) shows that the number of probable processes can be restricted further.

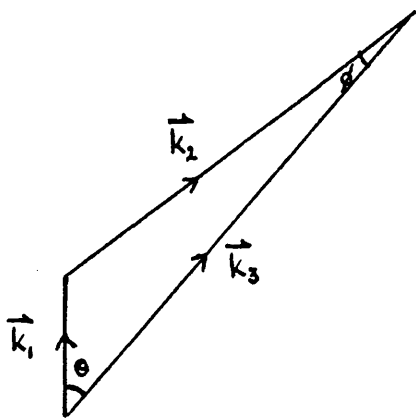


Figure (5.1) DIAGRAMMATIC REPRESENTATION OF EQUATION (5.6)

It follows because $|k_1| \ll |k_2| \approx |k_3|$ that $\cos \theta \approx 1$.
 Thus from Figure (5.1)

$$|k_1| \cos \theta + |k_2| = |k_3| \tag{5.7}$$

As $T \ll \theta_D$ and $|k_2| \approx |k_3|$ (where θ_D is the Debye temperature), the dispersion is very small and Equation (5.4) can be written as

$$(\nu_s)_1 |k_1| + (\nu_s)_2 |k_2| = (\nu_s)_3 |k_3| \tag{5.8}$$

from Equations (5.7) and (5.8)

$$|k_1| [(\nu_3)_1 - (\nu_3)_3 \cos \theta] = |k_2| [(\nu_3)_3 - (\nu_3)_2] \quad (5.9)$$

but as $|k_1| \ll |k_2|$ Equation (5.9) can only be satisfied if

$(\nu_3)_2 \approx (\nu_3)_3$. That is the initial and final thermal phonons must have the same polarisation. Four of the processes of the type (5.3) satisfy this requirement, they may be denoted as

$$l + l \rightarrow l \quad (5.10a)$$

$$l + t \rightarrow t \quad (5.10b)$$

$$t + t \rightarrow t \quad (5.10c)$$

$$t + l \rightarrow l \quad (5.10d)$$

where l and t represent longitudinally and transversely polarised phonons respectively. The order of the phonons is as in (5.3), i.e. the first letter represents the acoustic phonon. Having reduced the number of potentially significant three phonon processes to four, it is now necessary to consider whether these processes can simultaneously satisfy the selection rules described by Equations (5.4) and (5.6). This is conveniently done by means of a graphical construction described by HERRING (1954). The method is described in stages below.

(a) Firstly from the origin O in \vec{k} space the wave vector \vec{k}_1 of the acoustic mode is drawn, the vector ending at the point O' .

(b) Secondly for a particular angular frequency ω_2 ($\approx \frac{k_B T}{\hbar}$) of the initial thermal phonon, all the corresponding wave vectors \vec{k}_2 are drawn from O' (assuming the material to be non-dispersive). Because of the assumption of isotropy made previously the ends of the vectors \vec{k}_2 will describe the surface of a sphere.

(c) Thirdly the angular frequency ω_3 of the final thermal phonon is calculated from Equation (5.4), and all the corresponding wave vectors \vec{k}_3 are drawn from O . Again the ends of these vectors describe a sphere.

At any point of intersection of the two spheres.

$$\vec{k}_1 + \vec{k}_2 = \vec{k}_3$$

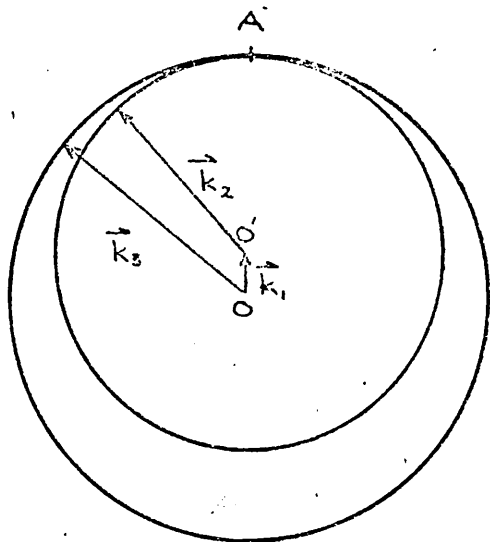
and \vec{k}_3 was chosen in such a way as to ensure that

$$\omega_1 + \omega_2 = \omega_3,$$

that is both the selection rules are simultaneously satisfied.

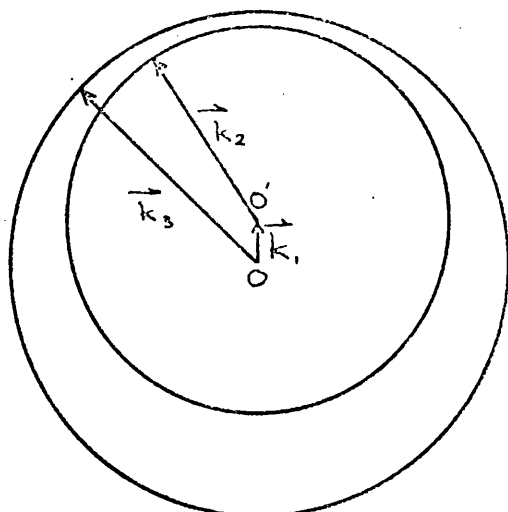
Figures (5.2a) to (5.2d) are representative of the results of carrying out the above construction in the cases of processes (5.10a) to (5.10d), respectively. The figures show sections through the constructions containing the vector \vec{k}_1 . That figures (5.2) represent correct constructions can be checked simply from the sign of the quantity $\Delta k = |k_3| - |k_2| - |k_1|$ for three collinear phonons. This is significant as it determines whether OA (see Figure (5.2a)) is equal to $|k_3|$ or $|k_1| + |k_2|$ i.e. whether the circles intersect.

As $(v_s)_2 = (v_s)_3$ for the processes of interest, it is easily verified from Equations (5.4) and (5.6) that for



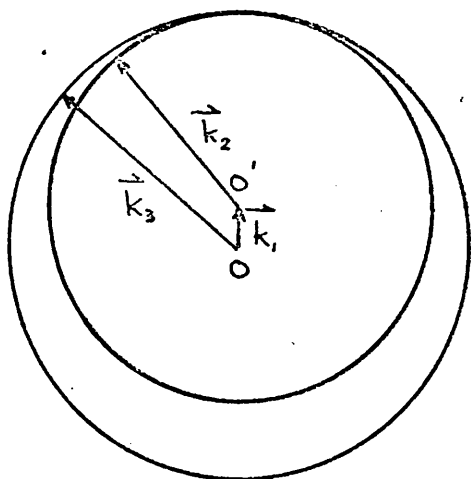
(a.)

PROCESS (5.10a) $l + l \rightarrow l$



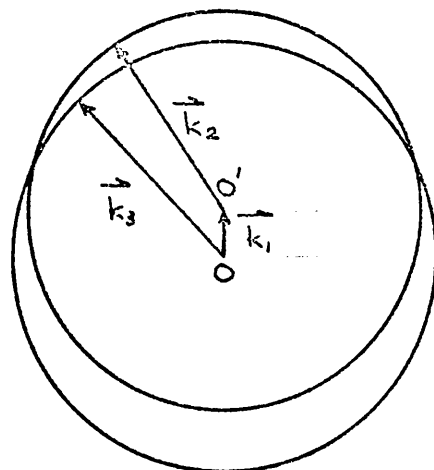
(b.)

PROCESS (5.10b) $l + t \rightarrow t$.



(c.)

PROCESS (5.10c) $t + t \rightarrow t$



(d.)

PROCESS (5.10d) $t + l \rightarrow l$

Figure(5.2) SECTIONS THROUGH THE HERRING CONSTRUCTIONS FOR PROCESSES(5.10).

the case of collinear phonons $\Delta|k| = \omega_1 \left[\frac{1}{(v_s)_2} - \frac{1}{(v_s)_1} \right]$

thus if $(v_s)_1 = (v_s)_2$; $\Delta|k| = 0$ and the spheres touch - processes (5.10a) and (5.10c) . If $(v_s)_1 > (v_s)_2$; $\Delta|k|$ is positive, and the spheres do not intersect - process (5.10b) . If $(v_s)_1 < (v_s)_2$; $\Delta|k|$ is negative, and the spheres intersect - process (5.10d).

From figure (5.2) it can be seen that for process (5.10d) both selection rules can be simultaneously satisfied, whereas for process (5.10b) they cannot. For the processes (5.10a) and (5.10c) the selection rules can only be satisfied with the special arrangement of three collinear phonons. Up to this point it has been assumed as a result of the low temperature and the fact that $|k_2| \approx |k_3|$, that the material could be assumed to be dispersionless. Although this is true to a first approximation, there will be a very small dispersion. Even though this dispersion is very small, it is sufficient to ensure that the spheres in Figures (5.2a) and (5.2c) do not quite touch. Thus the only one of the processes (5.10) which satisfies the selection rules is (5.10d). Therefore on the basis of the arguments advanced up to this point it may be concluded that, in the intermediate region, longitudinal acoustic waves cannot be attenuated by thermal phonons having energies of $\sim k_B T$, via three phonon processes. However such a process is possible for shear waves. This conclusion was originally reached by LANDAU and RUMER (1937).

Several processes which might cause the attenuation of a longitudinal wave have been considered by various authors. For four phonon processes the selection rules can be satisfied. POMERANCHUK (1941) (1942) has shown that such processes cause an attenuation of a longitudinal wave which will depend on acoustic frequency and temperature as

$$\Gamma = A_1 \omega_1^2 T^7$$

where A_1 is a constant for a given material, which is a function of the quartic terms in the expression for the elastic energy. ORBACH (1960) has shown that the attenuation arising from four phonon processes is, in general, very small.

SLONIMSKII (1937) has considered the interaction of low energy longitudinal acoustic phonons with thermal phonons of approximately the same frequency. Such interactions are not subject to the same restrictions as those between acoustic phonons and thermal phonons having energies of $\sim k_B T$. ORBACH (1960) and SIMONS (1961) have criticised the treatment of Slonimskii, and shown that the attenuation of a longitudinal wave caused by this mechanism can be represented by an expression having the form

$$\Gamma = A_2 \omega_1^4 T$$

Orbach has also shown that the attenuation would, in general, be very small.

HERRING (1954) has shown that in some circumstances the anisotropy of a crystal can modify the effects of the selection rules and permit processes which would be forbidden

in an isotropic material. It can be seen in general terms from the construction above, that if the wave vector surfaces had complicated shapes they might intersect when spherical surfaces would not. The attenuation resulting from this process will vary as

$$\Gamma = A_3 \omega_1^2 T^3$$

in the case of the crystal class (6 mm) to which the materials of interest belong.

In general, the attenuation of a longitudinal wave as a result of the above processes is small. Further the predicted temperature and frequency dependencies do not agree with the results of the present and other measurements. It is therefore necessary to look for another process to account for the attenuation of longitudinal waves.

In the case of shear waves however, interaction with thermal phonons having energies of approximately $k_B T$, via process (5.10d), has been shown to satisfy the selection rules. LANDAU and RUMER (1937) have obtained an expression for the attenuation to be expected as a result of this process, and have shown that it has the form

$$\Gamma = B(\delta) \omega_1 T^4. \quad (5.11)$$

where δ is a function of the lattice anharmonicity. An account of a similar calculation is given in Appendix A.

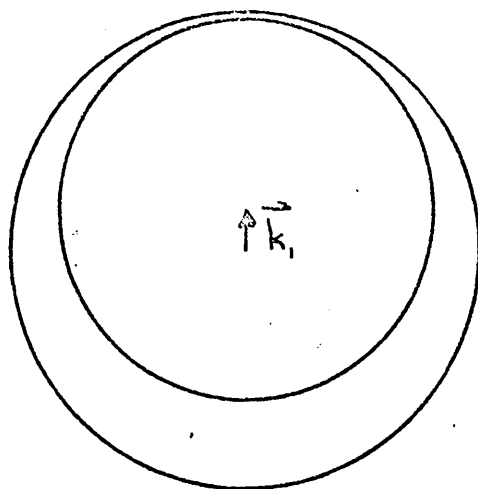
The same general expression is obtained for all the processes (5.10). The processes will not however occur if they do not satisfy the selection rules.

Mainly as a result of interactions involving only thermal phonons, the lifetimes of the thermal phonons are limited. As a consequence of its finite lifetime (τ_t) the energy and the crystal momentum of a thermal phonon will be uncertain. SIMONS (1963) (1964) and MARIS (1964) have considered the processes (5.10a) to (5.10c), which do not appear to satisfy the selection rules. They argued that if the uncertainties in the energies and crystal momenta of the thermal phonons ^{are} ~~is~~ greater than the amounts by which the selection rules are not satisfied, then the processes can not be considered to be forbidden by the selection rules. These processes will give rise to attenuations which can be represented by the expression (5.11). The effect of uncertainty in the thermal phonon crystal momentum on the Herring constructions has been illustrated in Figure (5.3) for the case of processes (5.10a) and (5.10c).

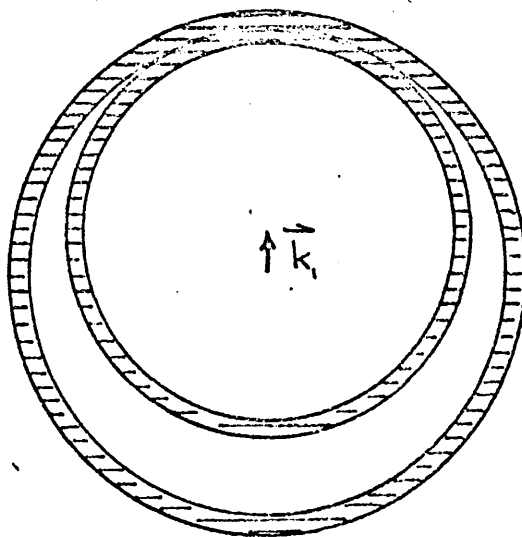
As the temperature varies the lifetime of the thermal phonons will vary, as will the uncertainty in their energies and crystal momenta. This has an interesting effect on the above argument concerning the selection rules. The effect can be illustrated by the following argument which is similar to that given by MARIS (1964). It is convenient to

Figure(5.3) EFFECT OF UNCERTAINTY IN THERMAL PHONON CRYSTAL MOMENTUM ON THE HERRING CONSTRUCTIONS

FOR PROCESSES (5.10a) AND (5.10c).



(a) $T_E \rightarrow \infty$



(b) T_E IS FINITE

consider the processes (5.10a) and (5.10c). The uncertainty in the thermal phonon energy is $\sim \frac{\hbar}{\tau_t}$, and the uncertainty in the crystal momentum $\sim \frac{\hbar}{v_s \tau_t}$. Where τ_t is the phonon lifetime and v_s is the appropriate velocity. As $T \ll \theta_D$ and $|k_2| \approx |k_3|$ the dispersion will be very small, so the true velocity dispersion relationship can be replaced by that for a linear chain of atoms namely

$$(v_s)\omega_2 = (v_s)_0 \cdot \frac{2(v_s)_0}{\omega_2 L} \cdot \sin \frac{\omega_2 L}{2(v_s)_0} \quad (5.12)$$

where L is the atomic spacing, and $\omega_2 \approx \omega_3$.

As $\frac{\omega_2 L}{2(v_s)_0} \ll 1$, Equation (5.12) may be written after expanding

$$\sin \frac{\omega_2 L}{2(v_s)_0} \text{ as}$$

$$(v_s)\omega_2 \approx (v_s)_0 - \frac{\omega_2^2 L^2}{24(v_s)_0} \quad (5.13)$$

From Equations (5.4), and (5.6), the minimum separation of the spheres in the Herring construction for processes (5.10a) and (5.10c) is

$$\omega_1 \left[\frac{1}{(v_s)\omega_2} - \frac{1}{(v_s)_0} \right] \quad (5.14)$$

From Equation (5.13) and (5.14) the separation can be written as

$$\frac{\omega_1 \omega_2^2 L^2}{24 (v_s)_0^3}$$

Thus in order that the selection rules should not be effective τ_t must have such a value that

$$\frac{1}{v_s \tau_t} > \frac{\omega_1 \omega_2^2 L^2}{24 (v_s)_0^3} \quad (5.15)$$

(where $\frac{1}{v_s \tau_t}$ is the uncertainty in the thermal phonon wave vector.)

The effect of this condition can be seen more clearly if ω_2 is replaced by $\frac{k_B T}{\hbar}$. It was shown previously that the phonon distribution is strongly peaked at an energy close to $k_B T$. This approximation is sometimes called the 'dominant phonon' approximation. Making this approximation the inequality (5.15) becomes

$$\frac{1}{v_s \tau_t} > \frac{\omega_1 L^2 k_B^2 T^2}{24 (v_s)_0^3 \hbar^2} \quad (5.16)$$

The fact that $\frac{\omega_2 L}{(v_s)_0} \ll 1$, was used in obtaining equation (5.13). Replacing ω_2 by $\frac{k_B T}{\hbar}$ this inequality becomes

$$\frac{L k_B T}{\hbar (v_s)_0} \ll 1 \quad (5.17)$$

From the inequalities (5.16) and (5.17) it is seen that when $\omega_1 \tau_t \approx 1$ the uncertainty in the wave vectors of the

thermal phonons must cause the surfaces of the Herring construction to overlap very substantially. As was discussed at the start of this chapter the condition $\omega\tau_t \approx 1$ sets the upper limit of the intermediate region, therefore at least in the higher temperature part of the intermediate region the selection rules will be satisfied. Under these conditions the attenuation should behave in the manner indicated by Equation (5.11).

In general the thermal phonon lifetime will increase more rapidly than T^{-2} as the temperature is reduced, so that at sufficiently low temperatures the inequality (5.16) will not be satisfied and the processes (5.10a) and (5.10c) will be forbidden by the selection rules. For process (5.10d) there will be no lower limit of the type discussed above. The amount by which the process (5.10b), fails to satisfy the selection rules is much larger than for processes (5.10a) and (5.10c), consequently the lower limit of the region in which this process is possible will occur at a higher temperature. In fact the process may not be permitted at any temperature.

In connection with the interpretation of the measurements, it is of interest to consider the variation with frequency, of the limiting temperatures of the regions in which the processes (5.10a) and (5.10c) may occur.

The lower limit is set approximately by the inequality (5.16), from which it is seen that as ω_1 increases the limiting value of τ_t must decrease i.e. the limit occurs at higher temperatures. The upper limit is $\omega_1 \tau_t \approx 1$, from which it is obvious that as ω_1 increases τ_t must decrease i.e. the limit again occurs at higher temperatures. Thus as the acoustic frequency increases the whole region moves upwards in temperature.

Treatments have been given by KWOK, MARTIN and MILLER (1965) and GUREVICH and SHKLOVSKII (1967) of the attenuation of acoustic waves at those temperatures at which the processes (5.10a) and (5.10b) are forbidden by the selection rules. The basis of this approach would appear to be that by using powerful thermodynamic Green's function techniques it is possible to extend the perturbation treatment to take account of higher order process involving the cubic anharmonicity.

The account of these higher order processes given below concentrates on their relation to the selection rules, a feature not discussed in previous treatments. A second order three phonon process might be viewed as two successive first order processes. The key to the operation of a process of this type would seem to be that the intermediate state should be short lived.

Provided that the intermediate phonon is sufficiently short lived, the uncertainty in its energy would be larger than any amount by which energy was not conserved in the two first order processes making up the second order one. Such a process is illustrated diagrammatically below.

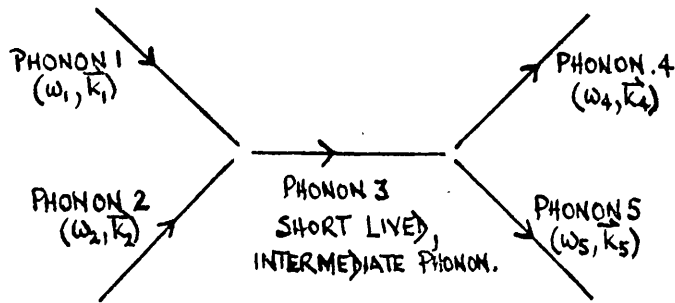


Figure (5.4) DIAGRAMMATIC REPRESENTATION OF SECOND ORDER THREE PHONON PROCESS

A process of this type would seem to have a number of interesting features. There are four long lived phonons, so that in the long term the process is able to satisfy the selection rules. However because the process proceeds via two three phonon processes the larger cubic rather than quartic anharmonicity will control the transition rates, so that the attenuation will be correspondingly larger. Because there is little restriction on the energy of the intermediate phonon, there will be a large number of possible

intermediate paths for the process. That is the second order processes are capable of simultaneously satisfying the selection rules and causing substantial attenuation.

Second order processes are possible in which the first of the first order processes has the form of any of the processes (5.10). Of particular interest in the present context are second order processes which lead to the attenuation of longitudinal waves, i.e. those in which the initial first order process has the form of processes (5.10a) or (5.10b). The work of Kwok, Martin and Miller and Gurevitch and Shklovskii, mentioned previously, shows that the attenuation resulting from such processes is expected to show two asymptotic regions. At high temperatures, provided $\omega, \tau_t \gg 1$, the attenuation is expected to vary as ω, T^4 , in agreement with the discussion above in terms of first order processes. At low temperatures both types of second order process are expected to result in an attenuation which is independent of frequency, but a difference in the temperature dependence is predicted. The process in which the initial first order process has the form of (5.10a), is expected to lead to an attenuation varying as T^7 ; whereas the attenuation resulting from the other type of process is expected to vary as T^9 . However SHIREN (1966) and KLEIN (1966) have shown that dispersion

and the anisotropy of the lattice anharmonicity can effect the form of the attenuation in the lower temperature region. A further difficulty in comparing theory with experiment, is that the range of temperatures in which the low temperature asymptotic behaviour occurs is very low in many materials. This results in the attenuation being so low that any measurements are subject to considerable uncertainty.

5.5 Summary of the Predicted Behaviour of the Acoustic Attenuation

The object of this section is to collect together the various predictions made in the course of the previous section, concerning the temperature and frequency dependence of the acoustic attenuation resulting from three phonon processes. These predictions may conveniently be divided into three groups. Those involving (a) the temperature dependence of the attenuation, (b) the frequency dependence of the attenuation and (c) the upper and lower temperature limits of the Landau-Rumer or T^4 regime. The present summary is restricted to the behaviour of the attenuation of longitudinal waves. In certain cases, i.e. when process (5.10d) is the dominant one, the attenuation of shear waves will behave differently at the lowest temperatures. This situation is treated in the fuller discussion of the previous section. Only longitudinal waves are considered here because the only measurements for which detailed results are presented in

Chapter 7, were made with longitudinal waves.

The attenuation is expected to show two asymptotic regimes. In the higher temperature regime it is anticipated that the attenuation will vary as the fourth power of the temperature, as predicted in Appendix A from a consideration of first order three phonon processes. The thermal phonon lifetime is expected to increase with decreasing temperature in such a manner that a situation is reached in which the uncertainty in the thermal phonon wave vector is less than the amount by which the selection rules are not satisfied. In this condition the first order process is forbidden by the selection rules, and it is necessary to consider higher order three phonon processes. The treatment including the effects of higher order processes, yields the same results in the high temperature regime as those obtained in Appendix A by considering only first order processes. This treatment predicts that the attenuation should also exhibit a lower temperature asymptotic region in which the attenuation varies as T^7 or T^9 depending on the nature of the process responsible for the attenuation.

It is anticipated that the attenuation should vary linearly with the acoustic frequency in the higher temperature or Landau-Rumer regime. In the lower temperature regime the attenuation is expected to be independent of frequency.

Both the upper and lower temperature limits of the

Landau-Rumer or higher temperature asymptotic regime, are expected to increase as the acoustic frequency increases.

Chapter 6 EXPERIMENTAL ASPECTS OF ACOUSTIC ATTENUATION
MEASUREMENTS AT LOW TEMPERATURES

6.1 Introduction

This chapter describes the experimental aspects of a series of measurements of acoustic attenuation as a function of temperature, carried out in the temperature range 15-120°K; at frequencies of 1.0, 3.6 and 8.8 GHz. Measurements were made on zinc oxide, cadmium sulphide and cadmium selenide.

The form of the chapter is described below. In Section (6.2) the basic form of the microwave systems is discussed. This is common to all three systems. Sections (6.3) and (6.4) contain detailed descriptions of ^{the} X, S and L band systems. In Section (6.3) the particular problems of making measurements on short rods are considered. The specially designed cryostats used in the low temperature measurements are described in Section (6.5). Especial attention is paid to the methods of temperature measurement and control. The method of preparing specimens is described in Section (6.6). Properties of the crystals from which specimens were prepared are also discussed; for example the resistivity of the material, and the presence of local strain in the crystals. The method of making attenuation measurements is described in Section (6.7). For a particular specimen and acoustic frequency a minimum attenuation is defined, below which any measurements are considered to be of doubtful value.

6.2 General Description of the Microwave Systems

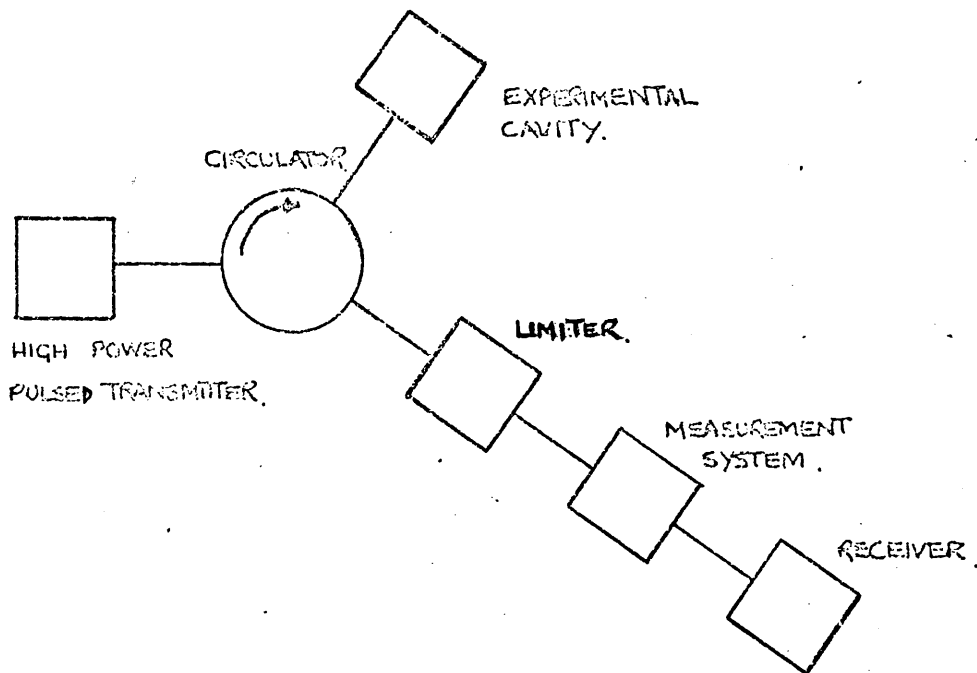


FIGURE 6.1 GENERALISED BLOCK DIAGRAM OF MICROWAVE SYSTEMS

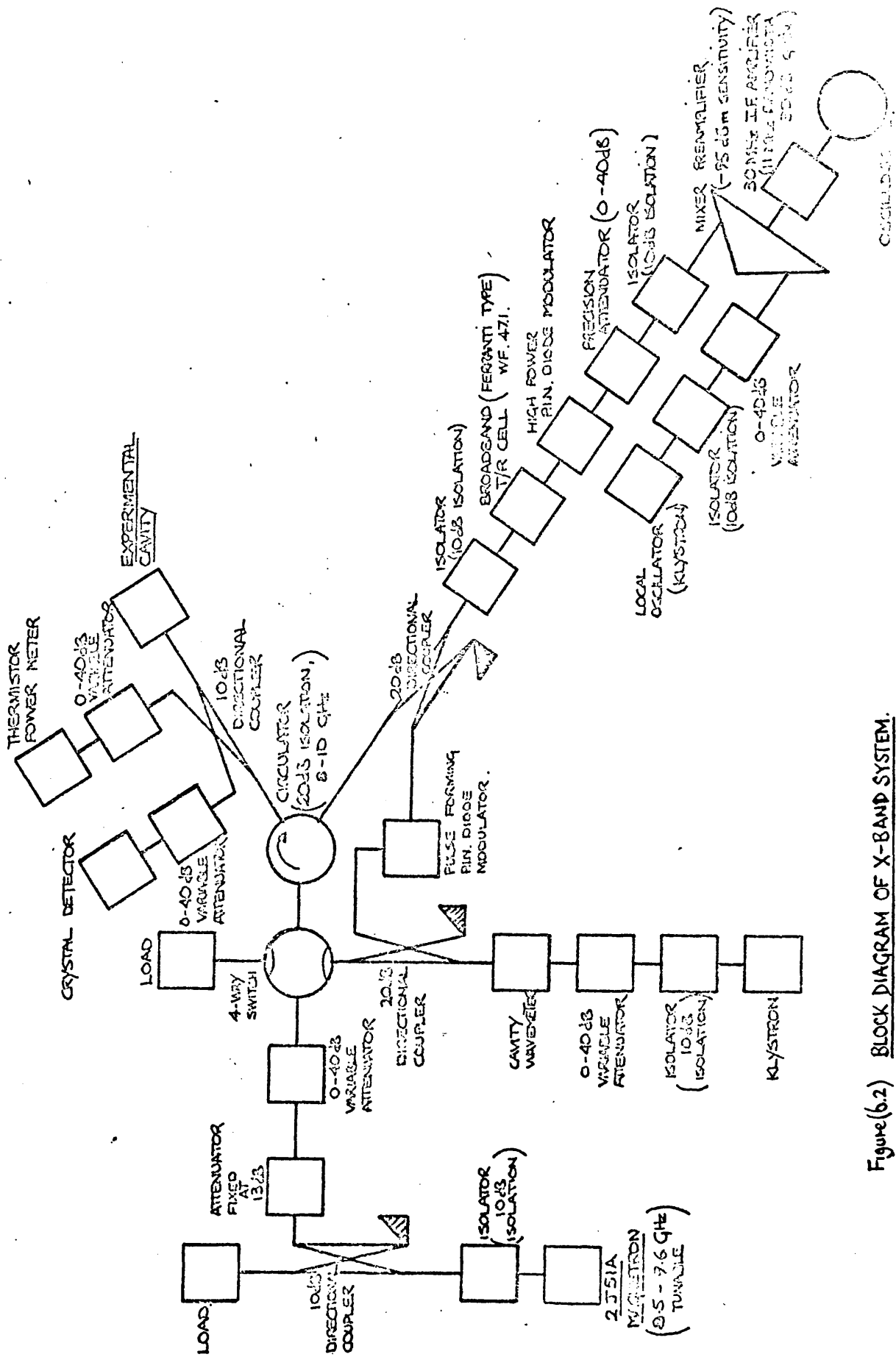
A separate microwave system was developed for each of the three frequencies at which measurements were made. These systems were basically similar but showed considerable variation in detail. They were used to launch the microwave frequency acoustic pulses by surface excitation, into rods of the materials of interest; and to receive the signals resulting from successive reflections of the acoustic pulses. Each of the systems was designed to have a large dynamic range, to permit measurements over a wide range of acoustic attenuation. This was achieved by using a high power pulsed

transmitter and a sensitive heterodyne receiver. The acoustic system was one-port in character, and it was therefore necessary to protect the receiver while the transmitter was firing. This was arranged by using a combination of a circulator and a limiter (Figure (6.1)). Measurements of the relative amplitudes of the signals or echoes from the specimens, were made by comparison methods using precision attenuators. The particular method employed varied from system to system.

6.3 X-Band microwave system

Figure (6.2) is a detailed block diagram of the X-band system, which was assembled using waveguide components. Figure (6.3) is a general view of the apparatus. A type 2J51A magnetron tunable over the range 8.5 to 9.6 GHz, was used as the transmitter. In normal operation the magnetron produced a peak power of about 60kW. In order to reduce the difficulties associated with this high level of peak power the magnetron was run close to its lowest stable output, at about 20kW peak power. This was arranged by using the minimum magnet field and reducing the amplitude of H.T. pulse applied to the magnetron.

The magnetron was driven from a standard radar transceiver (Decca type 625) which had been suitably modified. Three main modifications were needed. Firstly the adjustment of the amplitude of the driving pulse as indicated above. Secondly the reduction of the driving pulse length to 0.2 μ sec, which



Figure(6.2) BLOCK DIAGRAM OF X-BAND SYSTEM.

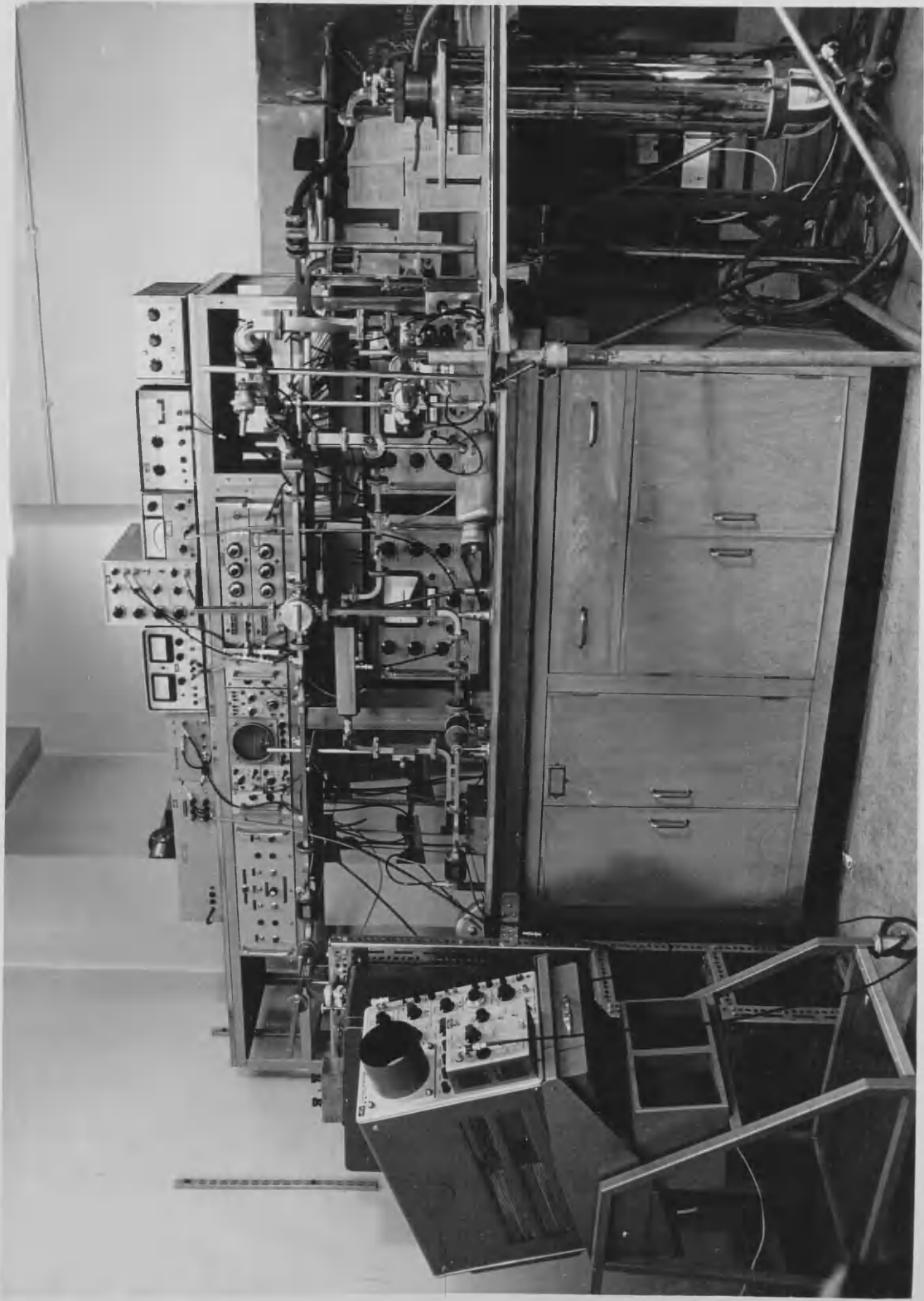


Figure (6.3) GENERAL VIEW OF X-BAND APPARATUS.

was the shortest well shaped pulse produced by the magnetron. This shorter pulse was needed to avoid overlap of successive echoes when making measurements with short specimens. Thirdly the circuit was modified to permit external triggering of the transceiver. This made it possible to arrange for the magnetron firing to be synchronized with the 1000 Hz power supply to the transceiver from a motor alternator, thus reducing the effect of pick up from this supply. An additional advantage of external triggering was that it made it possible to trigger the oscilloscope time-base before the magnetron fired. A difficulty arose when it was found that the transceiver could not be externally triggered at 1000 Hz, this was circumvented by the use of a frequency divider ($\div 10$). A pulse amplifier was needed to provide a sufficiently large pulse to trigger the transceiver. The complete triggering arrangement for the system is shown diagrammatically in Figure (6.4). The trigger to the pulse forming P.I.N. diode modulator was used to trigger the high current pulser in the deformation potential amplifier experiments.

In order to avoid breaking down the glass vane attenuators used to adjust the input microwave power to the cavity, a directional coupler was used as a 10 dB pad in the manner shown in Figure (6.2). The first attenuator was fixed at 13 dB to avoid the peak input power to the cavity exceeding 100W, as it was found that the cavity broke down if this power was greater than about 200W.

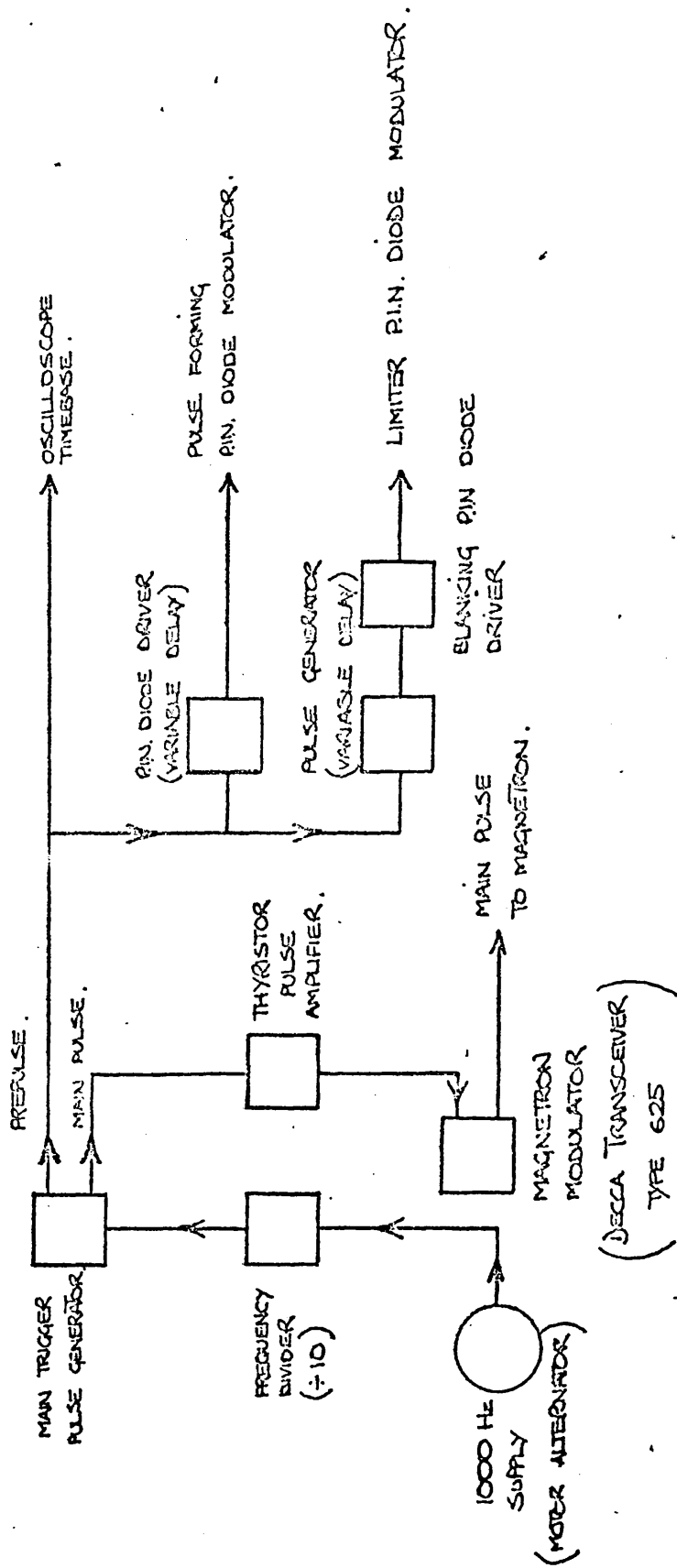


Figure (b4) TRIGGERING ARRANGEMENT FOR X-BAND SYSTEM.

The waveguide switch made it possible to switch conveniently between the magnetron and a klystron as the source of power. The functions of the klystron were purely diagnostic. When operated as a swept frequency source the klystron could be used in conjunction with the crystal detector and the wavemeter to check the Q and resonant frequency of the cavity at low temperatures. Using the klystron as a fixed frequency source in conjunction with the pulse forming P.I.N. diode modulator and the receiver it was possible to readily check the recovery time of the limiter under operating conditions, an important factor when making measurements on short specimens. This check was carried out as indicated below. When the waveguide switch was switched to the magnetron, the two 20 dB directional couplers (Figure(6.2)) still provided a path by means of which signals from the klystron could reach the receiver. These signals arrived at the receiver via the limiter, in addition to those arising from the magnetron pulse. The pulse forming P.I.N. diode modulator was used to provide pulses of power from the klystron, the delay of which could be adjusted with respect to the firing of the magnetron. The delay of the klystron pulse with respect to the breakthrough pulse from the magnetron was reduced and the attenuation of the klystron pulse noted. In this manner it was possible to make a good estimate of the recovery time of the limiter. The recovery time was found to be approximately 0.5μsec (to 0.1 dB attenuation). A further use of the klystron was in making a rapid approximate check of

the receiver sensitivity. This was particularly valuable if the receiver had been inadvertently exposed to an excessive amount of breakthrough, thus possibly damaging the mixer diodes. The first step in the check was to set the klystron output at some known level (usually 1mW), with the aid of the power meter. Then using the P.I.N. diode modulator to produce pulses of power, the relevant attenuators were adjusted until the signal was about twice the amplitude of the noise, on the display. The sensitivity was then readily obtained in -dBm. With undamaged diodes this was in the range -90 to -95 dBm.

When the magnetron was tuned to the cavity resonant frequency the circulator provided 20 dB isolation between the transmitter and receiver, over the tuning range of the magnetron. The four port directional coupler between the circulator and cavity (Figure (6.2), made it possible to measure the input power to the cavity and to monitor the reflected power from the cavity. The cavity was of the re-entrant coaxial type, details of which are given later. No provision was made to tune the cavity resonant frequency, the procedure being to tune the transmitter to the resonant frequency of the cavity. The initial tuning stage was to measure the resonant frequency using the klystron and the wavemeter. Fine tuning was affected by using the tuning facility of the magnetron to minimise the reflected power indicated by the crystal detector.

The circulator did not isolate the receiver sufficiently from the magnetron to prevent paralysis of the receiver and damage to the mixer diodes. Consequently while the magnetron was firing additional isolation was provided by the limiter. The limiter consisted of a T/R cell followed by a high power P.I.N. diode modulator. The T/R cell was a special development type obtained from Ferranti Limited, which operated over the whole tuning range of the magnetron and had a fast recovery time. The P.I.N. diode modulator was needed to prevent that initial part of the breakthrough pulse not reflected while the T/R cell was switching on, from damaging the mixer diodes. The particular type of P.I.N. diode modulator used had the advantage that the power needed to damage it was high ($\sim 100W$ peak). However when driven with a square voltage pulse it was found to have a very long recovery time of approximately $10\mu\text{sec}$. It was found possible to shorten this time to $\sim 0.5\mu\text{sec}$, by arranging that the negative driving pulse had a positive spike of about $10V$ on the trailing edge. The method of checking the limiter recovery time during a run has been described above.

Comparison of the amplitudes of the echoes from the specimen were made by a comparison method, which is described later, using a precision attenuator. The resetting accuracy of the attenuator was about ± 0.1 dB. For reasons of mechanical convenience a high quality glass vane attenuator was used, which was compared from time to time with a rotary

vane attenuator. No discrepancy greater than 0.1 dB was detected.

An isolator was placed between the precision attenuator and the receiver in order to improve the low (~ 6 dB) isolation between the local oscillator and the main line. This virtually eliminated any possibility of power from the local oscillator entering the main line, being reflected and effecting the measurements.

The mixer-preamplifier was a standard item, its characteristics

were	Operating Range	8.2-12.4 GHz
	Noise figure	6.5 dB
	Intermediate frequency	30 MHz
	I.F. gain	20 dB
	I.F. bandwidth	12 MHz.

After further amplification the video signals were displayed directly on a 30 MHz oscilloscope.

For the X-band measurements a cavity was used in order to produce the intense electric field at the end of the specimen required to launch an acoustic wave of significant amplitude. The type of cavity chosen was the re-entrant coaxial one described by HANSEN (1939), which has been used for this purpose by a number of workers. The high electric field region in this type of cavity is found in the gap between the top of the post and the end of the cavity.

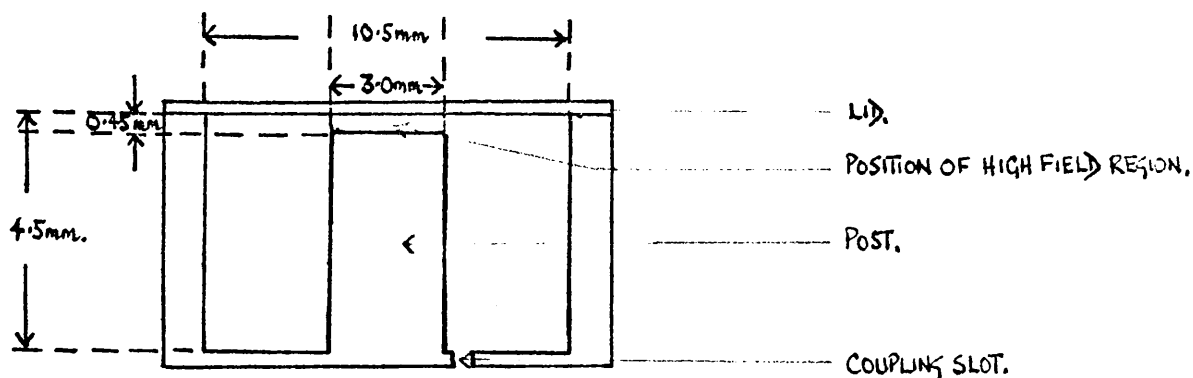


Figure 6.5 RE-ENTRANT COAXIAL CAVITY

Figure (6.5) shows the dimensions of the re-entrant cavity, the post diameter of 3mm, was chosen so that it would be larger than the 'diameter' of the smaller cross-section specimens (Section 6.6)). As a result if such a specimen were mounted with its end surface close to the top of the cavity post, the electric field would be predominantly normal to this end surface. Thus because the end surface is only exposed to a very small fringing field, the amplitude of any unwanted modes launched as a result of the fringing field would be correspondingly small. Given the diameter of the post, the remaining dimensions were chosen using the design data given by MORENO (1958) so that the resonant frequency of the cavity was 9.5 GHz. Coupling to the cavity was effected by cutting a narrow straight slot in the base of the cavity as shown in Figure (6.5), the length of the slot was slowly increased until the cavity was just undercoupled.

The cavity was machined from brass, and had a relatively low Q of about 300. The advantage of a relatively low Q was that the dimensional changes caused by making measurements at a series of different temperatures, had a smaller detuning effect than would have been the case with a cavity of higher Q .

For the reasons outlined in Section (6.6) the specimens were of two different cross-sectional areas. Two different methods of mounting the specimens were needed as it was required to excite only part of the face of the larger specimens in order to reduce the influence of the non-parallelism of the ends .

SMALL CROSS-SECTION ROD

LARGE CROSS-SECTION ROD

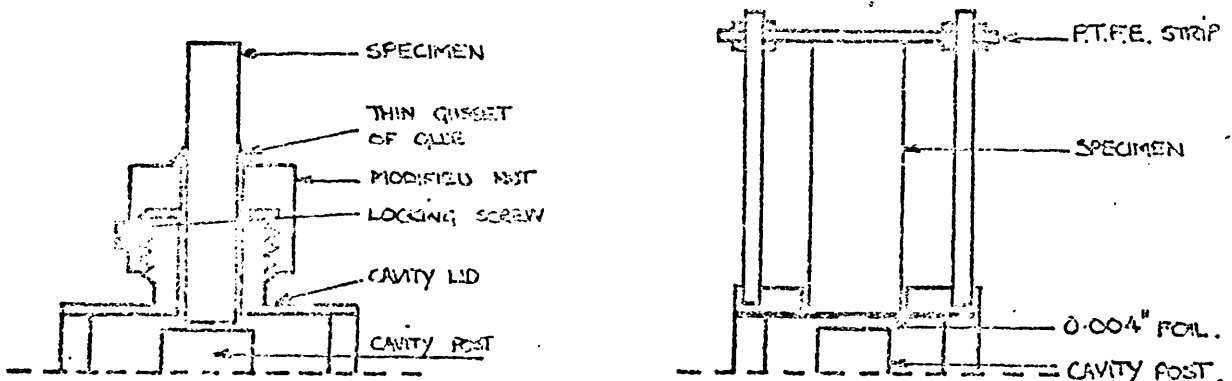


FIGURE (6.6) EXCITATION ARRANGEMENTS FOR X-BAND APPARATUS

Figure (6.6) illustrates both methods of mounting. The smaller cross-section rods were glued into modified 4BA nuts. Glue was used as the rods were too small to be conveniently held mechanically. The problem with this method is that inserting the specimen into the high electric field region of

the cavity causes a substantial change in the resonant frequency of the cavity. The mounting procedure was to screw the nut containing the specimen onto the screwed part of the cavity lid until the resonant frequency of the cavity was 8.9 GHz. The position of the nut was then locked with a grub screw. Measurement and approximate calculation showed that for the specimen size and dielectric constants involved, at a resonant frequency of 8.9 GHz the end of the specimen was just above the top of the cavity post. This ensured a substantially normal electric field at the end of the rod without damaging the highly polished face.

The sketch of the second arrangement is thought to be self explanatory. This method had the disadvantage that an unwanted mode was weakly excited, but this did not effect the measurements as it was not used with short specimens (Section (6.6)) The advantage of the method was that it reduced the cross-sectional area of the acoustic beam without cutting the specimen into small pieces.

6.4 S and L Band Microwave Systems

Figure (6.8) is a block diagram of the S-band microwave system, which was assembled using coaxial components. Figure (6.9) is a general view of the complete apparatus. The high power pulsed oscillator, consisted of type 2C39A planar triode mounted in a cavity resonator. This oscillator was one of several constructed in the Department by J. Richter for operation at frequencies around 1 GHz. It was necessary to

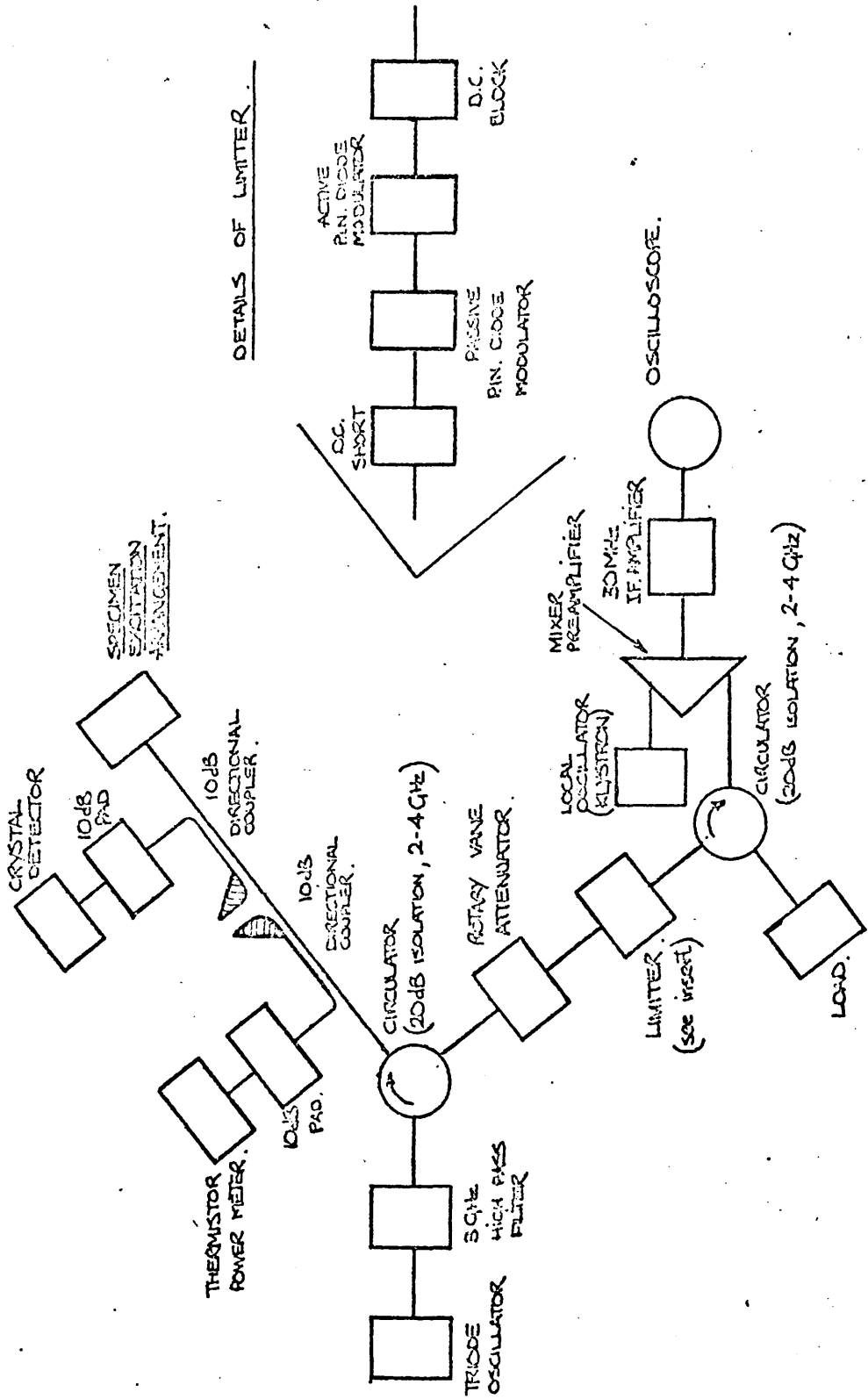


Figure (6.8) BLOCK DIAGRAM OF S-BAND SYSTEM

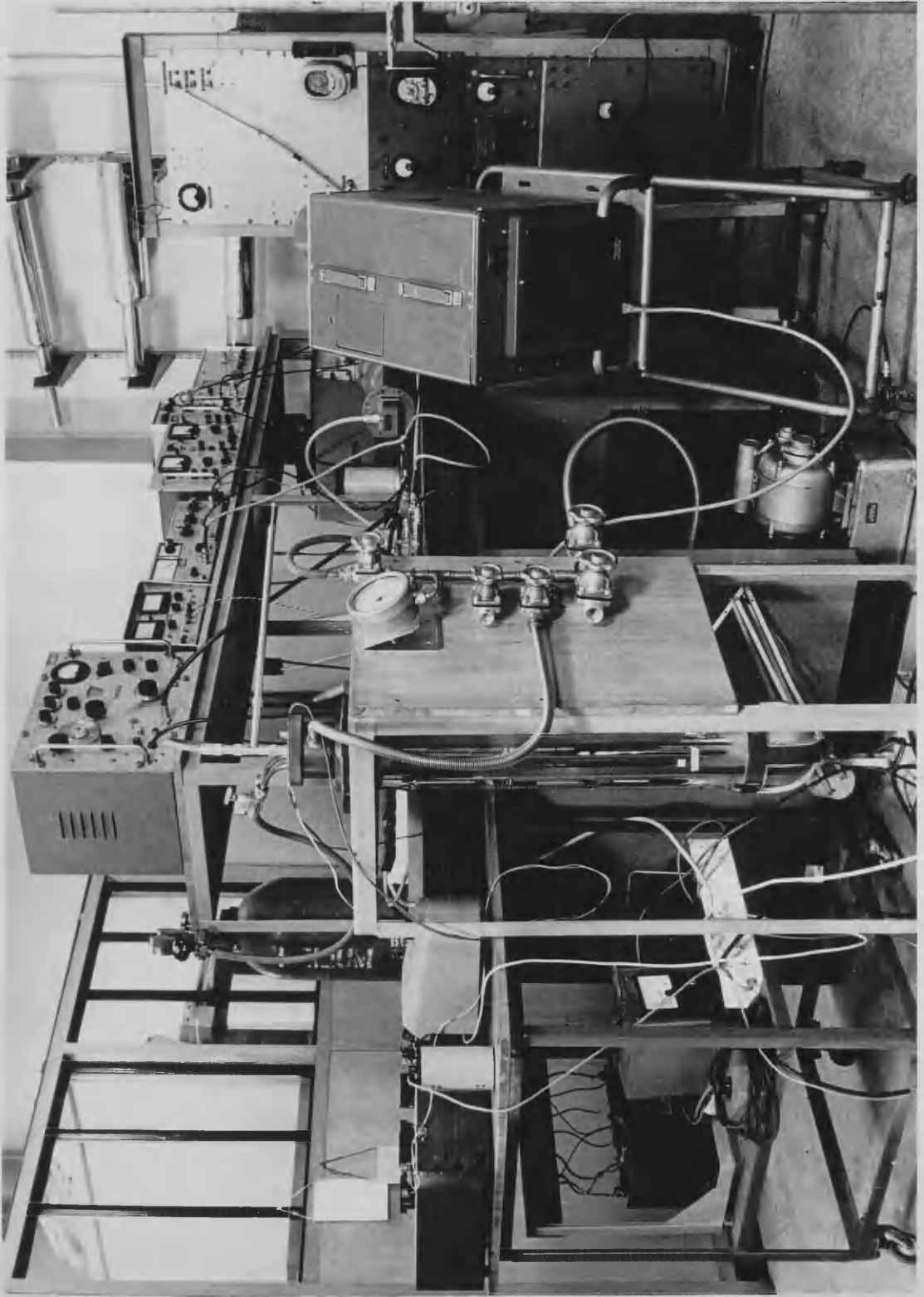


Figure (69) GENERAL VIEW OF S-BAND APPARATUS.

to change the length of the cavity and alter the feedback arrangement, in order to make this oscillator operate at 3.6 GHz. Full details of the design, construction, and mode of operation of this type of oscillator; together with details of the modulator used to derive it have been given by RICHTER (1966). The modulator driving the high power oscillator was triggered from the main pulse of a master pulse generator, via a trigger pulse amplifier. The repetition rate was 1000 Hz, and the r.f. pulse length 0.7 μ sec.

The length of the anode cavity of the triode oscillator was such that it must have been operating at the fifth harmonic of the cavity, i.e. the cavity fundamental was 720 MHz. Despite the preferential selection of a particular harmonic by the feedback arrangement, there was some possibility of a small amount of power being generated at the first (720 MHz) and third (2160 MHz) harmonics of the oscillator. The seventh harmonic at 5040 MHz was above the cut-off frequency of the triode (4 GHz). To attenuate the lower harmonics, a 3GHz high pass filter was placed in front of the oscillator.

The circulator, crystal detector, and power meter, fulfilled the same roles as the comparable components in the X-band system.

The arrangement for producing an intense electric field at the surface of the specimen was the same for both the S and L band systems. The method was to place the end of the specimen

in contact with the centre conductor of an open-circuited transmission line, and use a stub tuner to produce the maximum voltage across the open-circuited termination. The specimen mounting arrangement is illustrated in Figure (6.7).

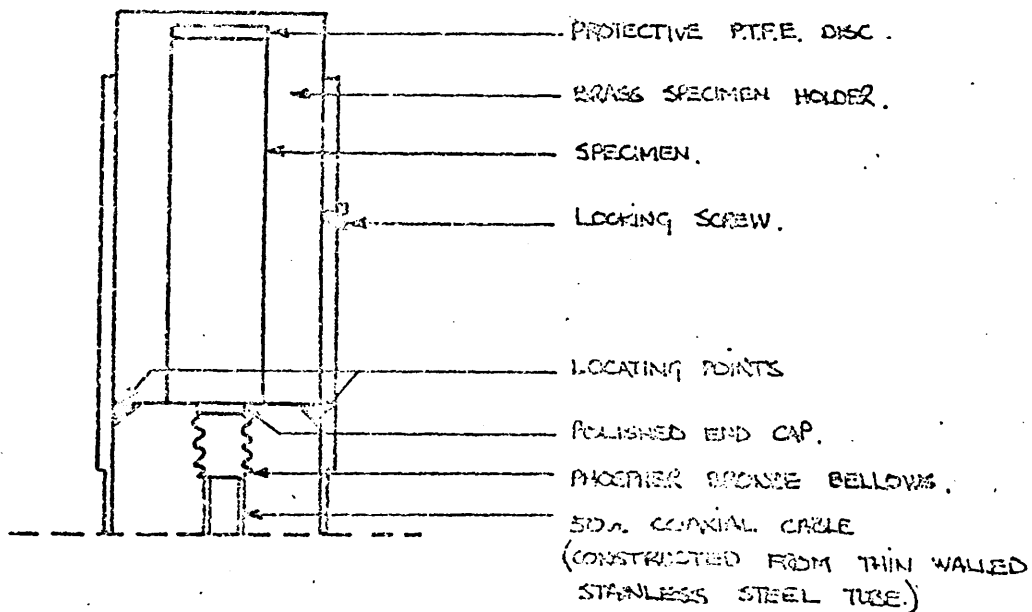


FIGURE 6.7 EXCITATION ARRANGEMENT FOR S AND L BAND APPARATUSES

The position of the locating points ensured that the bellows was slightly in compression, and therefore that the polished cap was in good contact with the end surface of the specimen. The method of tuning was simply to tune the stub tuner for maximum echo height on the oscilloscope display. As was expected, using this method an unwanted mode was weakly excited, however this was not ~~troublesome~~ ^{troublesome} as the method was not used with short specimens.

A waveguide rotary vane attenuator was used for the comparison of echo amplitudes, as no coaxial attenuator of sufficient precision appeared to be commercially available.

The components of the limiter are given in Figure (6.8). The passive P.I.N. diode allowed an initial spike of power to pass in the same manner as a T/R cell, so that a second active P.I.N. diode modulator was required. The d.c. short was needed to obtain the correct bias conditions for the passive P.I.N. diode. The d.c. block acted as a high pass filter which removed the substantial amount of noise generated at the intermediate frequency of the receiver, by switching the P.I.N. diodes. The active P.I.N. diode modulator was driven by a pulse generator which was capable of providing the 100 mA pulses needed for this purpose. This pulse generator was triggered by the trigger output of the master pulse generator. When driven by a square voltage pulse, the recovery time of the active P.I.N. diode modulator was approximately 2 μ sec. As only long specimens were measured with the L and S band systems, this recovery time was quite adequate and no special driving pulse was required.

The second circulator was used as an isolator, to increase the main line to local oscillator isolation, for the reasons outlined in the account of the X-band system.

The mixer-preamplifier was one which had been built in the department, it had the following characteristics.

operating range	2.0-4.0 GHz
noise figure	8 dB
intermediate frequency	30 MHz
I.F. gain	30 dB
I.F. bandwidth	6 MHz

After additional amplification the video signals were again displayed directly on a 30 MHz oscilloscope, the time-base of which was triggered from the trigger output of the master pulse generator.

The L band microwave system used was one built by J. Richter in the department, it has been fully described by RICHTER (1966).

6.5 Cryostats

The usual pair of glass dewars were used to contain the liquid helium. The method by which the liquid helium was transferred from the storage dewar to the experimental cryostat was the standard one.

Reported measurements of acoustic attenuation made at low temperatures on other materials and later confirmed in the present measurements, showed the attenuation to be a very sensitive function of temperature. Therefore it was considered to be of great importance that the temperature measurements should be made as accurately as possible; and further that a temperature control system should be devised, rather than

arranging to allow the specimens to warm up slowly. The reasons for the choice of a platinum resistance thermometer are given in Section (3.3). In the same section details of the accuracy and reproducibility of this type of thermometer are given.

The objection to the technique of making measurements as the specimen warms up; is that while the cryostat warms up temperature gradients may be set up in it. Thus it is possible that the thermometer will be at a temperature significantly different from that of the specimen. In the present measurements even small temperature differences will be important. With a temperature control arrangement the following measurement procedure was possible. The initial attenuation measurement was made at a short interval of time (\sim 20 seconds) after the thermometer had reached the required reading. The attenuation measurement was repeated after a further short interval, the thermometer reading being the same. The fact that no difference between the two attenuation measurements was ever detected, was taken to indicate that the first time interval was long enough for any temperature difference to be sensibly eliminated.

Two specially designed low temperature assemblies were built, one for use with the X-band apparatus and the other for use with the S and L band apparatuses. These assemblies differed only in their microwave components. For this reason only the X-band assembly is described. This assembly is illustrated in Figure (6.10).

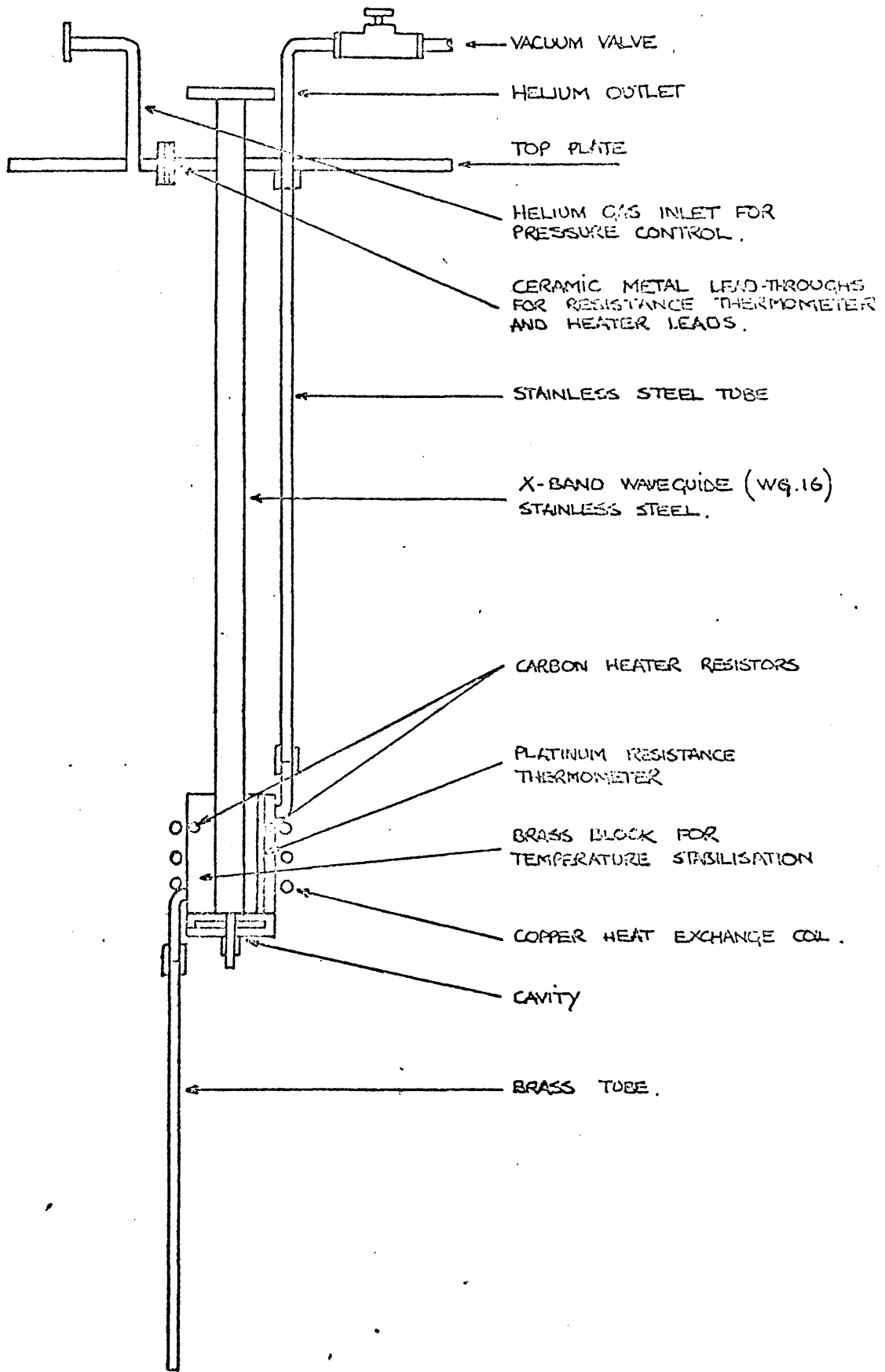


Figure (6.10) LOW TEMPERATURE ASSEMBLY FOR X-BAND APPARATUS.

The base of the microwave cavity was screwed into a brass block, through which a length of thin walled, stainless steel waveguide passed making a microwave connection between the cavity and the rest of the microwave system. The function of the brass block was to provide a large enough thermal capacity to prevent rapid fluctuations of the specimen temperature. Mounted in the brass block were two carbon heater resistors and the sensing element of the platinum resistance thermometer. The sensing element was slightly loose in its mounting hole at room temperature to allow for differential contraction on cooling. The importance of not changing the residual resistance of the sensing element by cold working is explained in Section (3.3).

A copper heat exchange coil was wrapped around the brass block. The upper end of the coil was attached to a thin walled, stainless steel tube, the other end of which could be closed by a vacuum valve. The lower end of the heat exchanger was connected to a brass tube, which was of such a length that when the assembly was screwed into place in the helium dewar, the open end of the brass tube was close to the bottom of the dewar. Apart from this composite exchanger tube, the components of the temperature control system were the heater and a pipe connecting the experimental helium dewar to a cylinder of helium gas. The function of this pipe was to enable the pressure of helium gas in the helium dewar to be raised above atmospheric when required.

The operation of the temperature control system is outlined

below. Liquid helium was transferred into the dewar until its level was a few inches below the brass block. In this condition the temperature controller had two modes of operation. The first was used when controlling the specimen temperature at a value fairly close to that of liquid helium, or when cooling the specimen rapidly. In this case control was achieved by opening the valve at the top of the exchanger tube and regulating the flow of helium gas from the cylinder to adjust the excess pressure in the helium dewar. The pressure in the dewar determined the specimen temperature as a result of controlling the height of the liquid helium in the brass tube and the flow of cold gas through the heat exchanger. The second mode of control was employed over most of the temperature range of interest, the required temperature was obtained by closing the valve at the top of the exchanger tube and balancing the heat flow down the brass tube by the power dissipated in the heater resistors.

The successful operation of the second mode of control depends on the brass tube having an appropriate thermal resistance. For the lower specimen temperatures of interest, the temperature gradient in the tube is small. Thus if the thermal resistance of the tube is too high, then the heat flow down the tube is small. This means that positive temperature fluctuations would take a long time to correct. However if the thermal resistance is too low then the heat flow required to maintain the specimen at the higher temperatures causes

the liquid helium to boil off at an unacceptably high rate.

The flow of helium gas from the cylinder in the case of the first mode of control, and the current to the heater resistors for the second mode; were controlled manually by a second operator using the resistance thermometer both as an indicator and a measuring instrument.

6.6 Specimens

The materials investigated were zinc oxide, cadmium sulphide and cadmium selenide. Hydrothermally grown zinc oxide crystals were obtained from Litton Industries, and vapour grown zinc oxide from the **3M** company. The cadmium sulphide and the cadmium selenide was vapour grown material. The sulphide was obtained from A.E.I. Limited and the Clevite Corporation, and the selenide from the Clevite Corporation.

The specimens studied were single crystals of the hexagonal form of these materials, having a structure belonging to the crystal class 6 m.m.

Attention was very largely concentrated on the piezoelectrically active acoustic modes along symmetry directions, commonly employed in acoustic-electric experiments and devices. These modes are the longitudinal mode propagating parallel to the c-axis, and the shear mode propagating along the a-axis and polarised parallel to the c-axis.

As the modes of interest were piezoelectrically active and the materials were semiconductors, acoustic attenuation caused by free current carriers was possible (HUTSON and WHITE (1962)). For this reason approximate measurements of the room temperature resistivity were made, under ambient illumination, on those crystals used in the acoustic attenuation measurements. The resistivity measurements were made by the usual four probe d.c. method, to eliminate the effects of contact resistance. Contacts were made by applying indium amalgam directly to freshly etched crystal surfaces. The voltage between the potentiometric contacts was measured with an electrometer. With the exception of one low resistivity crystal which will be considered separately later, the resistivity of all the crystals was $10^8 \Omega \text{ cm}$ or greater.

The theory of Hutson and White can be used to estimate the attenuation of the acoustic wave caused by free carriers. The attenuation is calculated below for the worst case, that of the longitudinal wave in zinc oxide. It is first necessary to calculate the values of the parameters ω_c and ω_D .

$$\omega_c = \frac{\sigma}{\kappa} = 1 \times 10^4 / \text{sec.} \quad (\text{if the resistivity is } 10^8 \Omega \text{ cm})$$

$$\omega_D = \frac{2V_s^2}{\mu k_B T} = 1 \times 10^{11} / \text{sec.}$$

this latter value depends on the assumption that the mobility (μ) is $100 \text{ cm}^2 / \text{Volt sec}$, which should be correct to within a factor of two.

As $\omega \gg \omega_c, \omega_p \gg \omega_c$, the expression for the attenuation given by Hutson and White (Equation (2.19) of their paper) reduces to

$$\Gamma = \frac{\omega_c K^2}{v_s \left[1 + \left(\frac{\omega}{\omega_p} \right)^2 \right]}$$

where K is the electromechanical coupling coefficient. It can be seen that the expression for the attenuation is only weakly dependent on the acoustic frequency ($\omega < \omega_p$).

Taking the value of v_s given by BATEMAN (1962) and the value of K given by CLAIBORNE, HEMPHILL and EINSBRUCH (1969), and assuming a frequency of 1 GHz.

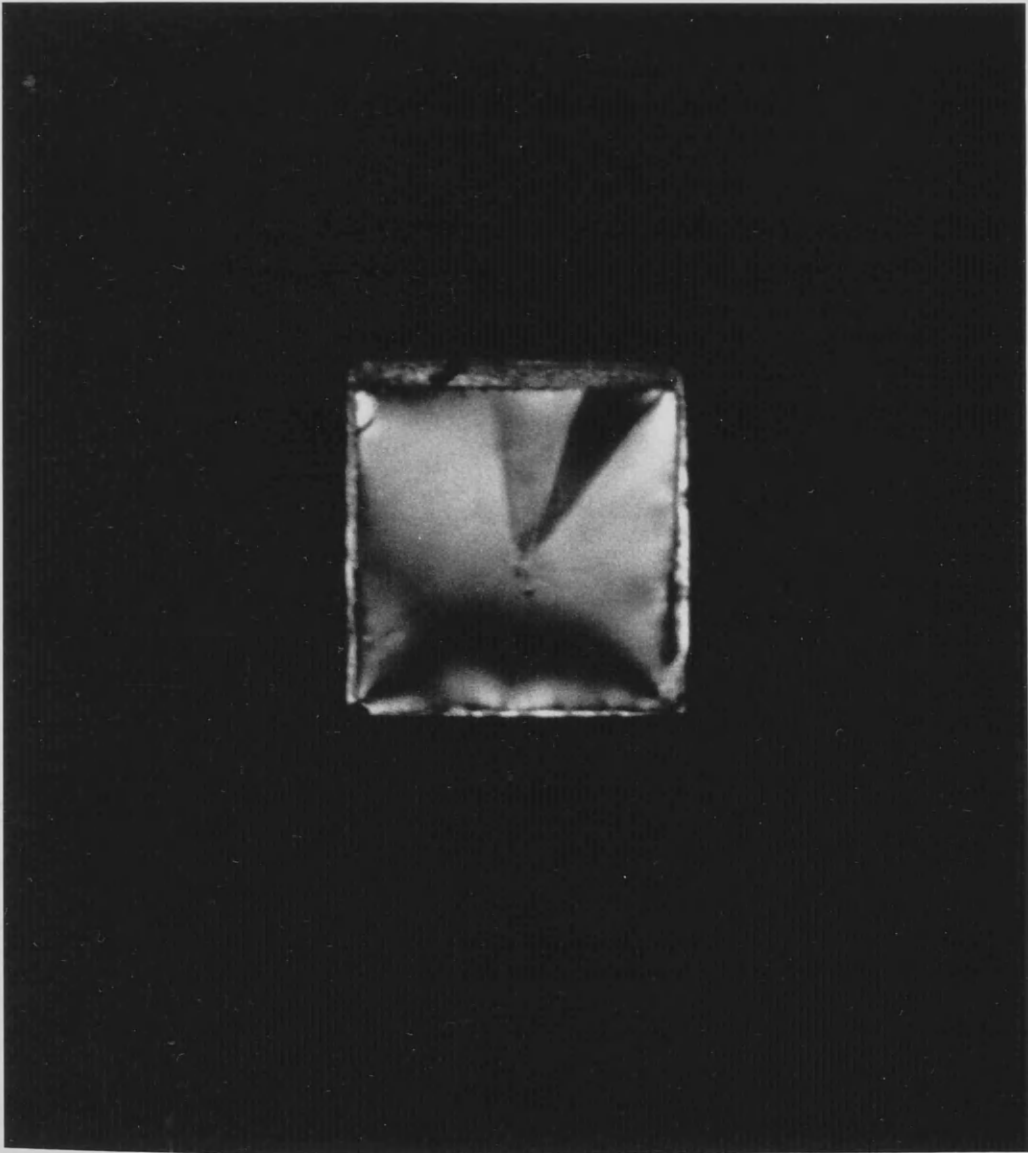
$$\Gamma = 1 \times 10^{-2} \text{ dB/cm}$$

This attenuation which is small enough to be neglected, represents the worst case. For other modes, materials, and frequencies, the attenuation will be smaller. This calculation is based on the measured room temperature resistivity, at the low temperatures at which the attenuation measurements were made the resistivity will probably be higher as a result of carrier 'freeze-out'. This will result in an even smaller attenuation caused by free carriers.

By utilising the photo-elastic effect, the crystals of interest were examined for local strain. The technique employed was the well known one of placing the crystal under test between crossed polaroids and making a visual inspection. Such an examination was carried out on the crystals of zinc

oxide and cadmium sulphide, but not on the cadmium selenide crystals as this material is opaque to visible radiation. Figure (6.11) is a photograph of a crystal examined in this manner. It shows the end face of a bar of low resistivity zinc oxide in which the axis of the bar was parallel to the c-axis. The sharply defined V-shaped region in the top right-hand section of the photograph is thought to be in some way different from the rest of the face, possibly of different crystallographic orientation. Obviously no measurements were made on this crystal. The crystals on which measurements were made showed much less evidence of strain than Figure (6.11), but in most cases some small evidence was observed.

The importance of the accurate crystallographic orientation of the specimens, and of obtaining the best possible flatness and parallelism of the end surfaces is indicated in Chapter 5. The crystallographic orientation was carried out by the X-ray 'back reflection laue' technique (CULLITY (1956)). The ease with which the orientation could be effected was considerably enhanced by the use of a jig which could be attached both to the X-ray generator and the crystal cutting machine. The accuracy of the orientation was always checked after cutting, and was found to be better than 2° in all cases.

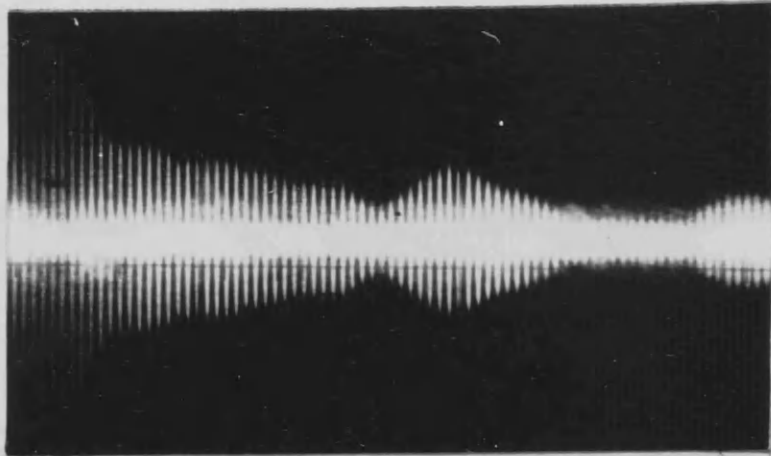


Figure(6.11) BADLY STRAINED ZINC OXIDE CRYSTAL VIEWED WITH CROSSED POLAROIDS.

The polishing of the end faces of the specimens was carried out in the Department, the technique has been described by BENNETT and WILSON (1966). The specimens were of two different cross-sectional areas. Those with the larger area ($\sim 4 \times 4$ mm) were polished after cutting. The smaller cross-section rods ($\sim 1.5 \times 1.5$ mm) however, were cut from the centre of a larger block of material after polishing. This approach was adopted as it was not found possible to polish rods of such small cross-section to the required flatness and parallelism after cutting. The end faces of the small rods and those parts of the end faces of the large rods which were excited, were thought to be more flat and parallel than the whole end surfaces of the larger rods. These larger surfaces were parallel to within 3 to 6 seconds of arc, which was about the limit of measurement; and were flat to within one-fifth a wavelength of visible light. The small cross-section rods were cut somewhat oversize and carefully lapped down to size by hand, to remove possible cutting damage.

Specimens of two lengths were used, that is rods of 2-3mm in length and long rods of ~ 12 mm in length. Although the short rods caused additional measurement problems they made it possible to extend the range of the attenuation measurements, and initially facilitated an experimental check of the maximum temperature at which measurements could be made.

a). 8.8 GHz, 4.2°K.



b) 450 MHz, room temperature.

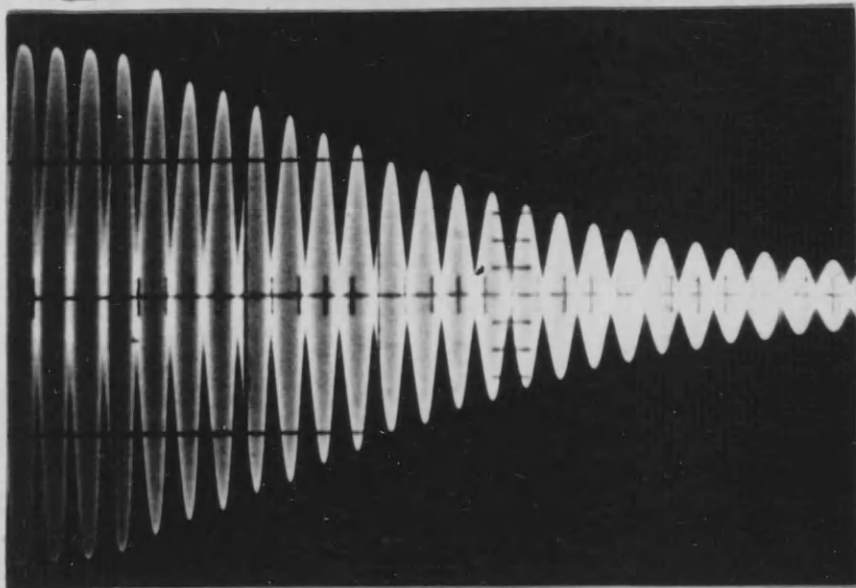


Figure (6.2) INFLUENCE OF THE EFFECTS DESCRIBED IN CHAPTER 5 ON ECHO PATTERNS
UNDER DIFFERENT EXPERIMENTAL CONDITIONS.

The small cross-section rods were initially used because they had the previously mentioned advantage that their cross-section was smaller than that of the post of the X-band cavities. So that by mounting these rods with the launching surface close to the post, no unwonted modes were detected. The absence of unwonted modes is a major advantage in the case of short rods when the echoes are closely spaced in time. The disadvantage of this method of excitation was that the small cross-section specimens were inconvenient for other measurements. This was particularly so with the long zinc oxide specimens, which were also required for the room temperature attenuation measurements described later. As this material was very expensive (£500/cc), the second mode of excitation described in Section (6.2) was used. This method is applicable to specimens of larger cross-sectional areas.

6.7 Measurement Technique

The normal procedure for making acoustic attenuation measurements by the pulse-echo method (McSKIMMIN (1964)), is not applicable when the echo pattern is disturbed by effects like those described in Sections (5.2) and (5.3) ^{(see figure (6.12))}. Therefore the attenuation relative to that at 4.2°K was measured, rather than the absolute attenuation. The measurement procedure was a well known one. It consisted of cooling the specimen to 4.2°K, and finding the attenuation of the smaller with respect to the larger of a particular pair, or pairs, of echoes.

This attenuation was termed the residual attenuation. It should be noted that as was discussed in Section (5.2) and (5.3), part of this attenuation is caused by processes which are not acoustic absorption processes. The measurements were repeated at each of a series of successively higher temperatures, and the relative attenuations obtained by subtracting the value at 4.2°K from each of those at the higher temperatures.

Using a precision attenuator placed in front of the receiver, the comparison of a pair of echoes could be made directly. This was done by finding the increase in attenuation which was needed to reduce the height of the larger of the pair, on the oscilloscope screen, to the initial height of the smaller. In order to ensure that no changes had occurred in the microwave system during an attenuation measurement, an additional check was carried out. Immediately after a measurement the attenuator was readjusted until the first echo reattained its initial height on the display, when a check was made to ensure that the attenuator was at its initial reading. On measuring the length of the specimen with a micrometer screw the specific attenuation was, ignoring thermal expansion, readily obtained. This temperature dependent part of the attenuation or relative attenuation, is the attenuation required for comparison with the theory discussed in Chapter 5.

In the case of the short rods, as both ends of the rod were exposed to the microwave electric field, both ends were

found to launch and detect acoustic pulses. This resulted in the separation of the echoes in time, being half the separation ^{that would have been} observed ^{if only one end of the rod had been exposed to the rf. field.} ~~with the longer rods.~~ Because it was anticipated that conditions might be different at the two ends of a short rod, measurements were carried out only on ^{even numbered} alternate echoes.

The method of measurement described above is dependent on the assumption that the part of the apparent attenuation not caused by thermal phonons, is independent of temperature. That is at all higher temperatures it is assumed that the residual attenuation is equal to its measured value at 4.2°K. This assumption is considered to be suspect, and to lead to possible error when the lattice dependent part of the attenuation is small compared to the residual attenuation. This situation appears to have been reached in some reported measurements of relative attenuations as low as 10^{-3} dB/cm; when the present work and other reported work, suggests that the residual attenuation was likely to be in the range 10^{-1} to 10^{-2} dB/cm.

The procedure adopted in the present work to avoid the effect of the residual attenuation on the results, was to limit the measurements to these temperatures at which the measured attenuation was greater than twice that at 4.2°K. That is the smallest relative attenuation measured was equal to the residual attenuation. The temperature dependence of the residual attenuation is expected to be small. Of the mechanisms discussed in Chapter 5, the only ones likely to lead to a

temperature dependent contribution to the residual attenuation would appear to be those influenced by thermal expansion. The contribution to the residual attenuation arising from the scattering of the acoustic wave as a result of local strain in a specimen is probably the most sensitive to thermal expansion. Consequently this contribution is probably the most temperature sensitive. It will be recalled that some evidence for the presence of local strain in the specimens was discussed in the previous section. However at the low temperatures at which measurements were made the thermal expansion is small, so that the approximate criterion discussed above is likely to be very adequate in ensuring that the influence of the residual attenuation on the results is negligible. An additional consequence of the minimum attenuation criterion was to ensure that measurements were made only at temperatures at which the echo pattern was approximately exponential.

It is interesting to note that it has been possible to measure attenuations in excess of 50 dB/cm in short specimens during the present work. The most important factor in making measurements at high attenuations is the pulse length. For a given acoustic mode in a given material, the pulse length controls the minimum specimen length that can be used without overlapping of echoes. Arising partly from the present work, a system is being actively investigated in the Department which is intended for use in making measurements at high attenuations (~ 1000 dB/cm). The basis of the system is to use very short pulses (~ 10 ns long) from a Gunn oscillator, and circumvent the limiter problem by

keeping the product of the peak power and short pulse length below the maximum permitted for the mixer diodes of the receiver.

CHAPTER 7 RESULTS AND INTERPRETATION OF ACOUSTIC
ATTENUATION MEASUREMENTS AT LOW TEMPERATURES

7.1 Introduction

The results of measurements of acoustic attenuation made at low temperatures by the methods described in Chapter 6, are presented in this chapter. These measurements are discussed in terms of the models of the attenuation mechanism described in Chapter 5. A number of accounts of measurements of acoustic attenuation, made on other materials, have appeared previously. However the present investigation is unusual in two ways. Firstly it has been possible to test experimentally all the predictions summarised in Section (5.5). Secondly measurements have been made on a group of closely related materials, rather than on a single material.

The layout of the chapter is as follows. The experimental results concerning the temperature and frequency dependence of the acoustic attenuation in zinc oxide, cadmium sulphide and cadmium selenide are given in Section (7.2). The results are presented graphically in Figures (7.1) to (7.5). In Figures (7.6) and (7.7) some of the data is displayed in an alternative manner, to facilitate the discussion of these results. In section (7.3) the results presented in the previous section are compared with the predictions of the three phonon theories summarised in Section (5.5). Additional experimental results not concerned with the temperature and frequency dependence of the attenuation, are contained in Section (7.4).

Section (7.5) contains a summary of the more important conclusions reached as a consequence of the low temperature attenuation results.

7.2 Experimental Results concerning the Temperature Dependence and the Frequency Dependence of the Acoustic Attenuation

All of the following results refer to piezo-electrically active longitudinal waves, propagating parallel to the c-axes of the crystals.

Figures (7.1) to (7.3) are composite graphs showing the behaviour of two specimens of different lengths, prepared from different crystals. Where possible, the two crystals were grown by different methods, and obtained from different crystal growers.

A number of the measurements shown in the subsequent graphs were repeated on further specimens cut from the same crystals as the original specimens. The maximum difference between the results obtained with any pair of similar specimens was $\pm 2\%$. This deviation is expressed as the difference in the temperatures at which the same value of attenuation was measured in different specimens. As a result of the increased temperature dependence of the attenuation at the lower temperatures, the same temperature difference represents a greater difference of attenuation (at the same temperature) at the lower temperatures than ^{at} the higher temperatures. No check was possible on the results obtained with the long zinc oxide ~~rod~~, as only one specimen was available.

RELATIVE ATTENUATION AS A FUNCTION OF TEMPERATURE IN ZINC OXIDE

AT 8.8 GHz

<u>Γ (dB/cm).</u>	<u>T ($^{\circ}$K).</u>
0.54.(L).	37.
0.92.(L).	40.
1.3.(L)	42.
1.9.(L).	45.
3.4.(L).	50.
5.4.(L).	55.
8.0.(S).	60.
10.8.(S)	64.
15.4.(S).	70.
24.5.(S).	78.
28.2.(S).	80.
43.(S).	90.
63.(S)	100.

The letter in brackets after the attenuation value denotes whether the measurement was made on a long or short rod.

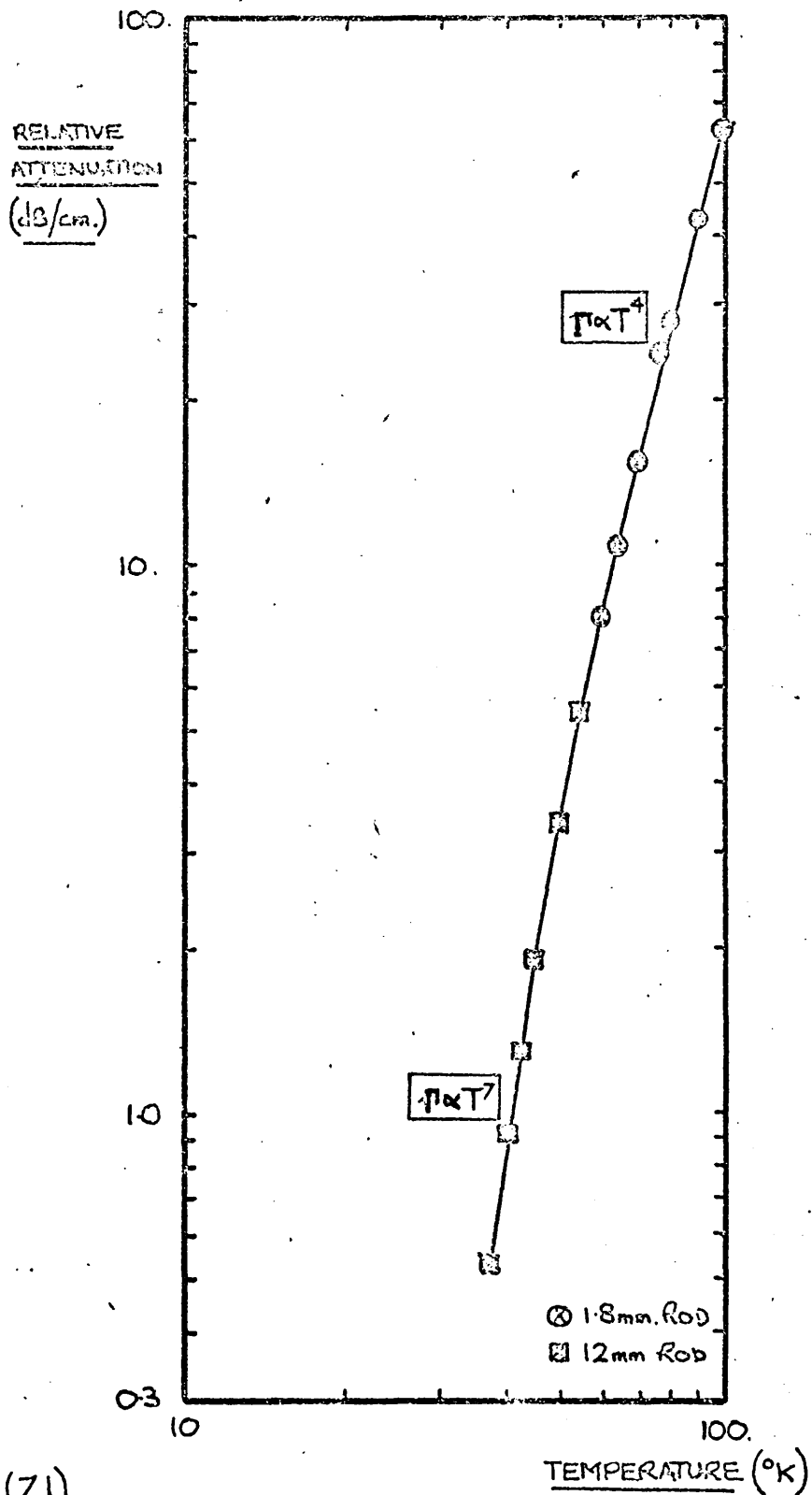


Figure (7.1)

ACOUSTIC ATTENUATION AS A FUNCTION OF TEMPERATURE IN ZINC OXIDE AT 8.8GHz

RELATIVE ATTENUATION AS A FUNCTION OF TEMPERATURE IN CADMIUM SULPHIDE

AT 8.8 GHz.

<u>Γ(dB/cm).</u>	<u>T(°K).</u>
0.58.(L).	19.
0.76.(L).	20.
1.45.(L).	22.
2.15.(L).	24.
3.1.(L).	26.
4.45.(L).	28.
6.65.(S).	30.
7.9.(L).	32.
9.3.(S).	33.
15.0.(S).	37.
20.(S).	40.
26.5.(S).	43.
31.(S).	45.
40.(S).	48.
48.(S).	50.

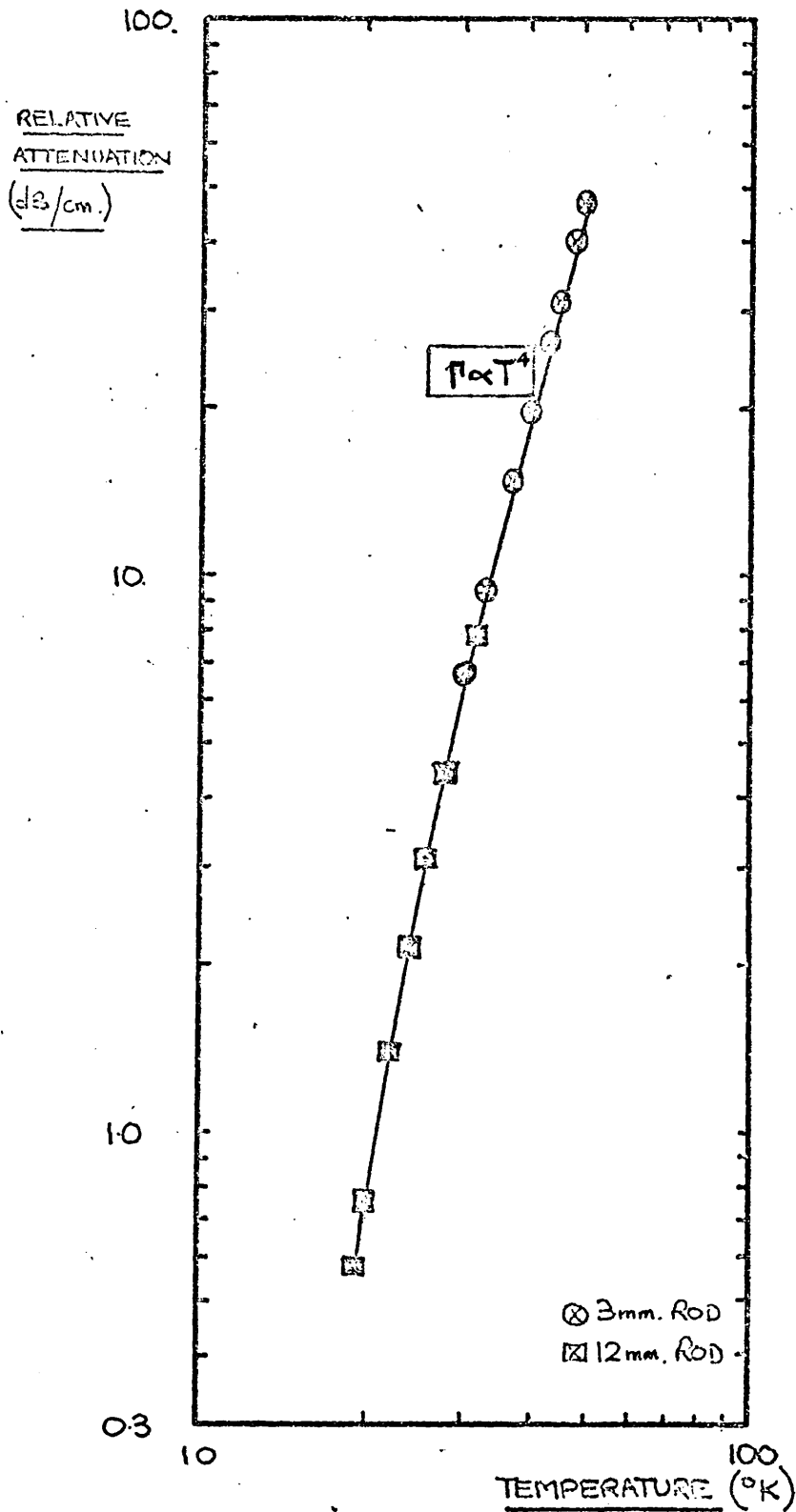


Figure (7.2)

ACOUSTIC ATTENUATION AS A FUNCTION OF TEMPERATURE IN CADMIUM SULPHIDE AT 8.8GHz.

RELATIVE ATTENUATION AS A FUNCTION OF TEMPERATURE IN CADMIUM SelenIDE

AT 9.0 GHz

Γ (dB/cm).

T(°K).

0.84.(L).

14.

1.75.(L).

16.

2.85.(L).

18.

4.5.(L).

20.

6.9.(S).

22.

7.9.(L).

23.

10.8.(S).

25.

15.2.(S).

27.

20.5.(S).

30.

26.(S).

32.

35.(S).

34.

51.(S).

37.

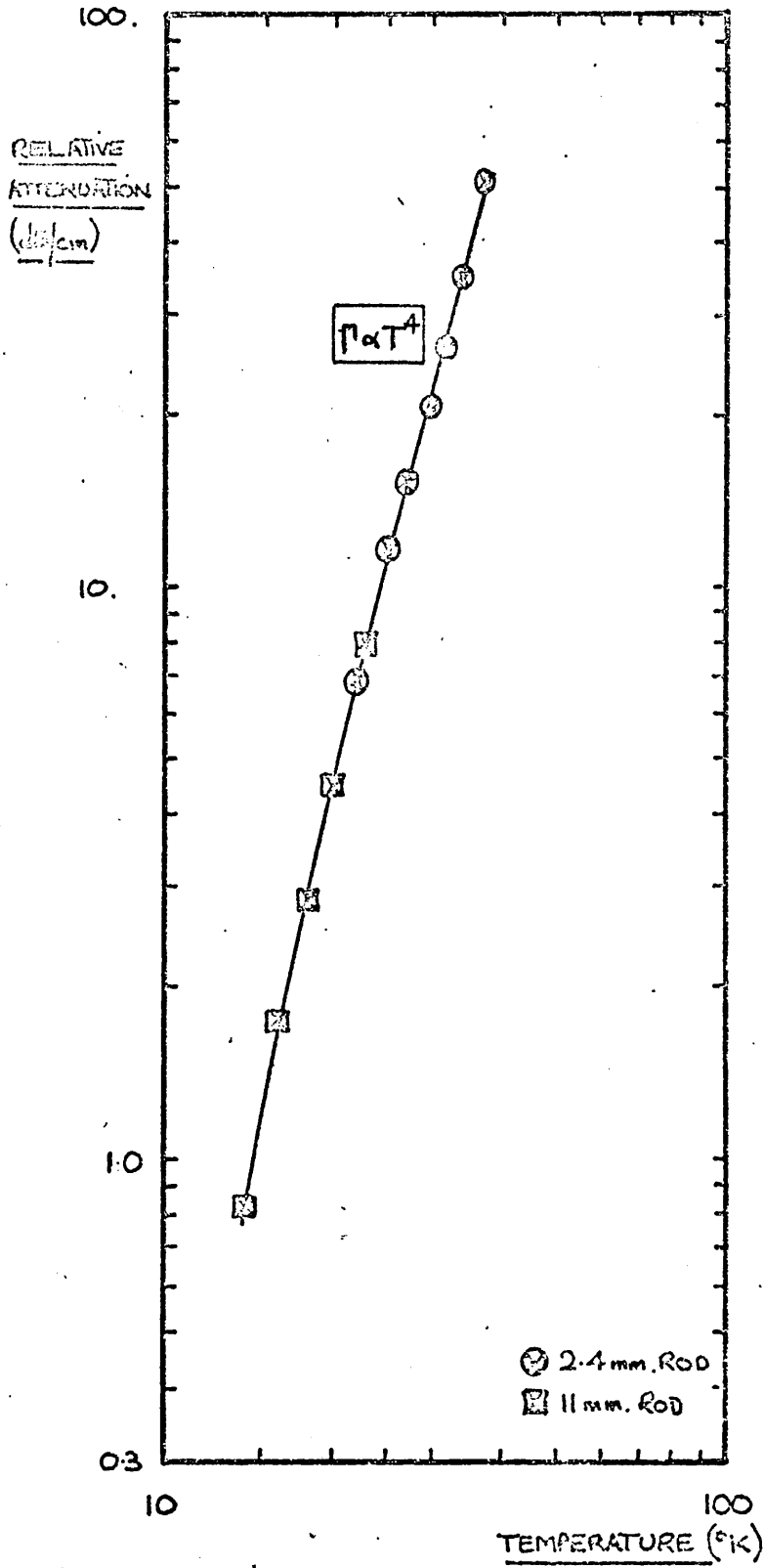


Figure (7.3)

ACOUSTIC ATTENUATION AS A FUNCTION OF TEMPERATURE IN CADMIUM SELENIDE AT 9.0CHz

RELATIVE ATTENUATION AS A FUNCTION OF TEMPERATURE IN ZINC OXIDE

AT 3.6 GHz.

<u>Γ (dB/cm)</u>	<u>T (°K)</u>
0.45.	38.
0.60.	40.
1.2.	45.
1.9.	50.
2.8.	55.
3.8	60.
5.8.	65.
7.0.	70.

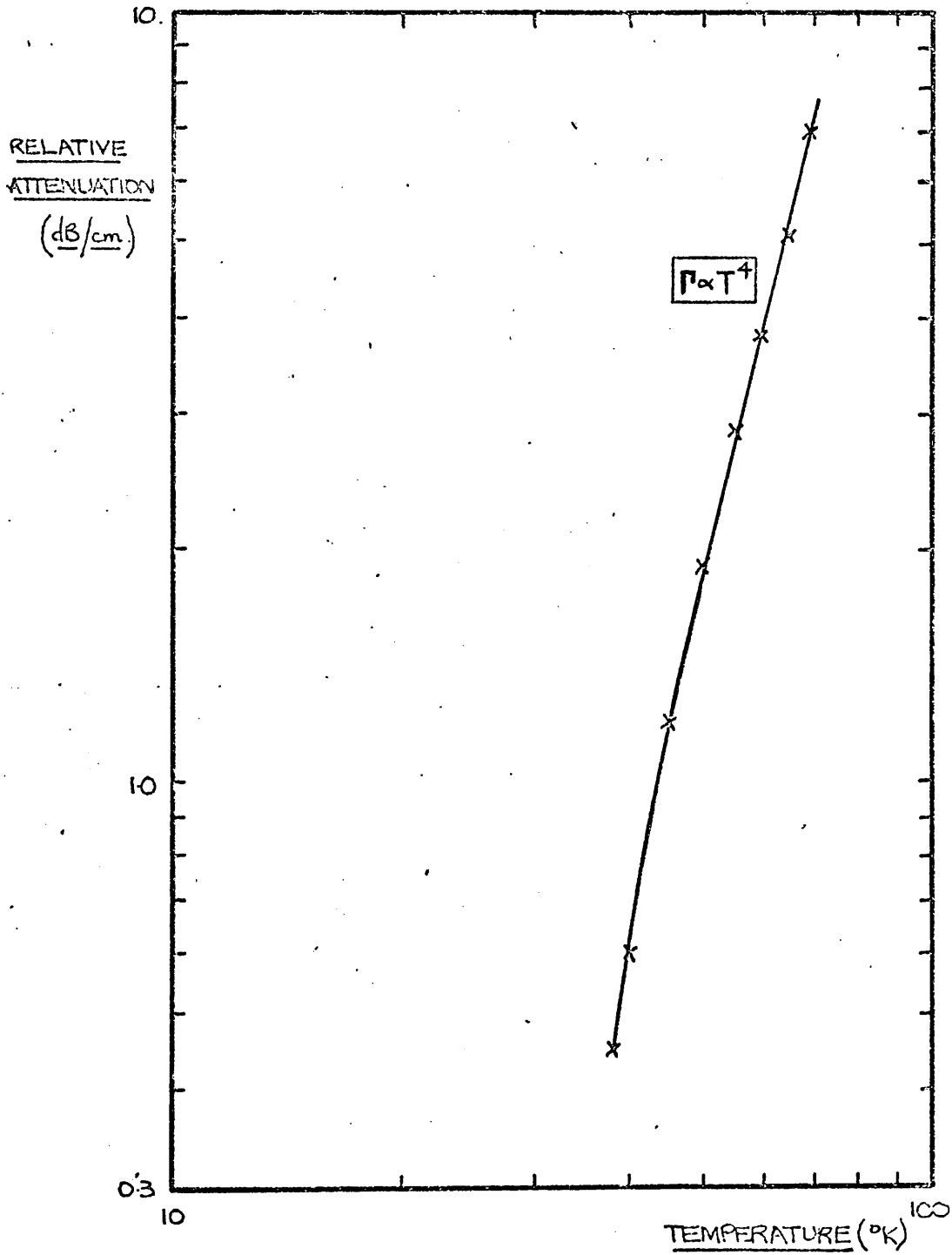


figure (7.4)

ACOUSTIC ATTENUATION AS A FUNCTION OF TEMPERATURE IN ZINC OXIDE AT 3.6GHz

RELATIVE ATTENUATION AS A FUNCTION OF TEMPERATURE IN ZINC OXIDE

AT 1.0 GHz.

<u>Γ (dB/cm).</u>	<u>T (°K).</u>
0.33.	45.
0.41.	47.
0.55.	50.
0.86.	55.
1.17.	60.
1.85.	70.
2.7.	80.
3.0.	85.
3.65.	90.
4.1.	95.
4.7.	100.
5.85.	110.
6.75.	120.
7.7.	130.

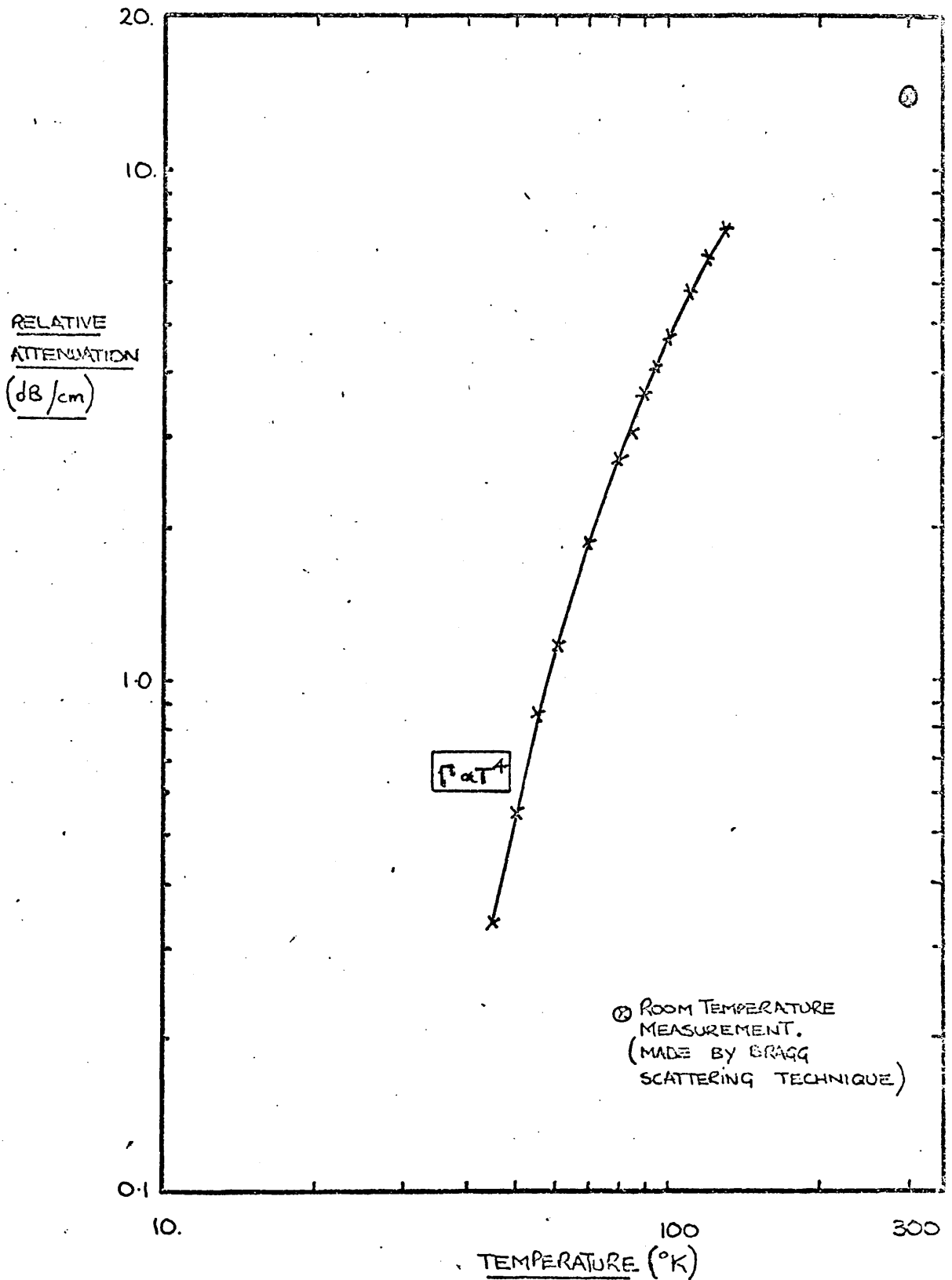


figure (7.5)

ACOUSTIC ATTENUATION AS A FUNCTION OF TEMPERATURE IN ZINC OXIDE AT 1.0 GHz.

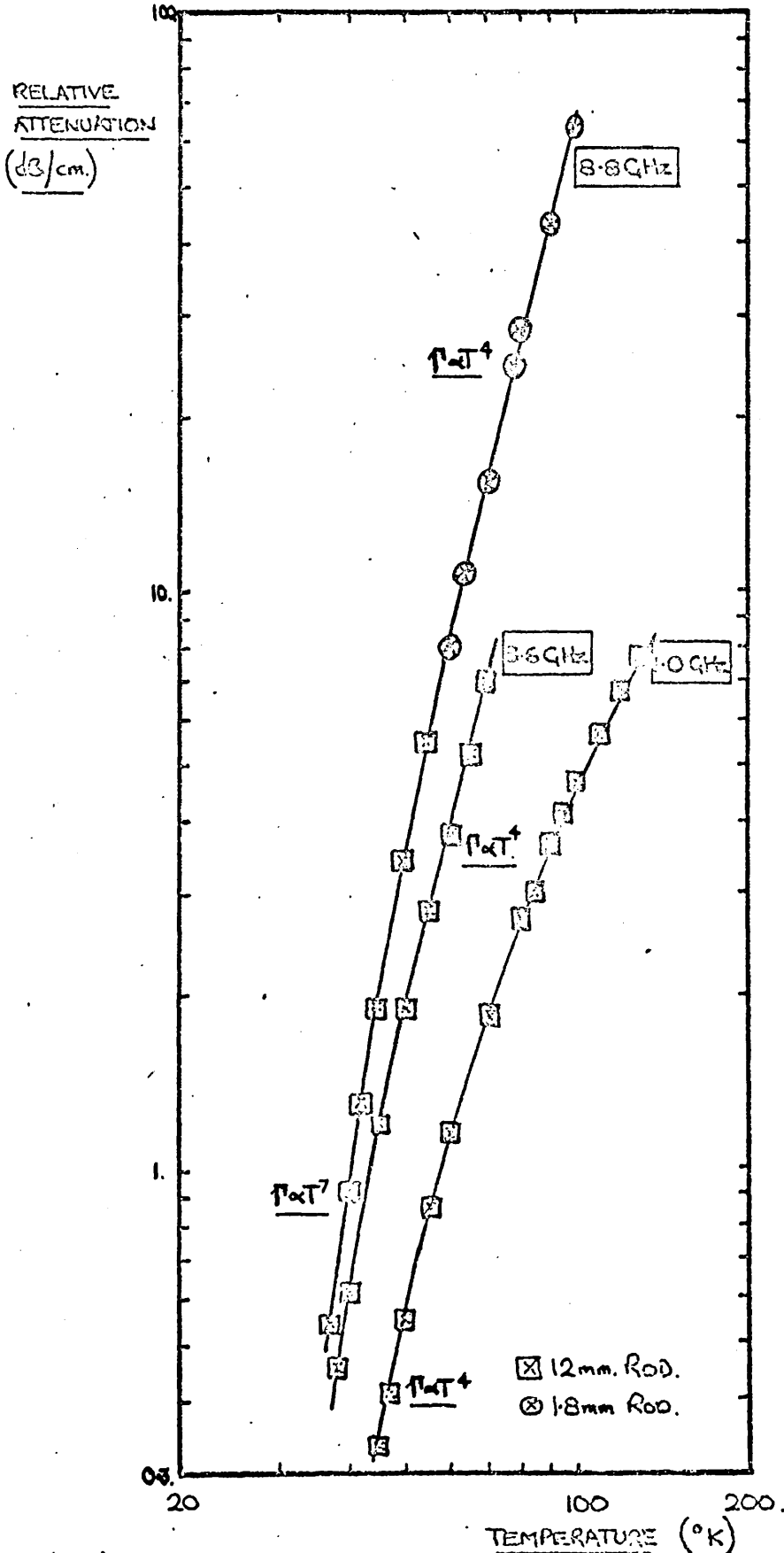
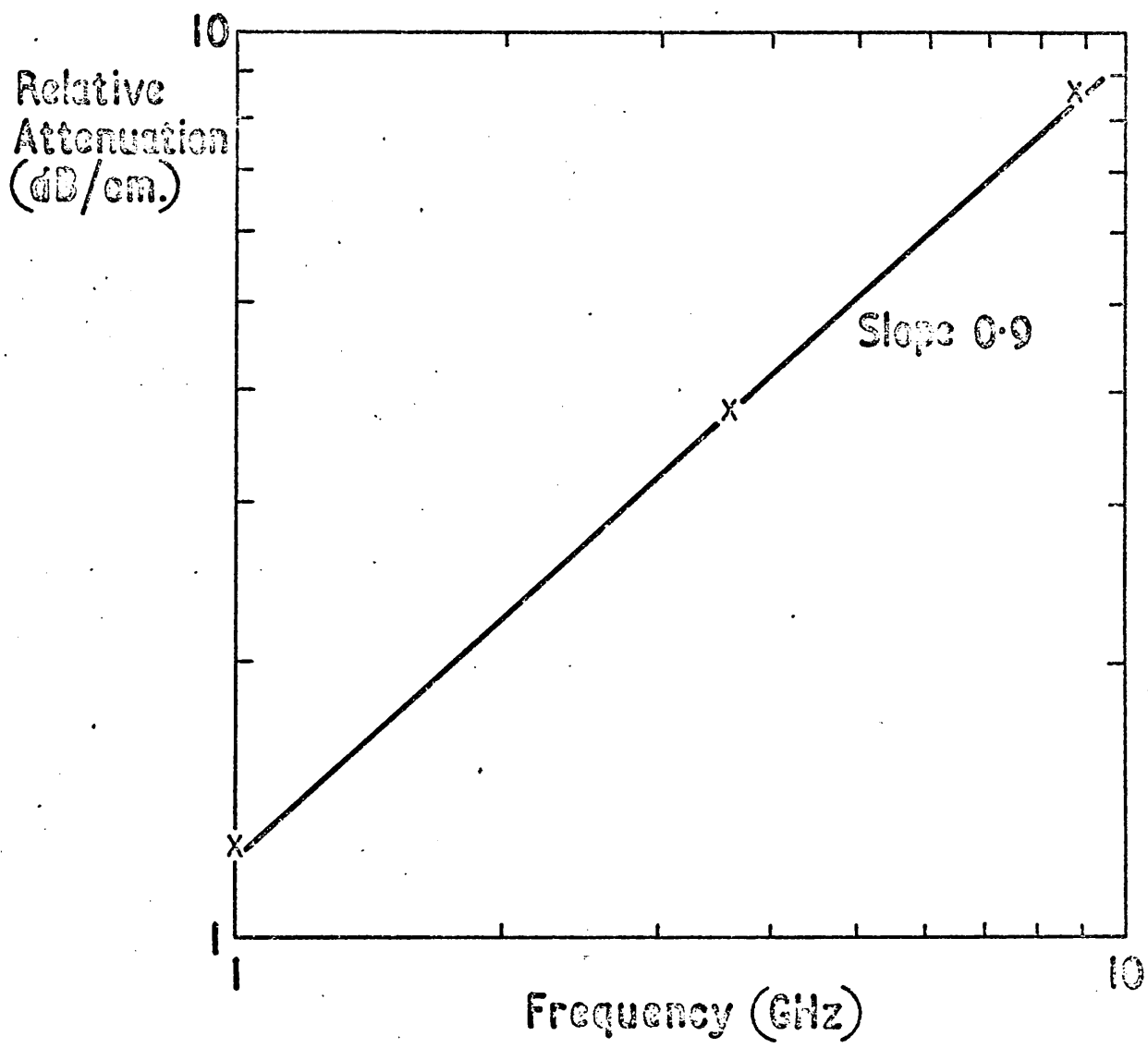
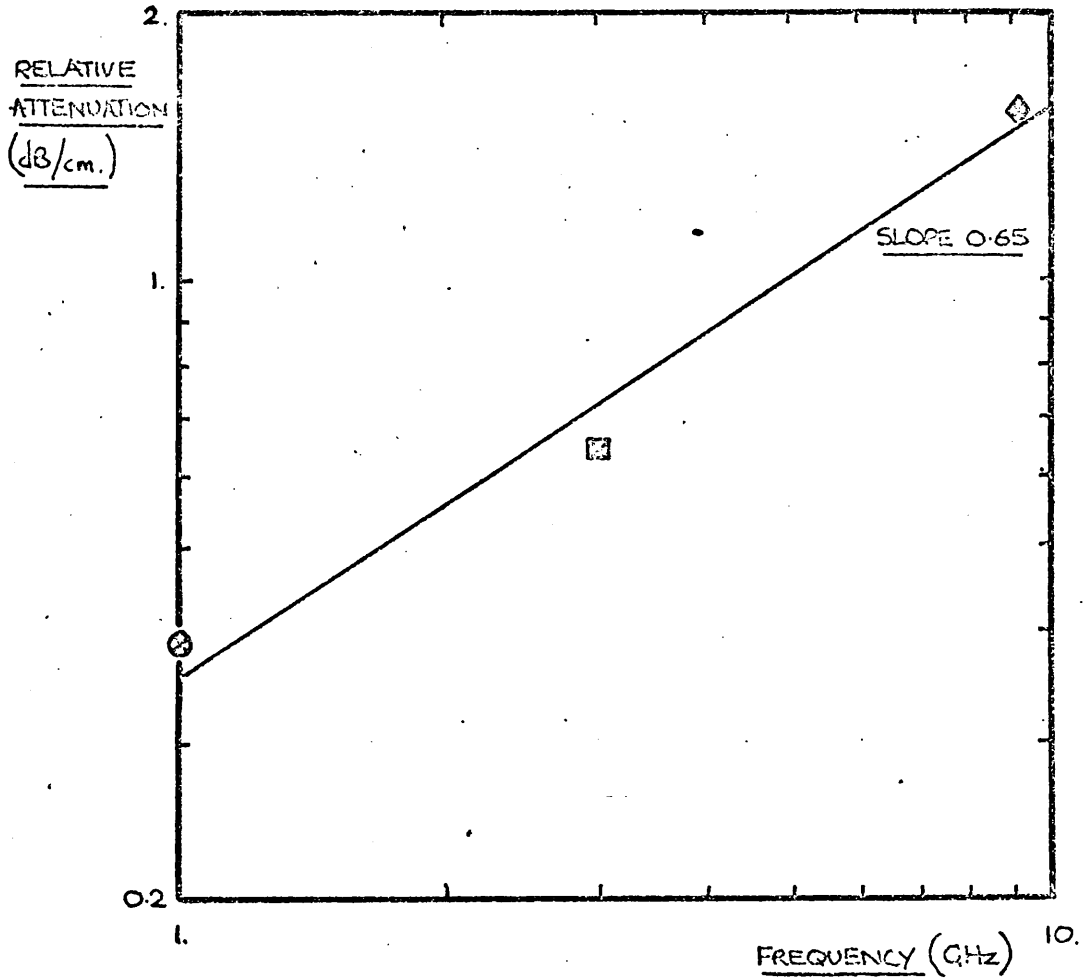


figure (7.6) ACOUSTIC ATTENUATION IN ZINC OXIDE AS A FUNCTION OF TEMPERATURE AND FREQUENCY.



Figure(7.7) FREQUENCY DEPENDENCE OF ACOUSTIC ATTENUATION IN ZINC OXIDE AT 60°K.



DATA FROM

- ⊗ MARIS (1964).
- ⊠ NAVA, ARZT, CICCARELLO AND DRANSFELD (1964)
- ◇ LEWIS AND PATTERSON (1967)

figure (7.8)

FREQUENCY DEPENDENCE OF ACOUSTIC ATTENUATION OF THE SLOW SHEAR MODE IN AC CUT QUARTZ AT 20°C

7.3 Interpretation of the Attenuation Results

The theoretical predictions summarized in Section (5.5) are conveniently divided into three groups; those concerning (a) the temperature dependence of the attenuation, (b) the frequency dependence and (c) the limits of the Landau-Rumer or T^4 region. As was mentioned in Chapter 5, the lack of information on the elastic anharmonicity of the materials of interest means that a quantitative prediction of the magnitude of the attenuation can not be made.

7.3.1 Temperature Dependence

A region where the attenuation varies as the fourth power of the temperature can be clearly seen in each set of measurements. This observation is in accordance with the prediction, made in Appendix A as a result of a consideration of first order three phonon processes.

The lower temperature limit of the T^4 or Landau-Rumer region is evident in Figures (7.1) to (7.4). At temperatures below the lower limit of the T^4 region the anticipated increase in the rate of change of the attenuation with temperature is apparent.

In some of the measurements presented in the previous section the behaviour of the attenuation at the lowest temperatures is not clear, owing to the limitations imposed by the residual attenuation. However, in Figure (7.1) and possibly Figure (7.2), the attenuation can be seen to vary as T^7 at the lowest temperatures. Such a temperature

dependence can be explained in terms of the second order three phonon processes considered in Chapter 5. The observed T^7 dependence, rather than a T^9 dependence, suggests that the processes responsible for the attenuation may be second order ones which have an initial first order process of the form of process (5.10a).

7.3.2 Frequency Dependence

Figure (7.6) shows the experimental results on zinc oxide plotted in a form suitable to illustrate the frequency dependence of the attenuation. It is apparent from this figure that at 60°K the attenuation is in the Landau-Rumer region at frequencies of 8.8 and 3.6 GHz. For the measurements at 1.0 GHz, 60°K is slightly above the upper temperature limit of the T^4 region. The value of the attenuation at 60°K if this temperature had been in the T^4 region at 1.0 GHz, can be obtained by making a short extrapolation of the T^4 region in Figure (7.5) to 60°K . The measured frequency dependence of the attenuation in the Landau-Rumer region is displayed in Figure (7.7), the value of the attenuation at 1.0 GHz being that obtained from the extrapolation described above. In view of the strong temperature dependence of the attenuation, the observed frequency dependence is in good agreement with the linear dependence predicted in Appendix A.

It can be seen from Figure (7.6) that at the lowest temperatures, that is when the measurements at 8.8 GHz show a T^7 dependence, the frequency dependence of the attenuation

is markedly less than that in the Landau-Rumer region at higher temperatures. At temperatures below the minimum at which measurements were made, it is expected that the attenuation of a 3.6 GHz wave would also vary as T^7 . At these temperatures it is predicted that the attenuation would be independent of frequency, at the frequencies of interest. Although the experimental results do not confirm this prediction, they provide a strong indication that had the residual attenuation in the specimen been lower permitting measurements at lower temperatures; then the predicted frequency independent regime would have been observed.

Measurements of the attenuation in cadmium sulphide of the longitudinal mode of interest in the present work, have been reported by GANAPOLSKI and TARAKANOV (1968) at a frequency of 1 GHz. The attenuation coefficients measured at 40⁰K were in the Landau-Rumer region both in the L-band measurements of Ganapolskii and Tarakanov and in the X-band measurements made in the course of the present work. Thus the frequency dependence in the T^4 region can be checked. The result of this check is shown below.

<u>ATTENUATION AT 1 GHz</u>	<u>ATTENUATION AT 8.8 GHz</u>	<u>INDEX IN RELATION</u>
		<u>$\Gamma \propto \omega^n$</u>
3.5 dB/cm	20 dB/cm	n = 0.8

Again this is in good agreement with the predicted linear frequency dependence.

Figure (7.8) is included for comparison with the present data, it shows the frequency dependence of the attenuation of the slow shear mode propagating along AC cut quartz rods at 20°K. The attenuation is in the Landau-Rumer region each case. The data is taken from the published literature.

7.3.3 Limits of the Landau-Rumer Region

It was predicted in Chapter 5, that both the upper and the lower temperature limits of the Landau-Rumer region should increase with increasing frequency. It can be seen from Figure (7.6) that both predictions are verified in the case of zinc oxide. A comparison of Figure (7.2) with the results of Ganapolskii and Tarakanov mentioned previously, shows that the same is true of cadmium sulphide.

7.4 Other Experimental Results

Measurements of acoustic velocity were made at liquid helium temperatures on all the specimens. The measurements were made by determining the time interval between echoes with an oscilloscope, and measuring the length of the specimens at room temperature with a micrometer screw. The results were compared with the published room temperature values for zinc oxide BATEMAN (1962), cadmium sulphide BERLINCOURT, JAFFE and SHIOZAWA (1963) and cadmium selenide CLINE, DUNEGAN and HENDERSON (1967). The agreement was good in each case. These

measurements were chiefly of value in checking, as far as possible, that the correct acoustic mode was in fact being propagated in the anticipated crystallographic direction.

Attempts were made to detect an influence on the observed echo pattern, of the level of input microwave power to the cavity. Such an effect has been observed by de KLERK (1966). In the present work no effect was detected. This was thought to be a consequence of the comparatively high insertion loss of the surface excitation method (~ 60 dB), which resulted in a relatively low acoustic power density in the crystal. Further if the effect is assumed to be the result of the harmonic generation mechanism discussed by RICHARDSON, THOMPSON and WILKINSON (1969), then the use of a one port system would have significantly reduced the probability of observing the effect. This mechanism concerns the transfer of energy from the fundamental to the acoustic harmonics, as a result of a non-linear process involving the lattice anharmonicity. However on reflection at a stress free boundary the process can be considered to be reversed, and energy is transferred from the harmonics back to the fundamental. Therefore a greater excess attenuation of the fundamental will be observed with a two port system like that used by deKlerk, than with the one port system used in the present measurements.

Of the four pieces of zinc oxide examined, only two were considered suitable for detailed investigation. One of the two unsatisfactory pieces was orientated for the launching of shear acoustic pulses. This crystal will be discussed further in Chapter 8. The objection to this crystal was that it showed a large residual attenuation at liquid helium temperatures. This was ~ 2 dB/cm at 1 GHz, and, ~ 5 dB/cm at 3.6 and 8.8 GHz. In this case the residual attenuation was an estimate of the exponential decay of the echo pattern at 4.2°K, and could not be explained in terms of a serious lack of flatness or parallelism of the end surfaces of the rod. That is it was an effect associated with the bulk of the crystal. Some measurements of the attenuation of piezoelectrically active shear waves propagating parallel to the 'a' axis at frequencies of 1.0 and 8.8 GHz were made using this crystal. In as far as it was possible to make measurements, it was found that the attenuation of the shear mode showed the same general behaviour as that of the previously mentioned longitudinal mode. But for the reasons outlined above and those discussed in Chapter 8, these results were considered to be of uncertain value and consequently are not presented. The other rejected piece of zinc oxide was the badly strained crystal shown in Figure (6.13).

Recently some measurements of the attenuation in zinc oxide of the longitudinal mode discussed in this work have been reported by CLAIBORNE, HEMPHILL and EINSBRUCH (1969) at

frequencies in the range 0.60 to 4.0 GHz. At temperatures above about 50°K the agreement with the present results is good. At lower temperatures however, the published results show no evidence of the temperature dependence becoming greater than a T^4 dependence. This result disagrees with both the theoretical predictions and the present results. It suggests that in the published work the attenuation at the lower temperatures was caused by mechanisms different from that considered in this work.

7.5 Conclusions

In Section (7.3) the predictions made in Chapter 5 on the basis of the three phonon models of the attenuation mechanism, were compared with the experimental results presented in Section (7.2). Whenever a comparison was possible the predictions were found to be verified. It is considered that the present work probably constitutes the most comprehensive test of the three phonon theories of acoustic attenuation attempted to date.

The use of specimens of different lengths had two advantages in the X-band measurements. Firstly, it enabled the range of attenuation investigated to be extended, while maintaining the minimum attenuation criterion. In this way it was possible to establish the Landau-Rumer regions in the attenuation of X-band frequency waves in the three materials. Secondly the overlaps in the measurements made on pairs of different specimens cut from different crystals, provides a strong indication that the measurements were of an intrinsic property of the materials.

During the course of the present work including that described in Chapter 8, a substantial body of evidence has accumulated which suggests that strain and crystalline imperfections are quite common in single crystals of the materials investigated, particularly in zinc oxide. This indicates that it is necessary to examine specimens thoroughly for local strain etc, and carefully note their residual attenuations; if reliable measurements are to be made.

The possibility that the residual acoustic attenuation of a specimen may be slightly temperature sensitive does not appear to have been taken into account in previous published work. As has been pointed out this temperature sensitivity may lead to errors in attenuation measurements made when the temperature dependent contribution to the total attenuation is small. The procedure of limiting the temperatures at which measurements are made on a given specimen to those at which the relative attenuation is greater than the residual attenuation, removes this problem.

In all the low temperature measurements the relative attenuation was found to be strongly dependent on the temperature, demonstrating the importance of accurate temperature measurement.

CHAPTER 8 ROOM TEMPERATURE ACOUSTIC ATTENUATION MEASUREMENTS

8.1 Introduction

This chapter deals with measurements of acoustic attenuation, made at room temperature, on specimens of zinc oxide. Because of their significance in acousto-electric studies, measurements were made on the same piezo-electrically active modes as in the low temperature work. These measurements extend the investigation of the behaviour of acoustic attenuation described in Chapters 5 to 7. In the nomenclature of Section 5.4, the measurements described in the present chapter relate to the high temperature region, whereas those described previously relate to the intermediate region. That is in the present case $\omega\tau \ll 1$.

Zinc oxide has a high electromechanical coupling coefficient and relatively low acoustic loss, as a result it is a material of considerable potential technological interest. There is substantial interest in information concerning the attenuation at frequencies of 10 GHz and higher, in order to estimate the maximum operating frequencies of various acousto-electric devices. At these frequencies the attenuation in zinc oxide is greatly in excess of the maximum measurable attenuation using the present techniques. For this reason measurements were made at lower microwave frequencies. Particular attention was paid to the frequency dependence of the attenuation; as it was considered that if

the predicted dependence was observed, more confidence would be justified in the extrapolation of the data to higher frequencies.

It was decided to use the method involving the Bragg scattering of a laser beam by the acoustic wave, to measure the attenuation of the wave. This is in contrast to the 'pulse echo' method used for the low temperature measurements. The optical method is more easily employed at room temperature, and it has several important advantages over the pulse echo method. Firstly it is not limited to information obtained at the ends of the specimen. The entire acoustic path may be probed to check for local changes in the attenuation and the direction of the acoustic beam. Secondly the optical method is relatively insensitive to changes of phase across the acoustic wavefront, so that the method avoids the signal cancellation difficulty described in Section 5.2. Thirdly, as microwave heterodyne receivers have relatively narrow frequency ranges of operation, it is usually necessary to use more than one when making measurements as a function of frequency. However no change in the detection system is needed with the Bragg scattering method.

The arrangement of this chapter is as follows. Section (8.2) contains a discussion of Bragg scattering in which emphasis is placed on the use of the phenomenon in the measurement of acoustic attenuation. Both scattering by a longitudinal acoustic wave and the more complex case of

scattering by a shear wave are discussed. In particular an explanation is advanced of the observation that the existence of a diffracted beam depended on which face of the shear wave specimen was illuminated by the laser beam. The experimental details are given in Section (8.3). In the discussion of room temperature acoustic attenuation contained in Section (8.4) and Appendix B, it is shown that a quadratic frequency dependence of the attenuation is anticipated. The experimental results are presented in Section (8.5). The attenuation of the longitudinal mode was found to vary as the square of the acoustic frequency, but the attenuation of the shear mode exhibited a more complex frequency dependence. An explanation of the frequency dependence of the shear mode is advanced in Section (8.6). In addition to the attenuation measurements it was possible to probe the direction and form of the acoustic beam at various positions along its length. As an illustration of the value of acoustic attenuation data in studies of acousto-electric devices, Section (8.7) contains a calculation of the maximum operating frequencies of microwave acousto-electric oscillators made using the data obtained in the present work.

8.2 Discussion of Bragg Scattering

The stress associated with an acoustic wave propagating through a crystal will, in general, cause a modulation of the refractive index of the crystal, via the photoelastic effect. This stress induced modulation of the refractive index may,

under certain circumstances, diffract a fraction of an optical beam passing through that part of the crystal occupied by the acoustic wave. The diffraction effect is usually denoted by the general term 'Brillouin scattering'.

The diffraction phenomena have been observed to be a function of the experimental conditions. The situation has been discussed by WILLARD (1949). Two situations have been distinguished. Firstly when the conditions are such that $\lambda d < \Lambda^2$ (where λ and Λ are the optical and acoustic wavelengths respectively, and d is the acoustic beam width). Under these conditions if a light beam is incident parallel to the acoustic wavefronts, the diffracted light appears on both sides of the main beam in the form of equally spaced spots. Secondly when $\lambda d > \Lambda^2$, the diffracted light appears as a single spot, which is of maximum intensity when the incident beam is at the Bragg angle. The former case is often termed the Raman-Nath regime, and the latter the Bragg regime. The two regimes run smoothly into each other. In the present measurements a typical acoustic wavelength was 6×10^{-4} cm. The beam diameter was 0.2 cm and the optical wavelength 6.3×10^{-5} cm. That is the conditions were those of the Bragg regime. As expected a single diffracted spot was observed in the experiments.

The observed fact that there is only one diffracted spot under the conditions of the Bragg scattering regime; suggests that it would be possible to treat the diffraction as a

phonon-photon scattering process, with the scattering probability a function of the appropriate photoelastic coefficient.

Such a process will be subject to two selection rules. The first is the conservation of energy, which can be expressed in the form

$$\omega_1 + \omega_2 = \omega_3 \quad (8.1)$$

and the second is the conservation of crystal momentum, which can be written as

$$\vec{k}_1 + \vec{k}_2 = \vec{k}_3 \quad (8.2)$$

where the index 1 refers to the phonon, and the indices 2 and 3 refer to the incident and diffracted photons respectively.

The scattering process is represented diagrammatically in Figure 8.1. The wavevector triangle represents the condition (8.2), from this construction it can be seen that

$$|k_1| = |k_2| \sin \theta_i + |k_3| \sin \theta_d \quad (8.3)$$

But the optical frequency was $\sim 10^{15}$ Hz whereas the acoustic frequency was $\sim 10^9$ Hz, so that from Equation (8.1) it is seen that $\omega_2 \approx \omega_3$. As a result $|k_2| \approx |k_3|$ neglecting dispersion. Therefore it can be seen that the

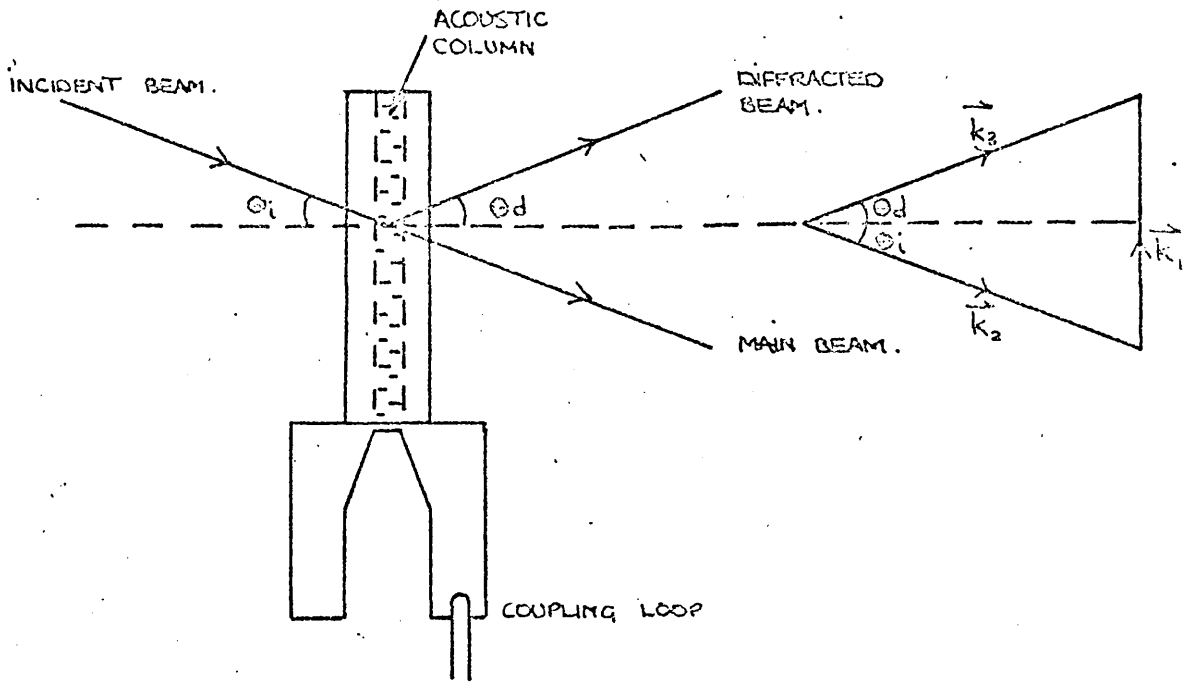


Figure (3.1) GEOMETRY AND WAVEVECTOR CONSTRUCTION FOR NORMAL BRAGG SCATTERING.

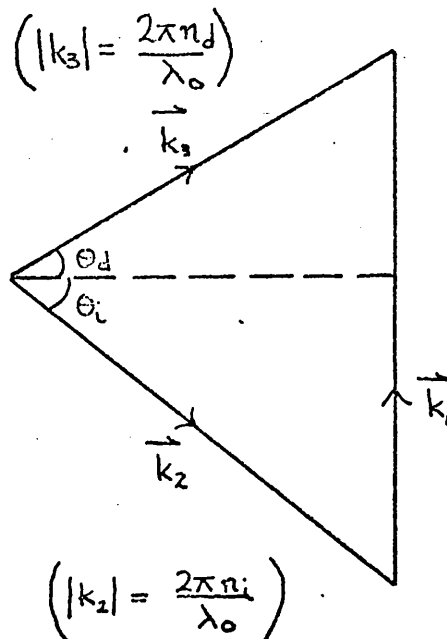


Figure (3.2) WAVEVECTOR CONSTRUCTION FOR ANOMALOUS BRAGG SCATTERING.

wavevector triangle is isosceles and consequently

$$\theta_i = \theta_d \quad (8.4)$$

From Equations (8.3) and (8.4) using the relation $|k_2| = \frac{2\pi}{\lambda}$, it is found that

$$\sin \theta_i = \frac{\lambda}{2\Lambda} \quad (8.5)$$

where λ and Λ are the optical and acoustic wavelengths respectively.

Thus the selection rules are satisfied if the angle of incidence of the light beam is given by Equation (8.5). When this condition is fulfilled maximum diffraction is expected. Further the angle of diffraction is equal to the angle of incidence. This situation is often referred to as 'normal' Bragg diffraction.

From Equation (8.1) it appears that the frequency of the diffracted light will be different from that of the incident light by an amount equal to the acoustic frequency. The difference in the optical frequencies will be very small however, because as was pointed out above $\omega_1 \ll \omega_2 \simeq \omega_3$. Equation (8.1) has been verified by QUATE, WILKINSON and WINSLOW (1965) to within an experimental uncertainty of about 10%.

It is necessary at this point to consider the properties of the photoelastic tensor of zinc oxide. The photoelastic tensor is a fourth rank tensor. The significance of the indices of the tensor (P_{ijkl}) can be seen from the following relation

$$E_i = P_{ijkl} E_j \epsilon_{kl} \quad (8.6)$$

where E_i and E_j are the electric fields of the diffracted and incident optical beams respectively and ϵ_{kl} is the strain resulting from the sound wave.

In order to employ the convenient matrix notation when treating the photoelastic tensor the number of independent indices must be reduced to two. The convention for affecting this reduction is given below.

INDICES IN FULL TENSOR NOTATION	11 ; 22 ; 33 ; 23 and 32; 31 and 13; 12 and 21.	(8.7)
INDICES IN MATRIX NOTATION	1 ; 2 ; 3 ; 4 ; 5 ; 6.	

The hexagonal form of zinc oxide belongs to the crystal class 6 mm. The form of the photoelastic tensor for this class has been given by NYE (1957) in matrix notation and is reproduced below.

<u>Longitudinal Wave</u>			<u>Shear Wave</u>			
p_{11}	p_{12}	p_{13}	0	0	0	<u>NO POLARISATION CHANGE</u>
p_{12}	p_{11}	p_{13}	0	0	0	
p_{31}	p_{31}	p_{33}	0	0	0	
0	0	0	p_{44}	0	0	<u>POLARISATION CHANGE</u>
0	0	0	0	p_{44}	0	
0	0	0	0	0	$1/2(p_{11} - p_{12})$	

(8.8)

The annotation was suggested by C.D.W. Wilkinson. The justification for this is based on (8.6) and (8.7) and is given below.

The first index in the matrix notation is concerned with the optical electric fields.

<u>VALUES OF MATRIX INDEX</u>	<u>RELATION BETWEEN INDICES IN FULL NOTATION</u>	<u>CORRESPONDING POLARISATION CHANGE</u>
1, 2, 3	$i = j$	No polarisation change
4, 5, 6	$i \neq j$	Polarisation change

The second index in the matrix notation is concerned with the strain.

<u>VALUES OF MATRIX INDEX</u>	<u>RELATION BETWEEN INDICES IN FULL NOTATION</u>	<u>CORRESPONDING TYPE CHANGE OF ACOUSTIC WAVE.</u>
1, 2, 3	$i = j$	Longitudinal
4, 5, 6	$i \neq j$	Shear

From the expression (8.8) it can be seen immediately that light diffracted from a longitudinal wave in zinc oxide will have the same polarisation as the incident light, because all the elements of the tensor corresponding to a longitudinal wave and a polarisation change are zero. However light diffracted from a shear wave will undergo a polarization change. These predictions were verified experimentally for the two modes used in the present experiments

The simple geometry of normal Bragg diffraction results from the fact that the optical wavevectors are effectively equal in magnitude. However if this is not so, then Equations (8.4) and (8.5) must be modified. The wavevectors will not be equal, if in an optically birefringent material the plane of polarisation of the diffracted wave differs from that of the incident wave. Both of these conditions are satisfied in the case of diffraction by a shear wave in zinc oxide. That is the refractive index for the incident beam (n_i) will, in general, be different from that of the diffracted beam (n_d), and consequently the amplitudes of the incident and diffracted optical wavevectors will differ. The wavevector construction representing the crystal momentum

conservation condition for this 'anomalous' case is shown in Figure (8.2). From this construction two relations between θ_i and θ_d are apparent, the first is Equation (8.3) and the second is

$$|k_2| \cos \theta_i = |k_3| \cos \theta_d \quad (8.9)$$

the following relations are also valid

$$|k_2| = \frac{2\pi n_i}{\lambda_0} \quad ; \quad |k_3| = \frac{2\pi n_d}{\lambda_0} \quad \text{and} \quad |k_1| = \frac{2\pi}{\Lambda} \quad (8.10)$$

where λ_0 is the optical wavelength in air.

Equations (8.3) and (8.9) can be solved for θ_i and θ_d , together with relations (8.10) they yield.

$$\sin \theta_i = \frac{\lambda_0}{2n_i\Lambda} \left[1 + \frac{\Lambda^2}{\lambda_0^2} (n_i^2 - n_d^2) \right] \quad (8.11a)$$

and

$$\sin \theta_d = \frac{\lambda_0}{2n_d\Lambda} \left[1 + \frac{\Lambda^2}{\lambda_0^2} (n_i^2 - n_d^2) \right] \quad (8.11b)$$

Equations (8.11) were first derived by DIXON (1967).

In general, in the case of anomalous Bragg diffraction the quantity $n_i - n_d$ is a function of θ_i . Therefore for measurements with shear waves in zinc oxide, $n_i - n_d$ varies with the acoustic frequency. However in the present measurements the incident and diffracted beams were in a plane perpendicular to the c-axis of the crystal. For this orientation in the case of zinc oxide the relevant section through the indicatrix

is a circle, so that the quantity $n_i - n_d$ is independent of θ_i .

The plane of polarisation of the light diffracted by the longitudinal acoustic wave was not rotated, so that normal Bragg diffraction was anticipated and observed experimentally. However because the plane of polarisation was rotated when light was diffracted by the shear acoustic wave, anomalous diffraction was anticipated. Qualitative checks of Equations (8.11) were carried out and the predictions verified.

The relation between the acoustic and diffracted optical powers is of particular importance in acoustic attenuation measurements made by the Bragg scattering method. This relation is now considered. Let β be the probability of a photon being scattered while traversing the acoustic beam. Further let N and n be the phonon and incident photon fluxes respectively. If β is small the diffracted flux is given by

$$n' = nN\beta. \quad (8.12)$$

And the acoustic and diffracted optical powers are given by

$$P_1 = N\hbar\omega_1 \quad (8.13a)$$

and

$$P_2 = n'\hbar\omega_2 \quad (8.13b)$$

where the suffices 1 and 2 refer to the acoustic and diffracted optical fluxes respectively. From Equation (8.12) and (8.13).

$$\omega_1 P_2 = \omega_2 n \beta P_1$$

But in a given experiment n , β , ω_1 and ω_2 are constant. Therefore the diffracted optical power is proportional to the acoustic power. This relation can form the basis of a method of measuring acoustic attenuation, because by measuring the variation of the diffracted optical power at various points along the crystal a direct measure of the variation of the acoustic power is obtained. The proportionality has been verified by QUATE, WILKINSON and WINSLOW (1965).

It was noted during the measurements on the shear specimen, that if the laser beam was incident on one of the pair of c-faces of the crystal, i.e. faces perpendicular to the c-axis; no diffracted beam was observed. This was so even though the laser beam was incident at the Bragg angle. Whereas if the beam was incident on one of the other pair of large faces of the crystal a diffracted beam was detected. This observation can be explained by reference to the photo-elastic tensor (8.8). In arriving at the form of (8.8) the convention of designating the c-axis (along which the shear wave is polarised) as the 3 axis was adopted. In order to specify the situation the acoustic propagation is assumed to occur along the 2 axis. By considering both directions of incident optical polarisation and using Equation (8.6), the

photoelastic coefficient required to cause diffraction was deduced. This deduction was made both for light incident on a c-face and on one of the other large faces of the specimen.

The required coefficients are indicated below.

<u>FACE ILLUMINATED</u>	<u>INCIDENTAL OPTICAL POLARISATION</u>	<u>DIFFRACTED OPTICAL POLARISATION</u>	<u>STRAIN</u>	<u>PHOTOELASTIC COEFFICIENT</u>
c	2	1	ϵ_{23}	$p_{12,23} \equiv p_{64}$
	1	2	ϵ_{23}	$p_{21,23} \equiv p_{64}$
Other	3	2	ϵ_{23}	$p_{23,23} \equiv p_{44}$
	2	3	ϵ_{23}	$p_{23,23} \equiv p_{44}$

But it is seen from (8.8) that $p_{64}=0$, whereas p_{44} is non-zero. Thus diffraction will not occur when the c-faces are illuminated, but will when the other faces are illuminated.

The argument as stated above is valid only when the incident light beam is at right angles to the acoustic beam. It can be generalised to any angle of incidence by considering the appropriate components of the photoelastic coefficients.

If the direction of acoustic propagation is chosen as the 1 axis instead of the 2 axis the same results are obtained.

The observation of diffraction involving the photoelastic coefficient p_{44} in this work shows the prediction of MALONEY and CHARLETON (1967), that such diffraction would not occur, to be incorrect.

8.3 Experimental details

8.3.1 Optical Apparatus

The optical system for the Bragg scattering measurements was very simple. The light source was a Spectra Physics type 132 helium neon laser, which had an output of 2mW . A laser is a particularly suitable light source for this type of experiment as it produces a well collimated, intense beam. The detector was a photomultiplier with an S-20 phosphor. The particular tubes used were an E.M.I. type 9558 and an R.C.A. type 7265. To protect the sensitive photomultiplier from stray radiation, all experiments were conducted in a darkened laboratory and a narrow band pass optical filter, centred at the laser wavelength of 6328\AA , was placed in front of the photomultiplier. The output of the photomultiplier was displayed on a detector incorporating a tuned amplifier, having a centre frequency of 3 kHz. The acoustic signals were also modulated at 3 kHz. A V.S.W.R. meter proved to be a convenient detector. The narrow band detection greatly improved the signal to noise ratio of the measurements. A precision attenuator was placed between the photomultiplier and the detector, so that the detector was used only as a comparative indicator. The photomultiplier was attached to a milling table mounted vertically, thus enabling the tube to be placed accurately.

8.3.2 Microwave System

The microwave systems used for the longitudinal wave and shear wave measurements differed slightly. The system used with the shear wave specimen is shown diagrammatically in Figure (8.3.) The microwave oscillator was internally modulated at a frequency of 3 kHz by a stable oscillator. In the longitudinal wave case the modulation was performed externally with a P.I.N. diode modulator. The microwave signal was amplified to about 10W peak power by the travelling wave tube. No T.W.T. operating at the required frequencies was available for the longitudinal wave measurements. The circulator and load acted as an isolator. The roles of the wavemeter and powermeter are self-evident. The crystal detector was used to tune the oscillator to the resonant frequency of the cavity. Because of the different frequency ranges of the measurements separate cavities were needed for the longitudinal and shear specimens. Both were re-entrant cavities, the resonant frequencies of which were adjusted by varying the length of the cavity. The one used with the longitudinal specimen was built by J. Richter, who has described its design and construction (RICHTER (1966)). The other cavity was of smaller dimensions but similar design. The cavity was mounted on a rotary table in such a manner that the specimen could be rotated and translated horizontally and vertically,

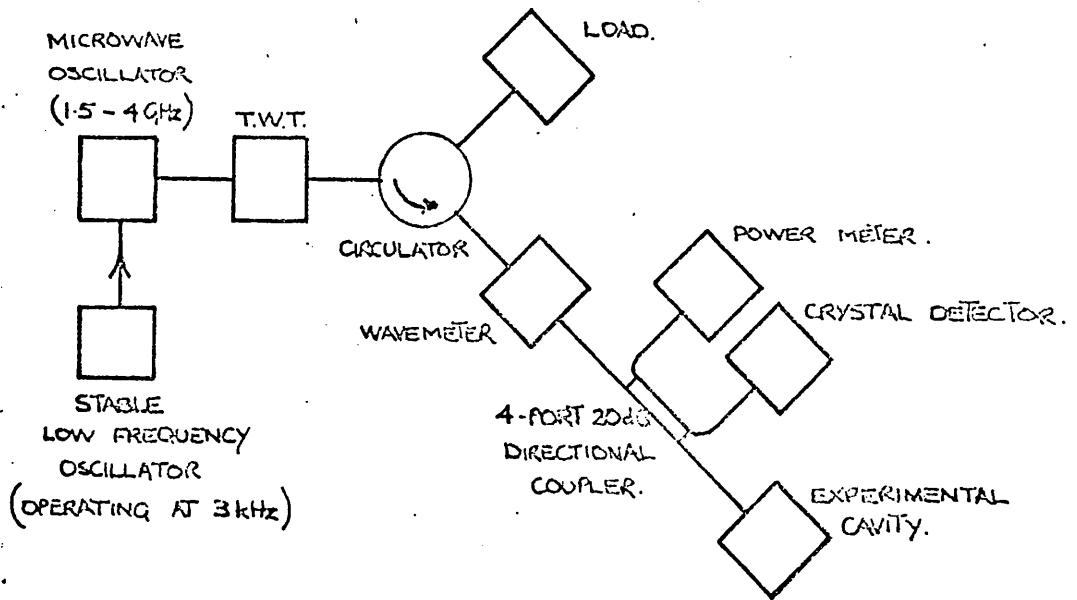


Figure (03)

MICROWAVE SYSTEM FOR BRAGG SCATTERING MEASUREMENTS

with respect to the laser beam.

8.3.3 Experimental Technique

The specimens of zinc oxide were the same ones as were discussed in Chapter 6 in connection with the low temperature measurements.

The method of measurement was to place the laser and photomultiplier so that the incident and diffracted angles were those for maximum diffraction, for the acoustic mode and frequency concerned. The equations derived in the previous section for θ_i and θ_d , were not in fact used to find these angles. It was always possible, with care, to locate the diffracted beam visually. The changes in the power of the diffracted beam were measured with the precision attenuator and V.S.W.R. indicator, as the crystal was successively displaced horizontally by equal distances; the laser and photomultiplier remaining fixed. The displacement of the crystal was measured with a clock gauge. After each displacement the crystal was rotated through a small angle to ensure that in the new position of the laser beam on the crystal, the angles of incidence and diffraction were those which gave the maximum diffracted signal. It was found that small corrections of a few minutes of arc were necessary. This was assumed to be the result of small changes in the direction of propagation of the acoustic wave along the crystal, probably due to changes in the crystallographic orientation of the specimen.

By measuring these corrections it was possible to obtain a very precise measure of the deviation of the acoustic beam as it propagated down the crystal. The largest derivation noted was five minutes of arc over a 5 mm length of specimen.

The linear relation between the acoustic and diffracted optical powers considered in the last section is the basis of the method of measurement. In order to justify using this relation it was necessary to show that the output ~~power~~^{current} of the photomultiplier was proportional to the optical power input, for the appropriate range of light intensities. This was established with a number of different calibrated neutral density filters. The calibration of these filters, which were obtained from Messrs Barr and Stroud could be traced to N.P.L. photometric standards. It was found that the output of the laser showed short term variations of a few percent probably due to mode changes. In order to take account of this, after the laser beam had passed through the crystal the intensity of the main beam (see Figure (8.1)) was monitored with a photodiode. A reading of the laser intensity was taken almost simultaneously with the attenuation reading after each displacement of the crystal.

Care was taken throughout the measurements to ensure that the acoustic power reflected from the end of the specimen was negligible (at least -20 dB down of the power of the unreflected acoustic signals), at the closest point to the reflecting surface at which measurements were made. This requirement had the effect of setting a minimum attenuation which could be measured. In the case of the longitudinal wave it was possible to reduce this minimum attenuation by mechanically loading the end of the specimen with mercury. A pool of the liquid was held in a specially designed cap, which fitted over the end of the specimen. The effect of reflected power on the attenuation measurements is shown in Figure(8.4)

8.4 Acoustic Attenuation at Room Temperature

At room temperature thermal phonon relaxation times are sufficiently small that $\omega\tau_t < 1$, even for microwave frequencies. That is in the classification of Section 5.4, the conditions are those of the high temperature region. Under these conditions the concept of discrete interactions between excitations, used in Chapter 5, is no longer helpful. A more useful picture is of the sound wave as a slowly varying field which interacts with the whole assembly of thermal phonons. The effect of the sound wave is to disturb the equilibrium of the 'gas' of thermal phonons. The disturbed thermal phonon distribution relaxes via irreversible processes, which are the cause of the

absorption of energy from the acoustic wave.

It is well known that the effects of a relaxation process on the acoustic properties of a solid can be treated by modifying the stress-strain relation of the solid. The effect of this modified relation is considered in Appendix B, where it is shown that the acoustic attenuation in such a solid is proportional to the square of the acoustic frequency; if $\omega\tau \ll 1$, where τ is the relaxation time of the relaxation process. This is a general result, independent of the particular relaxation process.

Two relaxation processes are of interest in connection with the acoustic attenuation. The first is the 'thermoelastic' process, which appears to have been first considered by Kirchoff in 1868 when treating acoustic attenuation in liquids. The propagation of a longitudinal wave sets up compressed and dilated regions in a solid. As a result a travelling periodic temperature variation occurs in the direction of acoustic propagation. The thermal conduction which takes place between the hotter and cooler regions is an irreversible process which results in the attenuation of the acoustic wave. A shear acoustic wave does not cause dilation of a solid and thus does not suffer thermoelastic attenuation.

The second relaxation process was suggested by AKHIESER (1939) and applies to both longitudinal and shear waves. As a result of the anharmonicity of the solid, the presence of a sound wave in the solid causes changes in the thermal phonon frequencies. The frequency change is a function of the polarisation and

propagation direction of the phonon. Because of the changes in the phonon frequencies and consequently in the energies of the phonons, these phonons are no longer in thermal equilibrium. As a result the thermal phonons relax towards a local equilibrium. Owing to the effect of the acoustic wave on the elastic properties of the medium, the local equilibrium differs from the equilibrium in the absence of the wave. The relaxation occurs by means of anharmonic phonon-phonon processes, similar to those considered in Chapter 5. ~~These processes are~~ ^{The relaxation process is} irreversible and leads to the attenuation of the wave.

Several calculations of the attenuation due to these processes have been made. This is equivalent to the calculation of the factor $\frac{\Delta c}{c}$ in Equation (B.13) of Appendix B. WOODRUFF and EHRENREICH (1961) have given a general treatment. An alternative has been given by MASON and BATEMAN (1964).

Accurate comparisons of the magnitudes of the measured values of attenuation with those predicted on the basis of the above calculations are not, in general, possible. This is due to a lack of information concerning quantities appearing in the theoretical expressions for the attenuation. With the exception of a few materials, no detailed data is available concerning the anharmonicity or third order elastic coefficients.

The thermal phonon relaxation time also appears in the theoretical expressions, an estimate of this can be obtained from measured values of the thermal conductivity. However the relaxation time obtained in this manner is the relaxation time for Umklapp processes only, whereas the attenuation occurs as a result of both Umklapp and normal processes. (The distinction between these two types of process was indicated in Section 5.4). Thus unless the Umklapp relaxation time is much shorter than the normal process relaxation time, the value of the thermal conductivity relaxation time will not be that required for the comparison.

The point concerning the thermal phonon relaxation times has sometimes been neglected in the literature. In certain cases, this neglect has led to significant errors. For this reason, the following simple argument first given by Peierls is included. Suppose that in some manner a state is set up in which there is a net crystal momentum.

$$P = \hbar \sum_{\mathbf{k}} \mathbf{k} N_{\mathbf{k}}$$

But the normal processes conserve crystal momentum, as is shown in Equation (5.6), and therefore they cannot effect P . However associated with P is an energy flow (Q), which in the absence of dispersion can be written as

$$Q = \hbar v_s \sum_{\mathbf{k}} \mathbf{k} N_{\mathbf{k}} = v_s P.$$

Thus if P is not affected by normal processes neither is Q .

But this means that a net energy flow can persist in the absence of a temperature gradient, which implies an infinite thermal conductivity. That is the normal processes do not contribute to the thermal resistance. Although they can have small second order effects, it is obvious that the thermal conductivity is almost independent of the normal process relaxation time. Therefore information concerning normal processes cannot be obtained from conventional thermal conductivity measurements.

These conclusions are of particular importance in a situation which is not directly related to the present work. This is the technologically important case of low acoustic loss materials. One characteristic looked for in a potential low loss material is a high Debye temperature (θ_D) (OLIVER and SLACK (1966)). But an argument was presented in Section 5.4, to show that when $\frac{T}{\theta_D} < 1$ (where T is the temperature) the incidence of Umklapp processes is significantly reduced. Thus the relaxation time obtained from the thermal conductivity data is likely to be too long.

8.5 Results

It is convenient to deal with the results obtained with the longitudinal and shear specimens separately.

8.5.1 Longitudinal Wave Specimen

The measured attenuation of the piezo-electrically active longitudinal wave propagating along the c axis is shown as a function of acoustic frequency in

Figure (8.4). It can be seen that the predicted quadratic frequency dependence was observed. This result disagrees with that reported by HEMPHILL (1966) who found that the attenuation of this mode varied as $\omega^{1.6}$. As the predicted dependence was obtained reasonable confidence may be placed in the extrapolated values of the attenuation, at higher frequencies. This point will be discussed again in Section 8.6. Because of the interest in extrapolating the attenuation data, the experimental results are tabulated in Figure (8.4). The uncertainties quoted are approximately equal to the ~~mean~~ ^{standard} deviations, of typically eight measurements.

Figure (8.5) shows the attenuation of a 1.004 GHz acoustic wave at various points along the longitudinal specimen. The zero is set at the initial point. The mercury which was used to mechanically load the specimen during the measurements, was removed in order to show the effect of the power reflected from the end of the specimen. The deviation from linearity at the points furthest from the initial point, i.e. those closest to the reflecting surface, is ascribed to the effect of reflected power.

In addition to the measurements of the deviations in the direction of acoustic propagation described in Section 8.3., a further demonstration of the facility of the Bragg scattering method to probe small volumes of the specimen is illustrated in Figure (8.6) This figure shows sketches

ATTENUATION (dB/cm)	5.8±0.3	10.0±0.3	13.7±0.5	23.2±0.7	33.0±0.7
FREQUENCY (GHz)	0.657	0.850	1.004	1.303	1.572

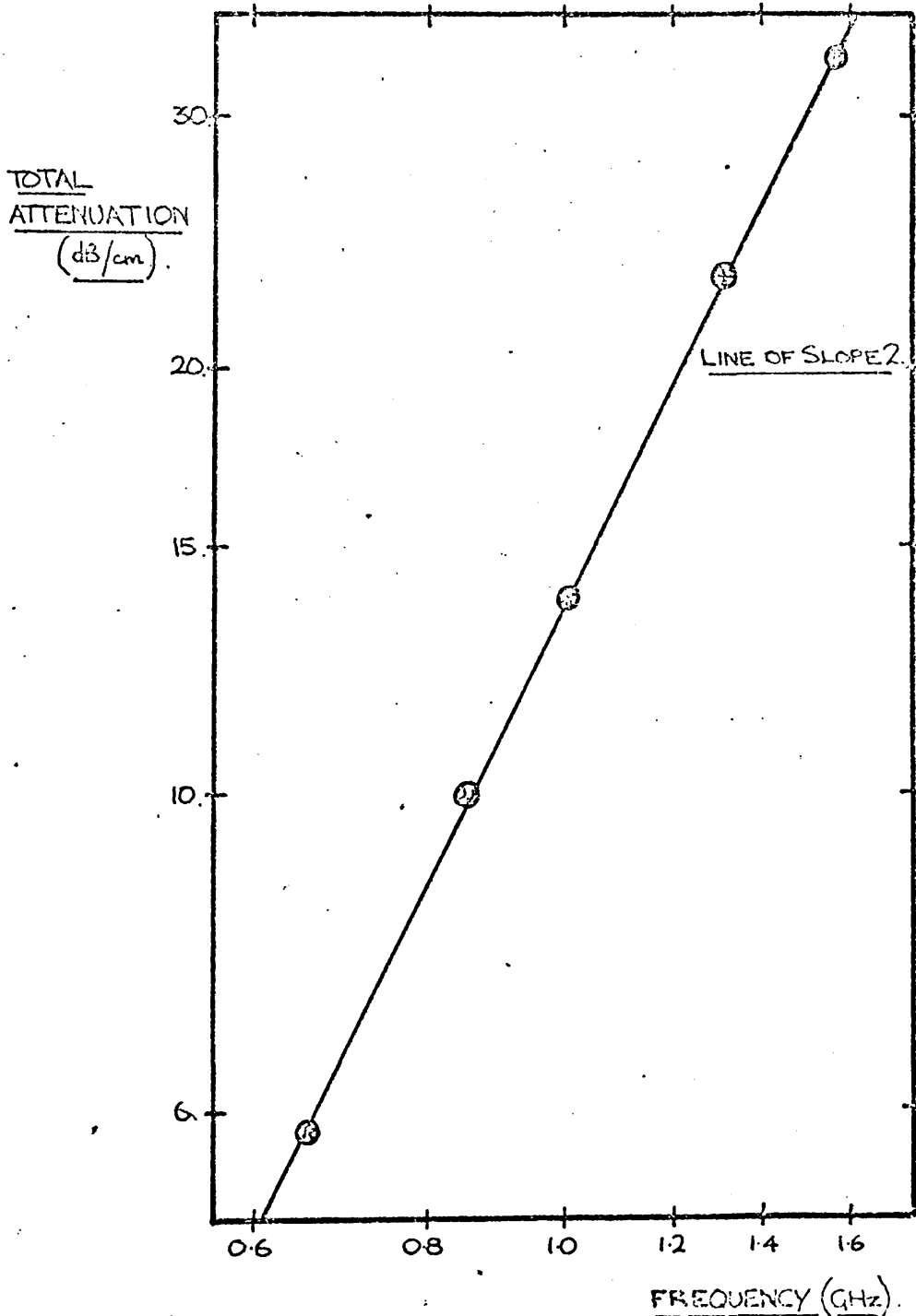


figure (8.4) ACOUSTIC ATTENUATION OF LONGITUDINAL MODE ALONG c-AXIS IN ZINC OXIDE AT ROOM TEMPERATURE.

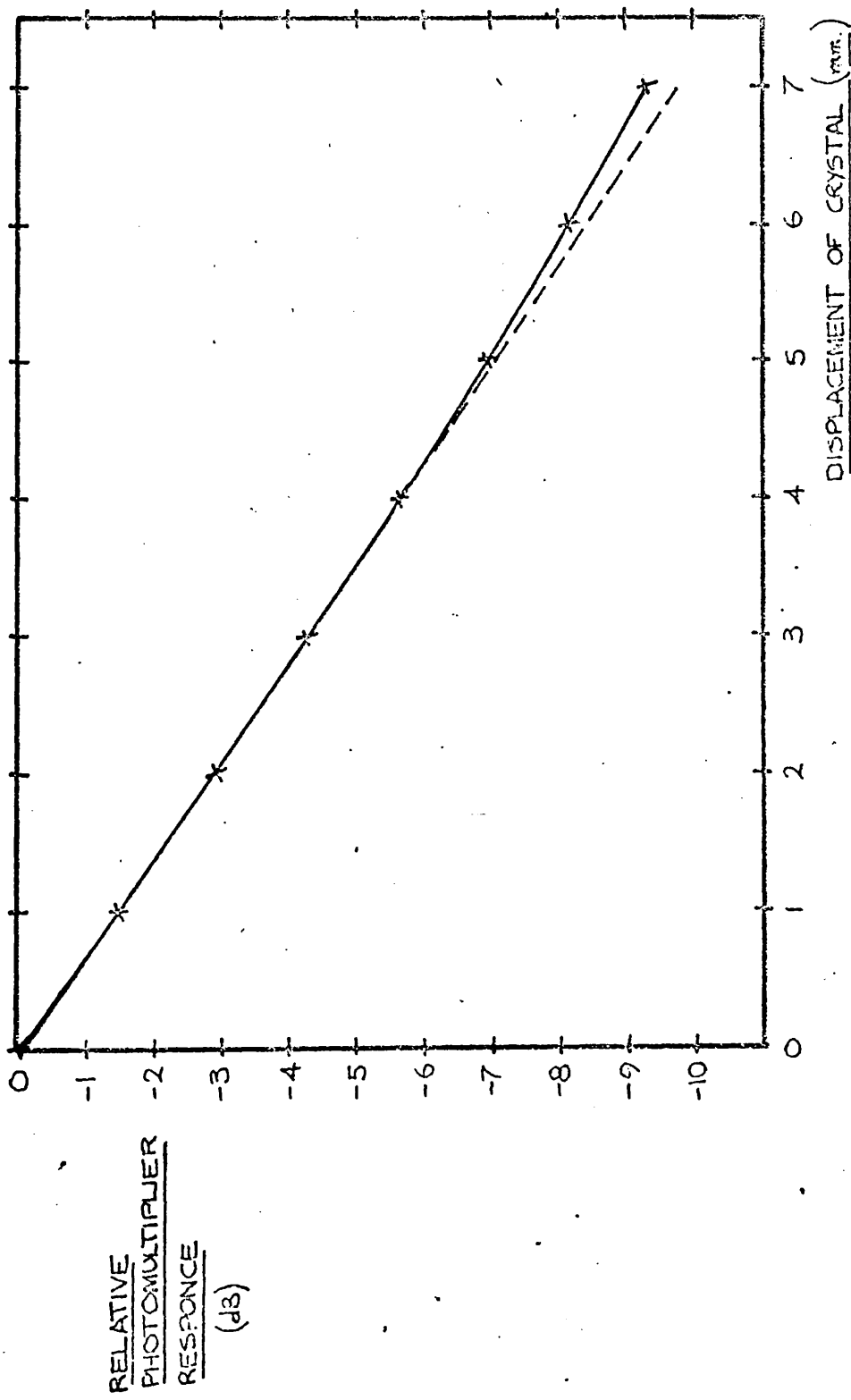


Figure (2.5) RAW ATTENUATION DATA FOR LONGITUDINAL MODE SHOWING THE EFFECT OF REFLECTED POWER.

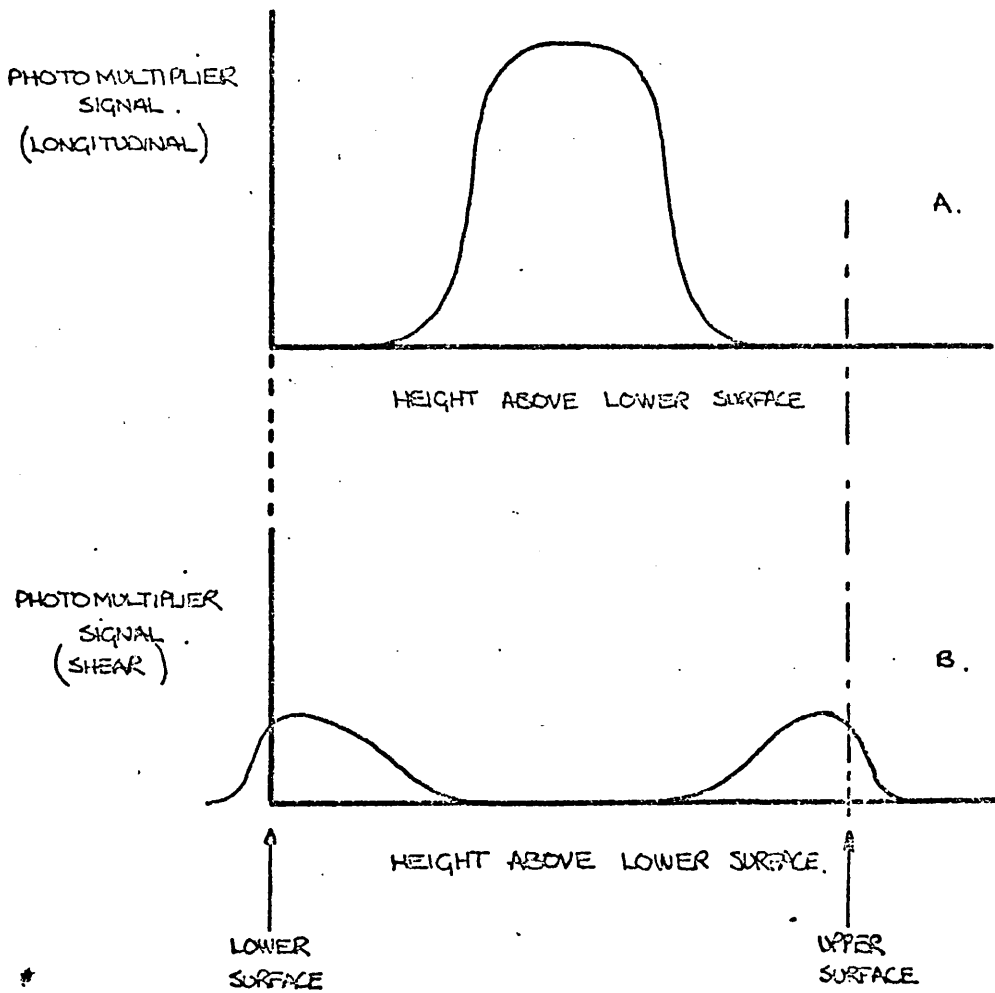
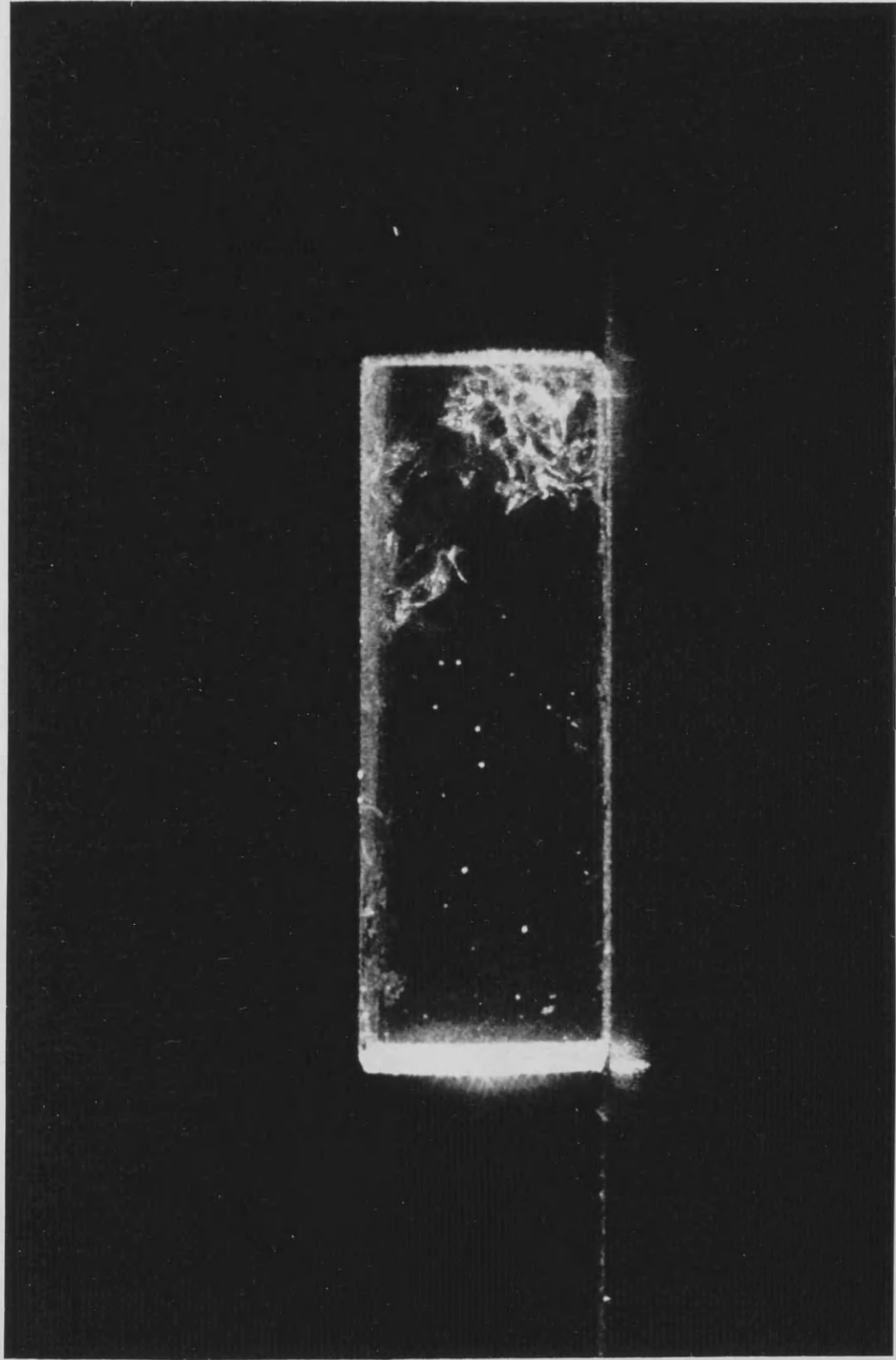


Figure (B.6) ACOUSTIC POWER FLOW ACROSS SECTION THROUGH LONGITUDINAL SPECIMEN PERPENDICULAR TO DIRECTION OF ACOUSTIC PROPAGATION.

of the variation of the signal from the photomultiplier as the longitudinal specimen was lowered through the laser beam. Sketches (a) and (b) show the signals observed when the system was set up to detect light diffracted from the longitudinal and shear waves respectively, propagating parallel to the c axis. The longitudinal wave as expected appears as a well defined beam propagating down the centre of the rod. The shear wave was launched by fringing fields, and as anticipated is concentrated near the sides of the rod.

8.5.2 Shear Wave Specimen

While carrying out diffraction measurements with the shear specimen, it was noted that this specimen was causing significantly greater random scattering of the laser beam than the longitudinal one. As all faces of both specimens were polished to a comparably high optical finish, it appeared that an examination of the optical properties of the shear specimen was required. An initial test was conducted by directing the laser beam along the axis of the specimen, i.e. parallel to the acoustic propagation direction, and observing the beam visually at right angles. Figure (8.7) is a photograph taken under these conditions, and clearly shows substantial scattering of the laser beam. The optical transmission of both specimens was also measured in the



Figure(8.7) SHEAR WAVE SPECIMEN ILLUMINATED BY LASER.

wavelength range $5\mu\text{m}$ to $0.2\mu\text{m}$, using a standard instrument made available by the Chemistry Department. Both specimens showed an absorption edge at a wavelength of $0.4\mu\text{m}$, which agrees with the known bandgap of zinc oxide ($\sim 3.3\text{eV}$ PUTLEY (1960)) and suggests that the bandgap is direct. But whereas the longitudinal specimen showed no variation in absorption between 5 and $0.4\mu\text{m}$, the shear specimen showed a small absorption peak at a wavelength of $2.3\mu\text{m}$.

The measured attenuation of the piezoelectrically active shear wave propagating along the a axis is shown as a function of acoustic frequency in Figure (8.8). The measurements were made at a part of the specimen where no appreciable light scattering was detected (see Figure 8.7). The form of the attenuation versus frequency curve is considered in the next section.

8.6 Interpretation of Shear Wave Attenuation Results

It is clear from Figure (8.8) that the acoustic attenuation measured in the shear specimen did not exhibit the predicted quadratic frequency dependence. This is thought to be a consequence of the fact that the measured attenuation was the sum of two components. The first component was the intrinsic attenuation, that is the attenuation due to thermal phonons considered in Section 8.4. The term intrinsic is not strictly justified because the attenuation due to thermal phonons can be affected by changes in the thermal phonon lifetime, due to the presence of paramagnetic impurities for example.

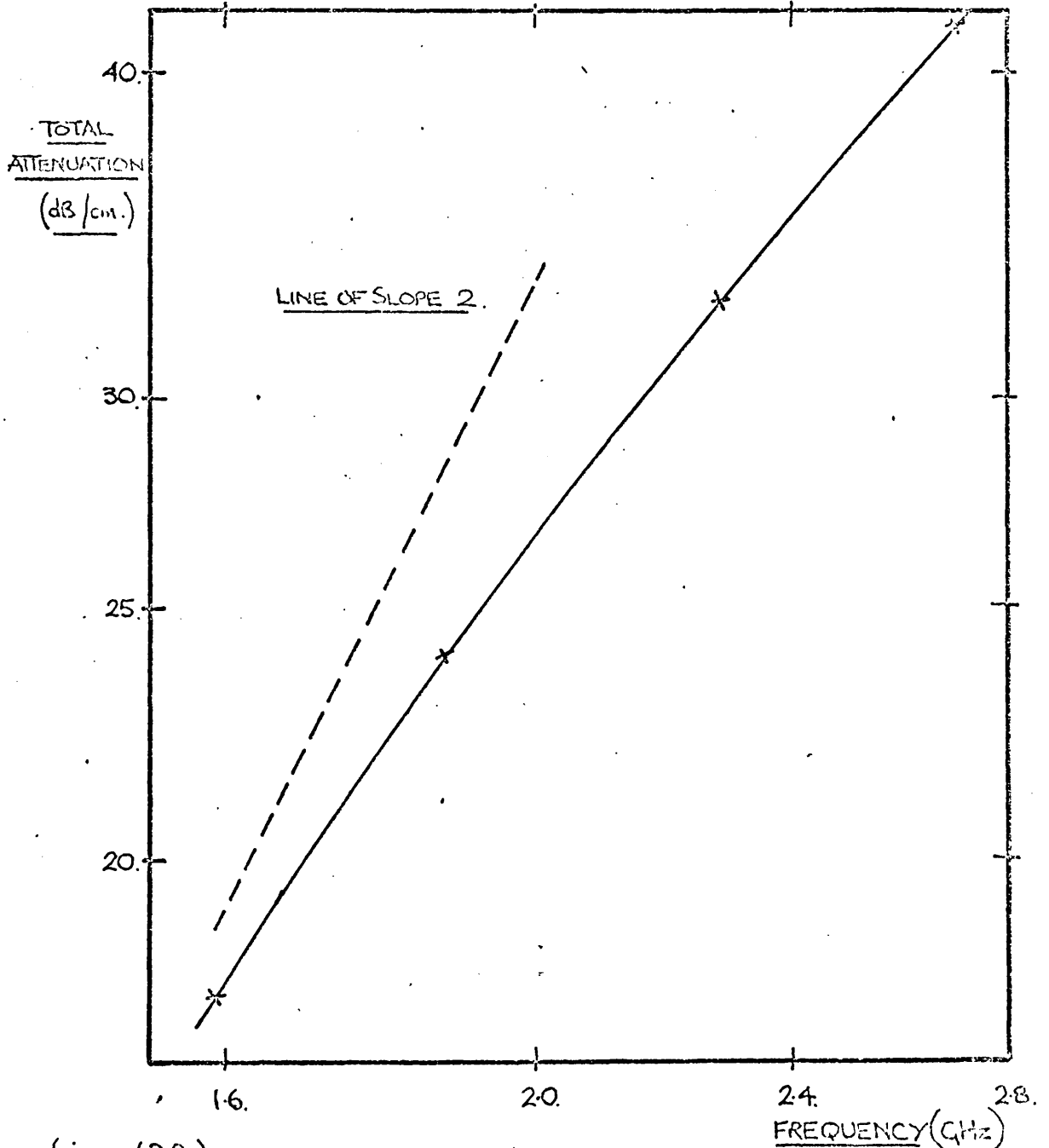


figure (B.B.) ACOUSTIC ATTENUATION AS A FUNCTION OF FREQUENCY FOR SHEAR MODE ALONG a-AXIS IN ZINC OXIDE AT ROOM TEMPERATURE.

However the term is convenient, and does not lead to ambiguity in the present discussion. The second component is thought to have been attenuation due to lattice imperfections. There is very strong evidence from the high residual attenuations detected in this specimen at liquid helium temperatures and from Figure (8.7), for the presence of lattice imperfections.

It was shown in Appendix B that the intrinsic component of the attenuation is expected to vary as the square of the acoustic frequency. Predictions of the frequency dependence of the impurity contribution can only be made in rather general terms, due to a lack of information concerning the concentration, size and mechanical properties of the imperfections. It is convenient at this point to describe briefly the experimental results of MERKULOV (1956) (1957). In measurements made in the frequency range 10-100 MHz on polycrystalline metallic specimens, it was found that the attenuation due to imperfections could be divided into three regions of simple frequency dependence separated by intermediate regions. In region I, at low frequencies, the attenuation was found to vary as the fourth power of the frequency, in the manner of Rayleigh scattering. In Region II the attenuation was found to vary as the square of the frequency. And in region III the attenuation was independent of frequency. The transition between regions II and III was found to occur when $\lambda \approx a$, where λ is the acoustic wavelength and a is the average linear dimension of the imperfections

(which could be estimated metallographically for the polycrystalline metal rods). These results are sketched in Figure (8.9). There have been a number of theoretical investigations of imperfection scattering for the case $\lambda > a$, for example BHATIA (1959) and BHATIA and MOORE (1959). These have led to predictions of the frequency dependence of the attenuation having the same form as in regions I and II of Figure (8.9). In region III when $\lambda < a$, a simple argument can be advanced to account for the observation that the imperfection attenuation does not depend on frequency. When $\lambda < a$, the acoustic wave will tend to propagate in the imperfections, possibly inclusions of lithium, as if they were separate media. As a result of the mechanical mismatch between the imperfections and the host lattice, the acoustic wave will be partly reflected at the boundaries of each imperfection. The resulting scattering will, in general, be in no fixed direction because the imperfections are assumed to have an irregular shape. When $\lambda < a$ the scattering at the boundaries of the imperfections and therefore the apparent attenuation of the acoustic wave will be independent of frequency.

Figure (8.10a) shows how the total attenuation is obtained from the intrinsic and imperfection contributions, at various frequencies. The total attenuation as a function of ω is redrawn in Figure (8.10b), on logarithmic scales, for direct comparison with Figure (8.8). It can be seen that region A of Figure (8.10b) has the same shape as the experimental curve

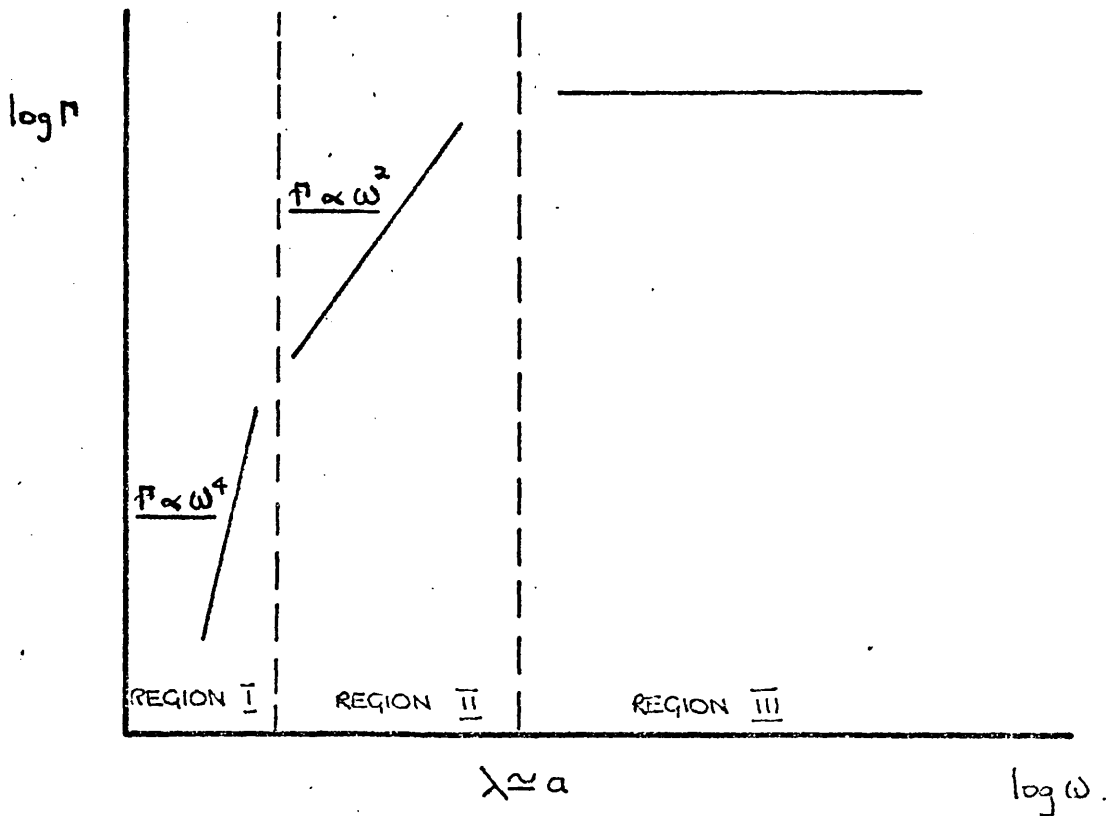


Figure (3.9) DIAGRAMMATIC REPRESENTATION OF FREQUENCY DEPENDENCE OF ACOUSTIC ATTENUATION ARISING FROM SCATTERING BY CRYSTAL IMPERFECTIONS.

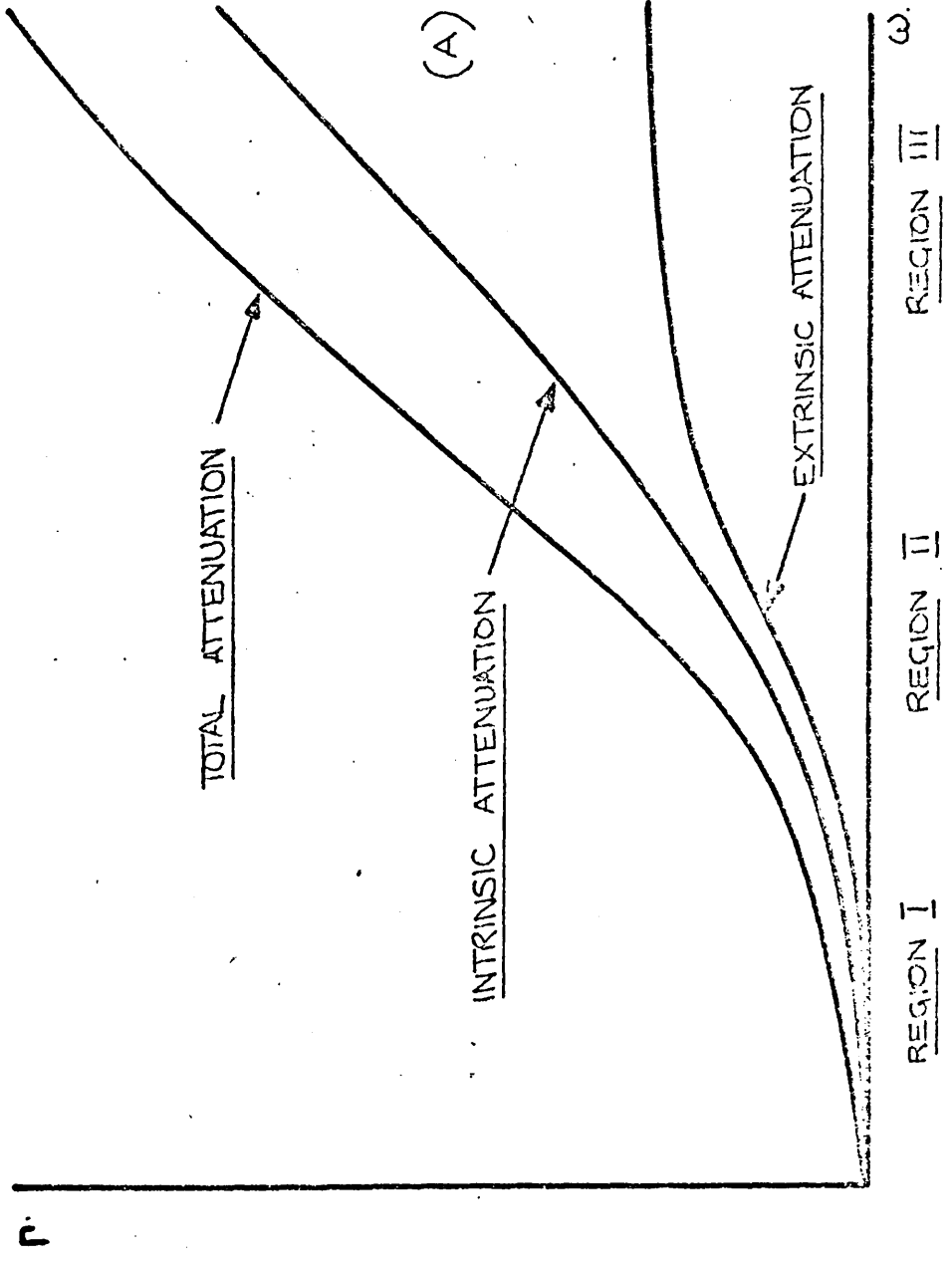


Fig. 8.10(A) FREQUENCY DEPENDENCE OF TOTAL ACOUSTIC ATTENUATION IN A SPECIMEN CONTAINING CRYSTAL DEFECTS.

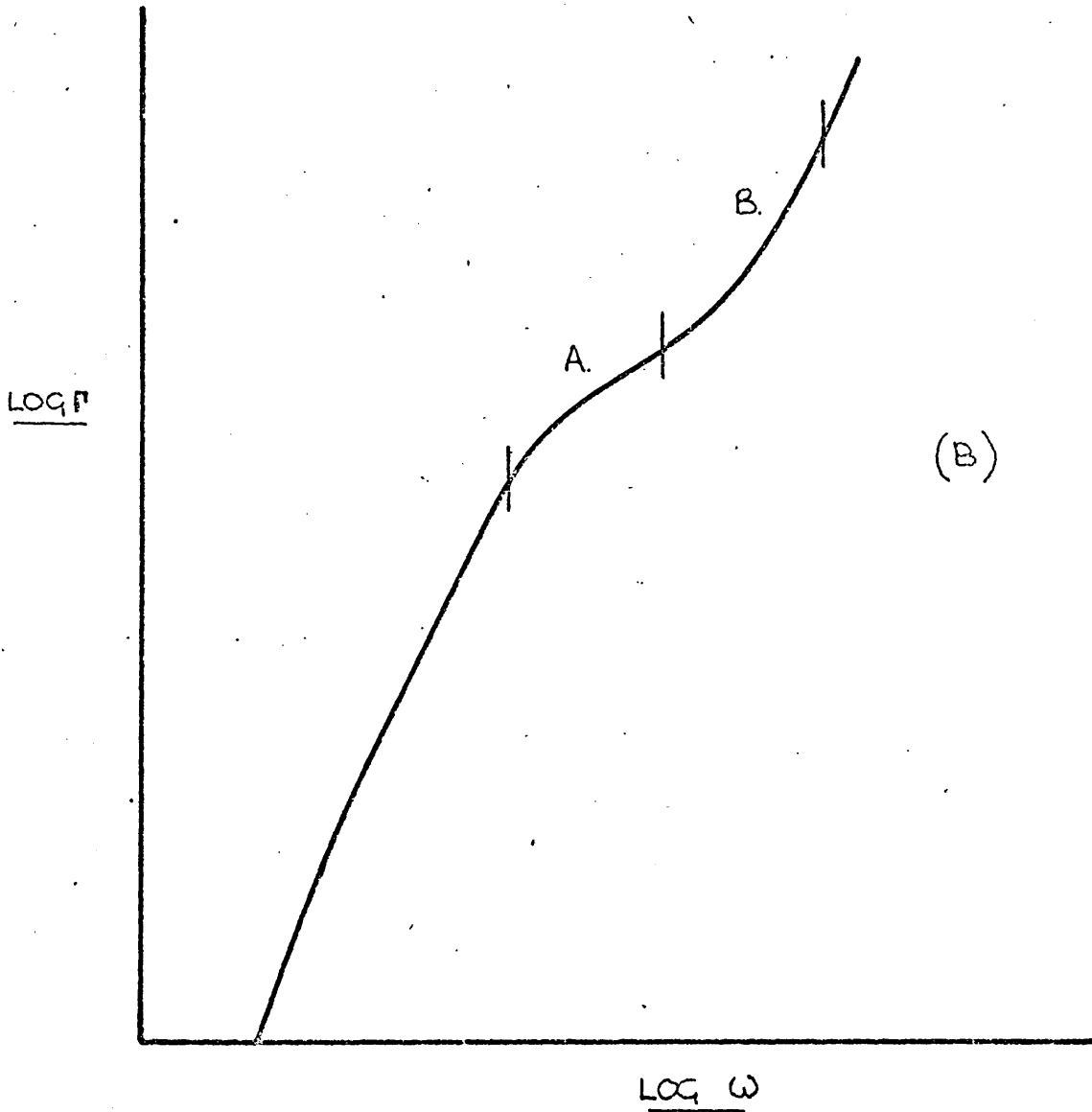


figure (8.10B) TOTAL ACOUSTIC ATTENUATION AS A FUNCTION OF FREQUENCY,
DISPLAYED IN FORM SUITABLE FOR COMPARISON WITH FIGURE (8.8).

Figure (8.8). Thus the form of the frequency dependence of the results obtained with the shear specimen can be explained in terms of the model described at the start of this section. From the slope of the curve in Figure (8.8) which is ~ 1.8 at the lowest frequency, it appears that the condition $\lambda = a$ is satisfied at some frequency a little below the minimum measured frequency. On this basis the average value of 'a' would appear to be 2-3 μm . It is interesting in this context to recall the optical absorption measurements made on the shear specimen, which showed a small absorption at 2.3 μm .

Acoustic attenuation measurements in rutile and sapphire, having a frequency dependence of the same form as region B of Figure (8.10b), have been reported by WILSON, SHAW and WINSLOW (1965). The interpretation of the results in this paper is based on the same model as used in the present work, however the application of the model is erroneous as it is assumed that the intrinsic attenuation varies linearly with the frequency. This error leads to a different explanation of the results to the one presented above.

It should be noted that the fact that the measured attenuation in a given specimen varies as the square of the acoustic frequency, is not sufficient to establish that the measurements are of the intrinsic attenuation. The measurements may have a component of imperfection attenuation which also varies as the square of the frequency, in a given range of frequencies. That is as in region II of Figure (8.9).

However in the case of the present longitudinal wave measurements the effect of scattering by imperfections can be neglected, as the residual attenuation in the specimen at liquid helium temperatures is known to be approximately 0.1 dB/cm.

8.7 Maximum Operating Frequencies of Acousto-Electric Devices

In order to illustrate the significance of acoustic attenuation measurements in acousto-electric device studies, the upper cut-off frequency of acousto-electric devices is considered below.

Potentially the most important applications of acousto-electric devices are in the microwave frequency range. Consequently the maximum operating frequency of such devices is a parameter of considerable importance. In general the high frequency cut-off will occur when the attenuation of the acoustic energy by the lattice is so large that no appreciable acousto-electric interaction is possible.

It is convenient to consider a particular acousto-electric device. Perhaps the most interesting of these devices is the acousto-electric oscillator WHITE and WANG (1966). A detailed investigation of the characteristics of this device has been carried out in the Department TWOMEY (1970). In this work it has been shown that the maximum cut-off frequency of such an oscillator is given by the expression

$$\nu_{\max} = \frac{\pi K^2}{8 + \nu_s} \left[1 + \frac{\pi K^2}{2 + \nu_s \nu_p} \right]^{-1/2} \quad (8.14)$$

where K is the electro-mechanical coupling coefficient, ν is the acoustic frequency and r and ν_D are defined by the relations

$$r = r\nu^2$$

and

$$\nu_D = \frac{1}{2\pi} \frac{e\nu_s^2}{\mu k_B T}$$

Equation (8.14) shows the dependence of the cut-off frequency on the magnitude of the acoustic attenuation.

It is interesting to estimate the values of the maximum operating frequencies of oscillators constructed from cadmium sulphide and zinc oxide, the two most promising oscillator materials. Using appropriate values of the quantities in Equation (8.14) including the value of r for zinc oxide obtained from Figure (8.4), the maximum operating frequencies for longitudinal wave oscillators are

MATERIAL	CdS	ZnO
ν_{\max}	4.5 GHz	17 GHz.

It is apparent that zinc oxide is likely to be the more useful material for the construction of microwave frequency acousto-electric oscillators.

APPENDICES

The objective of these appendices is to provide an account of the derivation of certain results of special importance in the discussions in Chapters 7 and 8. The derivations presented here are based on previously published work, and contain no original results.

In Appendix A it is shown that when acoustic attenuation can be considered to take place by means of first order three phonon processes, then the attenuation coefficient can be written in the form $\Gamma = A\omega T^4$. Where A is independent of ω , and T.

Appendix B is concerned with the situation when $\omega\tau \ll 1$; where ω refers to the acoustic wave and τ is the thermal phonon relaxation time. Under this condition it is shown that if the acoustic attenuation is caused by a relaxation process, then the magnitude of the attenuation is proportional to the square of the acoustic frequency. This result is found to be independent of the detailed nature of the relaxation mechanism.

In keeping with the form of the discussions in Chapters 7 and 8, the treatment in these appendices concentrates on the frequency dependence and the temperature dependence of the attenuation.

APPENDIX A

In this appendix the form of the expression for the acoustic attenuation coefficient is investigated in the case where the attenuation is caused by first order three phonon processes. This treatment is based on that given by LANDAU and RUMER (1937). For the reasons given in Chapter 5, attention is particularly directed to the temperature dependence and the frequency dependence of the attenuation.

The three phonon processes of interest are those for which the selection rules can be written as

$$\omega_1 + \omega_2 = \omega_3 \quad (\text{A.1})$$

$$\vec{k}_1 + \vec{k}_2 = \vec{k}_3 \quad (\text{A.2})$$

Where the suffix 1 denotes an acoustic phonon, and the suffices 2 and 3 refer to thermal phonons.

In order to obtain an explicit expression for the attenuation, it is necessary to consider a specific three phonon process from the group (5.10) discussed in Chapter 5. Process (5.10d) (i.e. $t+l \rightarrow l$) is chosen as an example. Using the method of Landau and Rumer or the alternative one discussed by PEIERLS (1955), an expression for the matrix element for the absorption process can be obtained. As $|k_1| \ll |k_2| \approx |k_3|$ and $\omega_1 \ll \omega_2 \approx \omega_3$, for the process under consideration the expression for the matrix element can be written

$$(N_1, N_2, N_3 | H | N_1-1, N_2-1, N_3+1) = \lambda (\vec{k}_2 \cdot \vec{k}_1) \left(\frac{\hbar N_1}{2m\omega_1} \right)^{1/2} \left(\frac{\hbar N_2}{2m\omega_2} \right)^{1/2} \left(\frac{\hbar N_3+1}{2m\omega_3} \right)^{1/2} V \quad (\text{A.3})$$

Where λ is a function of the anharmonicity of the material, the N 's are the numbers of acoustic and thermal phonons in the specimen, \vec{e}_1 is a unit vector in the direction of polarisation of the acoustic wave, m is the mass of the specimen and V its volume.

It is well known from the first order time dependent perturbation theory (SCHIFF (1955)); that assuming a single initial thermal phonon state, the transition probability per unit time for the absorption process has the form

$$\frac{2\pi}{\hbar} | (N_1, N_2, N_3 | H | N_1-1, N_2-1, N_3+1) |^2 \delta(\omega_1 + \omega_2 - \omega_3) \quad (\text{A.4})$$

Let ρ_2 be the number of phonon states for which \vec{k}_2 has a magnitude between $|k_2|$ and $|k_2| + d|k_2|$, and lies in the solid angle $d\Omega$. There are $\frac{V}{(2\pi)^3}$ allowed states per unit volume of k space, thus

$$\rho_2 dk_2 d\Omega = \frac{V k_2^2 dk_2 d\Omega}{(2\pi)^3}$$

Thus the total transition probability per unit time for the absorption process can be written.

$$\frac{1}{(2\pi\hbar)^2} \int | \langle N_1, N_2, N_3 | H | N_1+1, N_2-1, N_3+1 \rangle |^2 \delta(\omega_3 + \omega_2 - \omega_1) V k_2^2 dk_2 d\Omega \quad (\text{A.5})$$

Correspondingly for the reverse or acoustic phonon emission process, the total transition probability per unit time is

$$\frac{1}{(2\pi\hbar)^2} \int | \langle N_1, N_2, N_3 | H^\dagger | N_1+1, N_2+1, N_3-1 \rangle |^2 \delta(\omega_3 - \omega_1 - \omega_2) V k_2^2 dk_2 d\Omega. \quad (\text{A.6})$$

As far as the absorption of sound is concerned it is the difference between these two which is important. To find this difference the following properties of the creation and annihilation operators, from the theory of the harmonic oscillator (SCHIFF (1955)), are needed.

$$(N | A | N+1) \propto (N+1)^{1/2}$$

and

$$(N' | A^\dagger | N'-1) \propto (N')^{1/2}$$

Thus the difference between the transition probabilities per unit time is proportional to

$$N_2(N_3+1) - (N_3+1)N_2 \quad (\text{As } N_1 \approx N_1+1)$$

$$= N_2 - N_3$$

N_2 and N_3 are the thermal equilibrium numbers of these phonons so that

$$N_2 = \frac{1}{\exp\left(\frac{\hbar\omega_2}{k_B T}\right) - 1} \quad (\text{A.7})$$

$$\text{Thus } N_2 - N_3 = \frac{\exp\left(\frac{\hbar\omega_3}{k_B T}\right) - \exp\left(\frac{\hbar\omega_2}{k_B T}\right)}{\left[\exp\left(\frac{\hbar\omega_2}{k_B T}\right) - 1\right] \left[\exp\left(\frac{\hbar\omega_3}{k_B T}\right) - 1\right]} \quad (\text{A.8})$$

From Equation (A.1) it can be seen that

$$\exp\left(\frac{\hbar\omega_3}{k_B T}\right) = \exp\left(\frac{\hbar\omega_2}{k_B T}\right) \left\{ \exp\left[\frac{\hbar}{k_B T} (\omega_3 - \omega_2)\right] \right\} \quad (\text{A.9})$$

$$\exp\left[\frac{\hbar}{k_B T} (\omega_3 - \omega_2)\right] = 1 + \frac{\hbar}{k_B T} (\omega_3 - \omega_2) + \dots \quad (\text{A.10})$$

From Equation (A.8), (A.9) and (A.10)

$$N_2 - N_3 \approx \frac{\exp\left(\frac{\hbar\omega_2}{k_B T}\right) \frac{\hbar}{k_B T} (\omega_3 - \omega_2)}{\left[\exp\left(\frac{\hbar\omega_2}{k_B T}\right) - 1\right]^2} \quad (\text{A.11})$$

Differentiating (A.7) with respect to ω_2 , and substituting in Equation (A.11) yields

$$N_2 - N_3 = (\omega_3 - \omega_2) \frac{\partial N_2}{\partial \omega_2}.$$

From Equation (A.1)

$$N_2 - N_3 = \omega_1 \frac{\partial N_2}{\partial \omega_2} \quad (\text{A.12})$$

From Equations (A.3), (A.5) and (A.12) it can be shown that the transition probability per unit time for the net absorption of acoustic phonons ($\frac{dP}{dt}$) is

$$\frac{dP}{dt} = \frac{\hbar V^3}{(2\pi)^2} \frac{\lambda^2}{(2m)^3} \int \frac{(\vec{k}_2 \cdot \vec{k}_1)^2 (\vec{k}_2 \cdot \vec{e}_1)^2}{\omega_2^2} \frac{\partial N_2}{\partial \omega_2} \delta(\omega_1 + \omega_2 - \omega_3) k_1^2 dk_1 d\Omega \quad (\text{A.13})$$

Where the fact that $\omega_2 \approx \omega_3$ has been utilised.

If polar co-ordinates are introduced with \vec{k}_1 direction along the z-axis, the following substitutions may be made

$$(\vec{k}_2 \cdot \vec{k}_1)^2 = |k_2|^2 |k_1|^2 \cos^2 \theta; \quad (\vec{k}_2 \cdot \vec{e}_1)^2 = |k_2|^2 \sin^2 \theta \cos^2 \phi \quad (\text{A.14})$$

$$d\Omega = \sin \theta d\theta d\phi$$

Let $\Delta\omega$ be defined so that

$$\begin{aligned}\Delta\omega &= \omega_1 + \omega_2 - \omega_3 \\ &= \omega_1 - (\omega_3 - \omega_2)\end{aligned}$$

If $\omega_3(k_3) = \omega_3(k_1 + k_2)$ is expanded by Taylor's theorem, it is found that

$$\Delta\omega = \omega_1 - k_1 \cdot \frac{\partial\omega_2}{\partial k_2}$$

The process under discussion is process (5.10d). At the low temperatures of interest dispersion may be neglected and $\frac{\partial\omega_2}{\partial k_2} = v_l$ where v_l is the velocity of the longitudinal acoustic mode.

$$\therefore \Delta\omega = \omega_1 - |k_1| v_l \cos\theta \quad (\text{A.15})$$

It is convenient to rewrite Equation (A.13) as

$$\frac{dP}{dt} = \frac{\hbar V^3}{(2\pi)^2} \cdot \frac{\lambda^2}{(2m)^3} \cdot I \quad (\text{A.16})$$

Substituting into Equation (A.13) from Equations (A.14) and (A.15) yields

$$I = \int_0^{2\pi} \int_0^\pi \int_0^\infty \frac{|k_1|^2 |k_2|^4}{\omega_2^2} \frac{\partial N_2}{\partial \omega_2} \delta(\omega_1 - |k_1| v_l \cos\theta) k_2^2 dk_2 \cos^2\theta \sin^2\theta d(\cos\theta) \cos^2\phi d\phi.$$

In evaluating this integral the following result is required

$$\int_0^{2\pi} \cos^2 \phi \, d\phi = \pi. \quad (\text{A.18})$$

From the properties of the delta function

$$\omega_1 = |k_1| v_2 \cos \theta \quad (\text{A.19})$$

Using the result (A.18) and substituting (A.19) into (A.17) yields after rearrangement

$$I = \pi |k_1|^2 \frac{\omega_1^2}{|k_1|^2 v_2^2} \left[1 - \frac{\omega_1^2}{|k_1|^2 v_2^2} \right] \cdot \frac{1}{|k_1| v_2} \cdot \frac{1}{v_2} \int_0^{\infty} \omega_2^4 \frac{\partial N_2}{\partial \omega_2} \, d\omega_2 \quad (\text{A.20})$$

Let J be defined such that

$$J = \int_0^{\infty} \omega_2^4 \frac{\partial N_2}{\partial \omega_2} \, d\omega_2 \quad (\text{A.21})$$

Differentiating (A.7) with respect to ω_2 and substituting in Equation (A.21) yields

$$J = \int_0^{\infty} \omega_2^4 \left(\frac{h}{k_B T} \right) \exp\left(\frac{h\omega_2}{k_B T} \right) \left[\exp\left(\frac{h\omega_2}{k_B T} \right) - 1 \right]^2 \, d\omega_2 \quad (\text{A.22})$$

let γ be defined so that

$$\gamma = \left(\frac{\hbar \omega_2}{k_B T} \right)$$

Then making this substitution Equation (A.22) becomes

$$J = \left(\frac{k_B T}{\hbar} \right)^4 \int_0^{\infty} \frac{\gamma^4 \exp \gamma}{(\exp \gamma - 1)^2} d\gamma \quad (\text{A.23})$$

The integral in Equation (A.23) has the value $5! \zeta(5)$ (ABRAMOWITZ and STEGUN (1965)). Where $\zeta(5)$ is the Riemann zeta function of order five. The values of the Riemann zeta functions have been tabulated Abramowitz and Stegun, $\zeta(5) \approx 1.04$. From Equations (A.16), (A.20) and (A.23) the attenuation coefficient (Γ) may be written

$$= 120 \cdot 1.04 \cdot \frac{\hbar}{4\pi} \frac{\lambda^2}{\rho^3} \frac{v_t^2}{v_l^2} \left(1 - \frac{v_t^2}{v_l^2} \right) \frac{\omega_1}{v_t^2 v_l^8} \left(\frac{k_B T}{\hbar} \right)^4$$

Where v_t is the velocity of the transverse acoustic mode (because process (5.10d) is the one under discussion). It will be recalled that in Chapter 5 it was assumed that the material was isotropic.

It can be seen that the expression for the attenuation has the form $\Gamma = A \omega_1 T^4$. The same general form is found for the other three processes belonging to the group (5.10).

In the original paper of Landau and Rumer, as a result of a typographical error, the final expression has a different temperature dependence to the one shown here.

APPENDIX B

The object of this appendix is to investigate the frequency dependence of the attenuation coefficient of an acoustic wave propagating in a solid having a complex elastic coefficient. It is assumed that the conditions of the high temperature region, as defined in Section 5.4., are applicable. That is $\omega\tau_t \ll 1$, where ω refers to the acoustic wave and τ_t is the thermal phonon relaxation time.

Following ZENER (1948) the relation between stress (σ) and ^{strain} ϵ for the solid is written in the form

$$\sigma + \tau_\epsilon \dot{\sigma} = C_R (\epsilon + \tau_\sigma \dot{\epsilon}) \quad (\text{B.1})$$

If a stress σ_0 is suddenly applied at a time $t = 0$, the strain will initially adopt a value ϵ_0 . It will then relax with the strain relaxation time at constant stress (τ_σ), to an equilibrium value $\frac{\sigma_0}{C_R}$; where C_R is the relaxed elastic coefficient. This behaviour can be represented by a solution of Equation (B.1) having the form

$$\epsilon(t) = \frac{\sigma_0}{C_R} + \left(\epsilon_0 - \frac{\sigma_0}{C_R} \right) e^{-t/\tau_\sigma} \quad (\text{B.2}).$$

The constant τ_ϵ in Equation (B.1) is similar to τ_σ and represents the stress relaxation time at constant strain.

Equation (B.2) describes a form of the 'elastic after-effect'. This effect is characteristic of a solid with a complex elastic coefficient.

It is useful to introduce an additional parameter, the unrelaxed elastic coefficient C_u . Suppose that in a very short time δt the stress is changed by a small amount $\Delta\sigma$. If both sides of Equation (B.1) are now integrated with respect to time over the interval δt , then the first terms on each side of the Equation tend to zero as δt tends to zero. The result is

$$\tau_\epsilon \Delta\sigma = C_R \tau_\sigma \Delta\epsilon \quad (\text{B.3})$$

where the ratio $\Delta\sigma/\Delta\epsilon$ is the unrelaxed elastic coefficient (C_u). This relates to the initial strain resulting from a change in stress which is sufficiently rapid that no relaxation occurs before it is complete. From Equation (B.3) it is seen that the relaxed and unrelaxed elastic coefficients are related by

$$C_u = \frac{\tau_\sigma}{\tau_\epsilon} C_R \quad (\text{B.4})$$

As the acoustic wave is assumed to be harmonic, it is of interest to consider the stress and strain as periodically varying, so that

$$\begin{aligned}\sigma(t) &= \sigma_0 e^{i\omega t} & \text{and} & \quad \dot{\sigma}(t) = i\omega\sigma_0 e^{i\omega t} \\ \epsilon(t) &= \epsilon_0 e^{i\omega t} & \text{and} & \quad \dot{\epsilon}(t) = i\omega\epsilon_0 e^{i\omega t}\end{aligned}\tag{B.5}$$

Substituting in Equation (B.1) from (B.5)

$$(1 + i\omega\tau_\epsilon)\sigma_0 = C_R(1 + i\omega\tau_\sigma)\epsilon_0\tag{B.6}$$

the complex elastic coefficient is obtained from Equation (B.6) by setting

$$C^* = \frac{\sigma_0}{\epsilon_0}$$

thus

$$C^* = \frac{(1 + i\omega\tau_\sigma)}{(1 + i\omega\tau_\epsilon)} C_R$$

The angle (δ) by which the strain lags the stress is of interest, it's tangent is well known to be equal to the ratio of the imaginary part of C^* to its real part. If the usual method of separating the real and imaginary parts of C^* is employed, the ratio is found to be

$$\tan \delta = \frac{\omega(\tau_\sigma - \tau_\epsilon)}{1 + \omega^2\tau_\sigma\tau_\epsilon}\tag{B.7}$$

It is convenient to define a mean relaxation time

$$\tau = (\tau_o \tau_e)^{1/2} \quad (\text{B.8})$$

and a mean elastic coefficient.

$$c = (c_o c_R)^{1/2} \quad (\text{B.9})$$

If it is assumed that $c_o \approx c_R \approx c$, it follows from Equation (B.4) that $\tau_o \approx \tau_e \approx \tau$.

By using these approximations in conjunction with Equations (B.4), (B.8) and (B.9), it is possible to transform Equation (B.7) into

$$\tan \delta = \frac{(c_o - c_R)}{c} \frac{\omega \tau}{1 + \omega^2 \tau^2} \quad (\text{B.10})$$

As $\Gamma \ll \frac{\omega}{v_s}$, the attenuation coefficient and $\tan \delta$ are related by the expression

$$\Gamma = \frac{\omega}{2v_s} \tan \delta. \quad (\text{B.11})$$

From Equations (B.10) and B.11)

$$\Gamma = \frac{1}{2v_s} \cdot \frac{c_o - c_R}{c} \cdot \frac{\omega^2 \tau}{1 + \omega^2 \tau^2}. \quad (\text{B.12})$$

If the acoustic frequency is such that $\omega\tau \ll 1$, which was the case in the present measurements, then Equation (B.12) becomes

$$\Gamma = \frac{1}{2\sqrt{3}} \frac{\Delta c}{c} \tau \omega^2 \quad (\text{B.13})$$

where $\Delta c = c_v - c_R$.

which shows a quadratic dependence of attenuation on frequency. During the derivation of this result no assumptions were made concerning the nature of the relaxation process. That is the result is a general one applicable to the attenuation caused by any relaxation process.

REFERENCES

- ABAMOWITZ M. and STEGUN I.A. (Editors) (1965) Handbook of Mathematical Functions, Dover Publications, New York.
- AKHEISER A. (1939) J. Phys (U.S.S.R.) 1, 277.
- BARANSKII K.N. (1958) Soviet Physics - Doklady 2, 237.
- BARBER C.R. (1955) J. Sci. Instrum. 32, 416.
- BARDEEN J. and SHOCKLEY W. (1950) Phys Rev. 80, 71.
- BARDSLEY W. (1960) Progress in Semiconductors 4, 155.
- BATEMAN T.B. (1962) J. Appl. Phys. 33, 3309.
- BENNETT G.A. and WILSON R.B. (1966) J. Sci. Instrum 43, 669.
- BERLINCOURT D., JAFFE H. and SHIOZAWA R.L. (1963) Phys Rev. 129, 1009.
- BERZ F. (1965) Private Communication.
- BHATIA A.B. (1959) J. Acoust. Soc. America 31, 16.
- BHATIA A.B. and MOORE R.A. (1959) J. Acoust. Soc America 31, 1140.
- BLATT F.J. (1957a) Phys.Rev. 105, 1203.
- BLATT F.J. (1957b) J. Phys.Chem.Solids 1, 262.
- BRIGGS H.B. (1950) Phys.Rev. 77, 287.
- BROOKS H. (1951) Phys.Rev. 83, 879.
- BROOKS H. (1955) Advances in Electronics and Electron Physics 7, 87.
- BLOUNT E.I. (1959) Phys.Rev. 114, 418.
- CARR P.H. and STRANDBERG M.W.P. (1962) J. Phys. Chem.Solids, 23, 923.
- CICCARELLO I.S. and DRANSFELD K. (1964) Phys. Rev. 134, A1517.

- CLAIBORNE L.T., HEMPHILL R.B. and EINSBRUCH N.G. (1969)
J. Acoust. Soc. America 45, 1352.
- CLINE C.F., DUNEGAN H.L. and HENDERSON G.W. (1967)
J. Appl. Phys. 38, 1944.
- COHEN M.G. and GORDON E.I. (1965) Bell System Tech.J. 44, 693.
- CONWELL E.M. (1964) Proc.I.E.E.E. 52, 954.
- CSAVINSKY P. and EINSBRUCH N.G. (1963) Appl. Phys.Lett. 2, 1.
- CULLITY B.D. (1956) Elements of X-Ray Diffraction, Addison Wesley,
Reading Massachusetts.
- DALE J.R. (1966) Private communication.
- DEBYE P.P. and CONWELL E.M. (1954) Phys. Rev. 93, 693.
- de KLERK J. AND KELLY E.J. (1965) Rev. Sci. Instrum. 36, 506.
- de KLERK J. (1966) J. Appl. Phys. 37, 4522.
- de KLERK J. and KLEMENS P.G. (1966) Phys.Rev. 147, 585.
- DINGLE R.B. (1955) Phil.Mag. (Series VII) 46, 831.
- DIXON R.W. (1967) I.E.E.E. J. Quantum Electronics QE-3, 85.
- ECKSTEIN S.G. (1963) Phys. Rev. 131, 1087.
- ECKSTEIN S.G. (1964) J. Appl. Phys. 35, 2702.
- ERGINSOY C. (1950) Phys.Rev. 79, 1013.
- FOSTER N.F. (1964) I.E.E.E. Trans.Sonics and Ultrasonics
S.U.-11, 63.
- FOSTER N.F. (1967) J.Appl. Phys. 38, 149.
- FOWLER R.H. (1936) Statistical Mechanics, Cambridge University
Press, London.
- FRITZSCHE H. (1959) Phys. Rev. 115, 336.
- FRÖHLICH H. and PARANJAPE B.V. (1956) Proc. Phys. Soc. 69, 21.
- GANAPOLSKII E.M. and TARAKANOV V.V. (1968) Soviet Physics -
Solid State 10, 785.

- GANTSEVICH S.V. and GUREVICH V.L. (1967) Phys. Rev. 161, 736.
- GANTSEVICH S.V. and GURVICH V.L. (1969a) Soviet Physics - Semiconductors 2, 932.
- GANTSEVICH S.V. & GUREVICH V.L. (1969b) Soviet Physics - Semiconductors 2, 936.
- GIBSON R.W. (1966) Electronics Lett. 2, 213.
- GLASOE G.N. and LEBACQZ J.V. (1948) Pulse Generators, McGraw Hill, New York.
- GUREVICH L.E. and SHKLOVSKII B.I. (1967) Soviet Physics - Solid State 9, 401.
- GUREVICH V.L. and EFROS A.L. (1963) Soviet Physics - J.E.T.P. 17, 1432.
- HALL E.H. (1879) American J. Math. 2, 287.
- HAM F. (1955) Phys. Rev. 100, 1251.
- HANSEN W.W. (1939) J. Appl. Phys. 10, 38.
- HEARN C.J. (1965) Proc. Phys. Soc. 86, 881.
- HERRING C. (1954) Phys. Rev. 95, 954.
- HERRING C. and VOGT E. (1956) Phys. Rev. 101, 944.
- HILL R.W. and PARKINSON D.H. (1952) Phil. Mag. (Series VII) 43, 309.
- HUTSON A.R., MCFEE J.H. and WHITE D.L. (1961) Phys. Rev. Lett. 7, 237.
- HUTSON A.R. and WHITE D.L. (1962) J. Appl. Phys. 33, 40.
- ISENBERG I. RUSSELL B.R. and GREENE R.F. (1948) Rev. Sci. Instrum. 19, 685.
- JACOBSON E.H. (1960) J. Acoust. Soc. America 32, 949.
- JACOBSON E.H. (1961) Quantum Electronics, Townes C.H. (Ed), Columbia University Press, New York.
- KEYES R.W. (1960) Solid State Physics 11, 149.
- KEYES R.W. (1961) I.B.M. J. Research and Development 5, 266.

- KLEIN R. (1966) Phys. Lett. 23, 651.
- KWOK P.C. MARTIN P.C. and MILLER P.B. (1965) Solid State Comm. 3, 181.
- KYAME J.J (1949) J. Acoust. Soc. America 21, 159.
- LAMB J. and RICHTER J. (1967) J. Acoust. Soc America 41, 1043.
- LANDAU L.D. and RUMER G. (1937) Phys. Z. Sowjetunion 11, 18.
- LANGE J.N. (1968) Phys. Rev. 147, 585.
- LEVINGER B.W. AND FRANKL D.R. (1961) J. Phys. Chem. Solids 20, 281.
- LEWIS M.F. and PATTERSON E. (1967) Phys. Rev. 159 , 703.
- MALONEY W.T. and CHARLTON H.R. (1967) I.E.E.E. Trans, Sonics and Ultrasonics SU-14, 135.
- MANSFIELD R. (1956) Proc. Phys. Soc. 69, 76.
- MARIS H.J. (1964) Phil. Mag. (series VIII) 9, 901.
- MASON W.P. and BATEMAN T.B. (1964) J. Acoust. Soc. America 36, 644.
- MAY J.E. (1965) Proc I.E.E.E. 53, 1465.
- McDOUGALL J. and STONER E.C. (1938) Phil. Trans. Roy. Soc. (Series A) 237, 67.
- McKELVEY J.P. and LONGINI R.L. (1954) J. Appl. Phys. 25, 634.
- McLEAN T.P. and PAIGE E.G.S. (1960) J. Phys. Chem. Solids 16, 220.
- McSKIMMIN H.J. (1953) J. Appl. Phys. 24, 988.
- McSKIMMIN H.J. (1964) Physical Acoustics volume 1A, Mason W.P. (Ed), Academic Press, New York.
- MERKULOV L.G. (1956) Soviet Physics - Technical Phys. 1, 59.
- MERULOV L.G. (1957) Soviet Physics - Technical Phys. 2, 953.
- MORENO T. (1958) Microwave Transmission Design Data, Dover Publications, New York.
- MOTT N.F. (1936) Proc. Camb. Phil. Soc. 32, 281.

- NAVA R., AZRT. R., CICCARELLO I. and DRANSFELD K. Phys. Rev. 134, 1542.
- NYE J.F. (1957) Physical Properties of Crystals, Oxford University Press, London.
- OLIVER D.W. and SLACK G.A. (1966) J. Appl. Phys. 37, 1542.
- ORBACH R.L. (1960) Ph. D. Thesis, University of California.
- PAIGE E.G.S. (1964) Progress in Semiconductors 2, 1.
- PARMENTER R.H. (1953) Phys. Rev. 89, 990.
- PEIERLES R.E. (1955) Quantum Theory of Solids, Oxford University Press, London.
- POMERANCHUK I.J. (1941) J. Phys. (U.S.S.R.) 4, 259.
- POMERANCHUK I.J. (1942) J. Phys. (U.S.S.R.) 6, 237.
- POMERANTZ M., KEYES R.W. and SEIDEN P.E. (1962) Phys. Rev. Lett. 9, 312.
- POMERANTZ M. (1964) Phys. Rev. Lett. 13, 308.
- POMERANTZ M. (1965) Proc. I.E.E.E. 53, 1465.
- PUTLEY E.H. (1960) Hall Effect and Related Phenomena, Butterworths, London.
- PUTLEY E.H. (1967) Private communication.
- QUATE C.F., WILKINSON C.D.W. and WINSLOW D.K. (1965) Proc. I.E.E.E. 53, 1604.
- REDWOOD M. (1960) Mechanical Waveguides, Pergamon Press, Oxford.
- RICHARDSON, B.A., THOMPSON R.B. and WILKINSON C.D.W. (1968) J. Acoust. Soc. America 44, 1608.
- RICHTER J. (1962) Notes of a Post-graduate Lecture Course, Department of Electrical Engineering, University of Glasgow.
- RICHTER J. (1966) Ph.D. thesis, University of London.
- SCALAR N. and BURNSTEIN, E. (1956) J. Phys. Chem. Solids 2, 1.
- SCHIFF L.I. (1955) Quantum Mechanics, McGraw Hill, New York.

- SEAVEY M.H. (1963) Trans. I.E.E.E. Ultrasonic Eng. 10, 49.
- SEKI H., GRANATO A. and TRUPELL R (1956) J. Acoust. Soc. America 28, 230.
- SHIREN N.S. (1966) Phys. Lett. 20, 10.
- SIMONS S. (1961) Proc. Camb. Phil. Soc. 57, 86
- SIMONS S. (1963) Proc. Phys. Soc. 82, 401.
- SIMONS S. (1964) Proc. Phys. Soc 83, 749.
- SLONIMSKII G.L. (1937) J. Exp. Theor. Phys. 7, 1457
- SMITH R.A. (1959) Semiconductors, Cambridge University Press, London
- SPECTOR H.N. (1962) Phys. Rev. 127, 1084.
- SPECTOR H.N. (1965) Appl. Phys. Lett. 7, 82.
- STRATTON R. (1957) Proc. Roy. Soc. (Series A) 242, 355.
- SUZUKI K. and MIKOSHIBA N. (1966) Phys. Lett. 23, 44.
- TWOMEY J. (1970) Ph.D. thesis, University of Glasgow.
- VALDES L.B. (1954) Proc. I.R.E. 42, 420.
- van der PAUW L.J. (1958) Philips Research Reports 13, 1.
- WEINREICH G. (1956) Phys. Rev. 104, 321.
- WEINREICH G. (1957) Phys. Rev. 107, 317.
- WEINREICH G and WHITE H.G. (1957) Phys. Rev. 106, 1104.
- WEINREICH G, SANDERS T.M. and WHITE H.G. (1959) Phys. Rev. 114, 33.
- WHITE D.L. and WANG W-C (1966) Phys. Rev. 149, 628.
- WHITE G.K. (1961) Experimental Techniques in Low Temperature Physics, Oxford University Press, London.
- WHITFIELD G.D. (1961) Phys. Rev. 121, 720.
- WILLARD G.W. (1949) J. Acoust. Soc. America 21, 101.
- WILSON A.H. (1953) Theory of Metals, Cambridge University Press, London.
- WOODRUFF T.O. and EHRENREICH H. (1961) Phys. Rev. 123, 1553.
- ZENER C. (1948) Elasticity and Anelasticity in Metals Chicago University Press, Chicago.

ACKNOWLEDGEMENTS

The author wishes to express his thanks to Professor J. Lamb for his keen interest in, and encouragement of, this work.

Many helpful discussions have been held with Drs. J. Richter, J. Twomey, J.A. Wilkinson and C.D.W. Wilkinson. The first named is also thanked for the loan of a complete L-band microwave system. The last named introduced the author to the technique of the diffraction of light by sound.

Messrs C. Mullen and T. Wright were responsible for most of the specially constructed equipment used in this work. Mrs. E. Scott carried out the precision polishing of the various specimens. Without their assistance the experiments would have been extremely difficult.

This work was supported in part by the Ministry of Defence (C.V.D.). Thanks are expressed to the sponsors of the research contract Drs. E.G.S. Paige and F.G. Marshall for their interest in the work.